Functional Analysis of Zebrafish Paralogs, *parla* and *parlb,* by CRISPR-Cas9 Mediated Mutagenesis

Megan Jung

This thesis is submitted to the Faculty of Graduate and Postdoctoral Studies in partial fulfillment of the requirements for the Degree of M.Sc. in Biology

Department of Biology
Faculty of Science
University of Ottawa

Abstract

Parkinson's disease is a highly prevalent multifactorial neurodegenerative disorder caused by a complex cascade of interactions between various genetic and environmental factors. Due to this, the majority of cases are termed idiopathic. However, about 10% of PD cases are due to defined genetic factors. Interestingly, both idiopathic and familial cases of PD share mitochondrial dysfunction as a central component in the pathology of the disease. The mitochondrial protease, presenilin-associated rhomboid-like (PARL), is one such Parkinson's disease-linked gene, and is associated with diverse processes including mitochondrial dynamics, active inhibition of unnecessary apoptosis and mitophagy in *Drosophila* and yeast. Here, I investigated the role of the two zebrafish *parl* paralogs, *parla* and *parlb*, through stable CRISPR-Cas9 mediated mutagenesis. I injected wild type embryos with sgRNAs targeting *parla* and *parlb* loci, successfully producing indel mutations in *parlb* and multi-exon deletions in *parla* at mutation efficiencies of 74% and 40%, respectively. Through whole mount *in situ* hybridization experiments against *th1,* I saw no change in dopaminergic (DA) neuron development displayed by *parlb* mutants compared to wild types. Injection of *parla* splice blocking morpholinos into *parlb* mutants indicates that proper DA neuron development may depend principally on Parla function and loss of both Parla and Parlb function increases larval mortality. These results suggest a negative epistatic relationship between the *parl* paralogs as seen by the more severe phenotype observed in the loss of both Parla and Parlb function compared to the individual effects.

La maladie de Parkinson est un des plus communs troubles neurodégénératifs. Cette maladie résulte d'interactions complexes entre des facteurs génétiques et environnementaux. Ainsi, la plupart des cas de maladie de Parkinson sont classés comme étant idiopathiques. Il existe cependant environ 10% de cas dont la cause est génétique. Il est intéressant de noter que les cas idiopathiques et familiaux ont en commun une mal fonction des mitochondries comme cause de la pathologie. La protéase mitochondriale, "presenilin-associated rhomboid-like" (PARL), codée par un gène associé à la maladie de Parkinson, est associée à divers processus Ceux-ci incluent la dynamique des mitochondries et l'inhibition de la mitophagie et de l'apoptose non-essentielle, tel que l'ont montré des études chez la drosophile et la levure. Dans cette thèse, j'ai étudié le rôle de deux gènes paralogues du poisson-zèbre, *Danio rerio*, en produisant des lignées de mutants à l'aide de l'approche CRISPR-Cas9. J'ai injecté des embryons de poisson-zèbre avec des ARN guides (sgRNA) ciblant les loci *parla* et *parlb* et ai obtenu des mutations de type indel pour *parlb* et des délétions multi-exoniques pour *parla* avec des taux d'efficacité de 74% et 40%, respectivement. La détermination de l'expression de *th1* par hybridation in situ n'a montré aucune perturbation du développement des neurones dopaminergiques chez les mutants. L'injection, dans des embryons mutants *parlb*, de morpholinos dirigées contre une jonction intron-exon de *parla* a suggéré que le développement des neurones dopaminergiques dépend principalement de *parla* et que la survie des larves est affectée lorsqu'il y a perte de fonction des deux gènes *parl*. Ces résultats suggèrent une relation épistatique négative entre les gènes paralogues *parla* et *parlb* comme le montre un phénotype plus sévère lors d'une perte combinée de fonction, comparée à une perte individuelle.

Table of Contents

List of Figures

List of Tables

List of Abbreviations

A	Alanine
Afg3l2	atpase family gene 3-like 2
ASK1	apoptosis signal-regulating kinase 1
β-actin	beta actin
β-globin	beta globin
BCA assay	bicinchoninic acid assay
Bp	base pairs
BSA	bovine serum albumin
Cas9	CRISPR-associated protein 9
ClpP	caseinolytic mitochondrial matrix peptidase proteolytic subunit
Chr	chromosome
CNS	central nervous system
CRISPR	clustered regularly interspaced palindromic repeat
crRNA	chimeric RNA
Cyt-c	cytochrome c
D	aspartic acid
DA	dopaminergic
dat	dopamine transporter gene
Dpf	days post-fertilization
ECL	enhanced chemiluminescent
Ef1α	elongation factor 1 alpha
EJC	exon-exon junction complexes
ETC	electron transport chain
F	phenylalanine
FASP	filter-added sample preparation
FBS	fetal bovine serum;
G	glycine

GABA	gamma-amino-butyric acid
GAPDH	glyceraldehyde 3-phosphate dehydrogenase
GFP	green fluorescent protein
GLUT	glutamate
GPe	globus pallidus external
GPi	globus pallidus internal
H	histidine
HDR/HR	homology directed repair
HIFα	hypoxia inducible factor alpha
HRP	horseradish peroxidase
Ig	immunoglobulin
I-Clips	intramembrane cleaving proteases
Indel	insertion or deletion mutation
IMM	inner mitochondrial membrane
IMS	mitochondrial intermembrane space
iRhoms	inactive rhomboid-like proteases
K	lysine
kDa	kilo Dalton
LHON	Leber hereditary optic neuropathy
LRRK2	leucine-rich repeat kinase 2
MAPK	mitogen-activated protein kinase
MEF	mouse embryonic fibroblast
MFN	mitofusin
MO	morpholino
MRS	mitochondrial retrograde signaling
NHEJ	nonhomologous end-joining
NMD	nonsense-mediated mRNA decay
NMTR	nonsense-mediated translational repression
OMM	outer mitochondrial membrane

OPA1	optic atrophy 1
PAGE	polyacrylamide gel electrophoresis
PAM	protospacer adjacent motif
PARL	presenilin-associated rhomboid-like (human protein)
PARL	presenilin-associated rhomboid-like (human gene)
Parl	presenilin-associated rhomboid-like (zebrafish protein)
parl	presenilin-associated rhomboid-like (zebrafish gene)
PBS	phosphate buffered saline
PBS-T	phosphate buffered saline, 0.1% Tween-20
PCR	polymerase chain reaction
PD	Parkinson's Disease
PFA	paraformaldehyde
PGAM5	phosphoglycerate mutase 5
PINK1	PTEN-induced putative kinase 1
PMPcβ,	peptidase mitochondrial processing beta subunit
PNS	peripheral nervous system
PTC	premature termination codon
PTP	permeability transition pore
PTU	phenylthiourea
PVDF	polyvinylidene difluoride
qRT-PCR	quantitative real-time polymerase chain reaction
R	arginine
RIP	regulated intramembrane proteolysis
ROS	reactive oxygen species
RPL13α	ribosomal protein L13a
S	serine
SCX	strong cationic exchange
SDS-PAGE	sodium dodecyl sulfate polyacrylamide gel electrophoresis
SEM	standard error of the mean

sgRNA	single guide RNA
Sima	Similar gene
SNc	substantia nigra pars compacta
SNCA	alpha-synuclein
SNP	single nucleotide polymorphisms
SOD2	Mn-superoxide dismutase
STN	subthalamic nucleus
T	threonine
TALEN	transcription activator-like effector endonuclease
TGFβR2	transforming growth factor β-receptor type 2
Th-1	tyrosine hydroxylase 1
TMD	transmembrane domain
TMH	transmembrane helix
tracRNA	transactivating RNA
T7E1	T7 endonuclease 1
V	valine
VDAC	voltage-dependent anion channel
vDc	ventral diencephalon
W	tryptophan
W.I.S.H.	whole mount *in situ* hybridization
Wt	wild type
YWHAZ	tyrosine 3-monooxygenase/tryptophan 5-monooxygnase activation protein, zeta polypeptide
ZFN	zinc finger nuclease

Acknowledgements

I would first like to express my gratitude to my supervisor, Dr. Marc Ekker, for his guidance and support throughout my project and for allowing me the opportunity to work in his laboratory. I would also like to thank my committee members, Dr. Marie-Andre Akimenko, Dr. Tuan Bui and Dr. Bruce McKay for providing many helpful suggestions and for their advice.

I am sincerely thankful to my fellow lab mates in Dr. Ekker's and Dr. Akimenko's labs, for all their support and assistance. I greatly appreciated the mentorship and guidance provided by Dr. Sandra Noble, Dr. Jonathan Keow, and Khang Hua. Dr. Noble taught me a great deal of lab techniques and has shared many insights which were invaluable. Dr. Keow for always being willing to act as a sounding board for my ideas and for being a constant source of entertaining commentary and advice. I am gratefully indebted to Khang for offering fresh perspectives on each new challenge and for editing this thesis. Without their advice, insights and continued encouragement, this thesis would not have been possible. Jordan Nhan was a major force during genotyping and was integral to completing this project. Hannah Almira and Robert Lalonde were of great help for their counsel and aid in immunoblot and CRISPR-related experiments.

Thank you Gary Hatch, Vishal Saxena and Dr. Philip Peletier for your technical support and suggestions when it came to troubleshooting. I would also like to thank Vishal Saxena, Christine Archer, William Fletcher for their aid with zebrafish husbandry and training. Dr. Marie-Andre Akimenko (University of Ottawa) for providing the MLM3613 and DR274 plasmids.

Finally, I must express my gratitude to my family for providing me with unfailing support and encouragement through the process of researching and writing this thesis. This accomplishment would not have been possible without them.

1. Introduction

1.1 Rhomboid Proteases

Rhomboid proteases constitute a conserved protein superfamily that specifically bind and cleave membrane proteins at serine residues, directing their substrates into a diverse set of crucial signaling pathways. More specifically, rhomboid proteases, along with the presenilin aspartyl proteases and the Site 2 metalloproteases, belong to a class of highly hydrophobic proteins called intramembrane-cleaving proteases (I-CliPs). These I-CliPs catalyze the hydrolysis of peptide bonds within their membrane-embedded targets (Brown *et al.*, 2000; Pellegrini and Scorrano, 2007).

Rhomboid integral membrane proteases reside within cellular membranes with their active sites buried within their transmembrane domains (TMD). They cleave in, or immediately adjacent to, the transmembrane domains of their substrates (Lemberg, 2013), thereby liberating the biologically active nuclear or secreted domains from their membrane-tethered precursor proteins, as effectors or reporters (Sík et al., 2004). The resulting activated proteins have been identified to play pivotal roles in inter and extracellular signaling, cell regulation and protein processing (Meissner *et al.*, 2011; Weihofen and Martoglio, 2003) (Figure 1.1). This release of protein domains from membrane sequestration is a particularly powerful control mechanism and in most cases are part of highly controlled processes. Therefore, rhomboid proteases are considered proteins involved in regulated intramembrane proteolysis (RIP) (Weihofen and Martoglio, 2003).

The rhomboids exist throughout all kingdoms of life, making them some of the most widely spread transmembrane proteins yet identified. In fact, the conservation of these intramembrane proteases has brought to attention the possibility that they may be some of the most ancient regulatory enzymes of modern cells (Brown *et al.*, 2000; Koonin *et al.*, 2003; Urban and Freeman, 2002). Additionally, it has been argued that rhomboid proteases are potentially the most widely distributed membrane proteins in nature (Koonin *et al.*, 2003).

In bacteria, rhomboid proteases have been implicated in quorum sensing during bacterial growth (Urban and Dickey, 2011). In eukaryotic parasites, like *Toxoplasma gondii* and other apicomplexan parasites, rhomboids are involved in the intracellular signaling for host cell invasion via the dismantling of adhesive junctions, allowing the host membrane to seal and the parasite to be internalized (Freeman, 2008; Urban and Dickey, 2011). The *Saccharomyces cerevisiae* rhomboid, Pcp1p/Rbd1p, is a mitochondrial I-CliP which cleaves Mgm1, mediating mitochondrial fusion, respiration and growth rate (McQuibban *et al.*, 2003). Rhomboid-1 (RHO-1), the *Drosophila* rhomboid, plays a role in EGF signaling, growth and development through the cleavage and activation of Spitz. The *Caenorhabditis eleg*ans (*C. elegans*) rhomboid has also been implicated in EGF signaling (Freeman, 2004; Urban and Dickey, 2011). A presenilin associated rhomboid-like (PARL)-/- mouse model, links mammalian mitochondrial rhomboid function to the regulation of apoptosis and mitochondrial dynamics through the cleavage of OPA1 and PINK1 (Cipolat *et al.*, 2006).

The eukaryotic rhomboids are classified as active rhomboids, inactive rhomboid-like proteins that lack a catalytic domain (iRhoms) and a third group of inactive homologues (Freeman, 2008). The active rhomboids themselves are divided into two major subfamilies including the

secretase RHO subfamily, like *Drosophila* RHO-1, and protease PARL-type rhomboids, which are mitochondrial proteins (Figure 1.2). The RHO subfamily proteases typically have extra transmembrane helices (TMH) at the carboxyl (C-) terminus of the 6-TMH rhomboid core (6+1 structure). The PARL subfamily, similarly have an extra TMH, except it is added to the amino terminus (1+6 structure) (Hill and Pellegrini, 2010; Koonin *et al.*, 2003).

1.2 Mitochondrial Rhomboids

Mitochondria are integral and functionally versatile organelles, crucial in various cellular processes including energy conversion and intermediate metabolism (Danial *et al.*, 2003), and in several integrated signaling pathways, like Ca^{2+} signaling (Rizzuto *et al.*, 2000), and apoptosis (Green and Kroemer, 2004). Their functional versatility is paralleled by their complex and dynamic morphology, regulated through fusion and fission events in response to the different physiological needs of the cell (Cipolat *et al.*, 2006). Changes in mitochondria shape play critical roles in vertebrate development via programmed cell death, and in various processes of normal cell physiology, such as reactive oxygen species (ROS) production, and lifespan. Recently, rhomboid proteases have been implicated as mitochondria-shaping proteins and thus in mitochondrial membrane remodeling (Jeyaraju *et al.*, 2006).

The yeast Pcp1p/Rbd1p protein regulates and cleaves Mgm1p, an intermembrane space dynamin family member that participates in mitochondrial fusion events (Jeyaraju *et al.*, 2006). The short isoform of Mgm1p produced by Pcp1p/Rbd1p is required to maintain mitochondrial

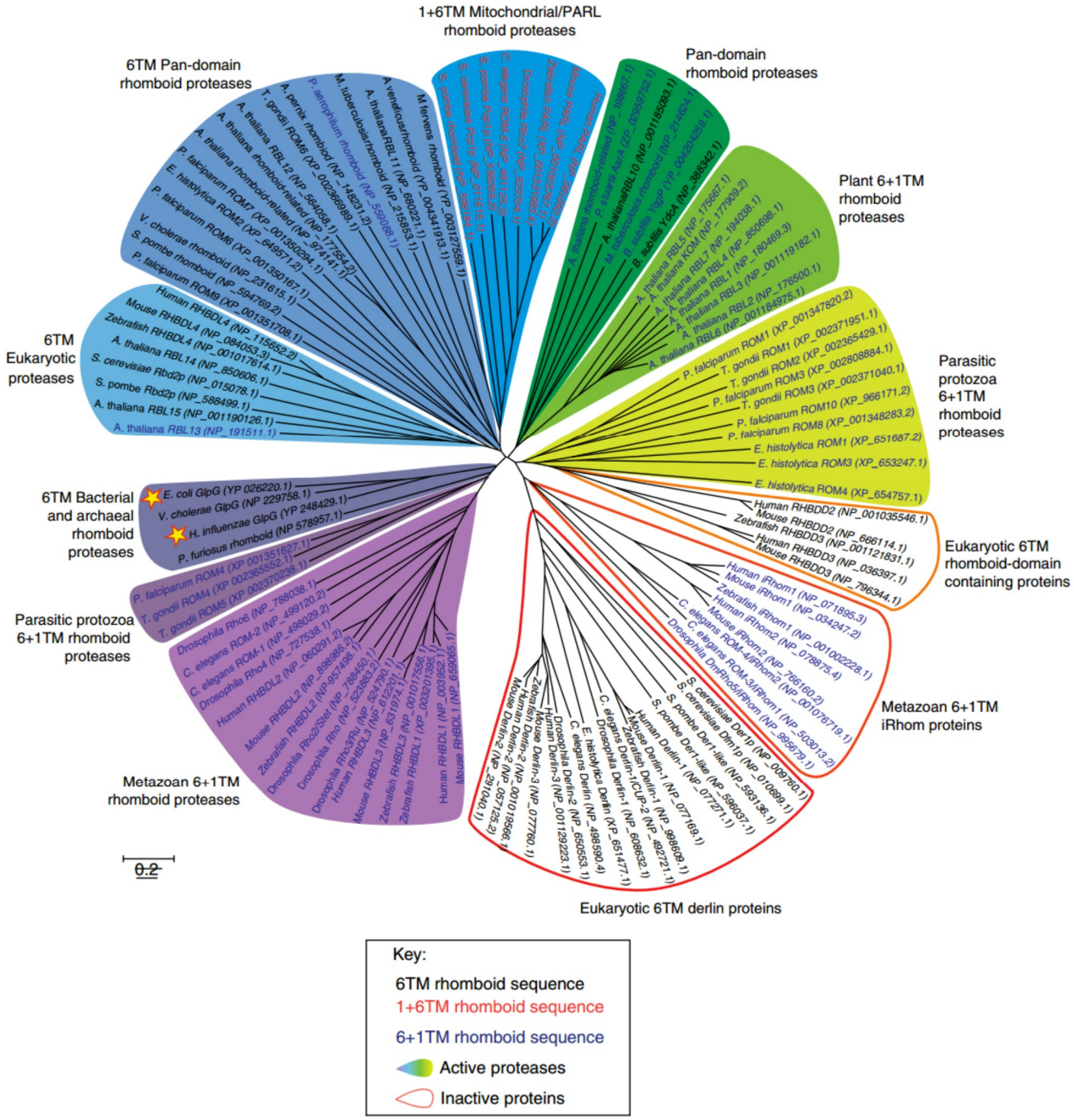
1+6TM Mitochondrial/PARL rhomboid proteases
Pan-domain rhomboid proteases
Plant 6+1TM rhomboid proteases
Parasitic protozoa 6+1TM rhomboid proteases
Eukaryotic 6TM rhomboid-domain containing proteins
Metazoan 6+1TM iRhom proteins
Eukaryotic 6TM derlin proteins
Metazoan 6+1TM rhomboid proteases
Parasitic protozoa 6+1TM rhomboid proteases
6TM Bacterial and archaeal rhomboid proteases
6TM Eukaryotic proteases
6TM Pan-domain rhomboid proteases
0.2
Key:
6TM rhomboid sequence
1+6TM rhomboid sequence
6+1TM rhomboid sequence
Active proteases
Inactive proteins

Figure 1.1: Phylogenetic tree of rhomboid proteases. A subset of 109 Rhomboid and Derlin family protein reference sequences, retrieved from the NCBI RefSeq database, was chosen to illustrate their diversity. Mega 5.05 was used to align sequences by MUSCLE and construct an unrooted neighbor-joining phylogenetic tree. Branches are labeled according to their common characteristics and are shaded or outlined to denote active or inactive protease sequences, respectively. Individual sequence names are colored black, blue, or red to indicate a 6TM, 6+1TM, or 1+6TM arrangement, respectively, with each RefSeq accession number included within parentheses. Despite the tremendous number and diversity of rhomboid proteins, structures of only two 6TM rhomboid proteases have been solved (yellow stars). (From Urban and Dickey, 2011)

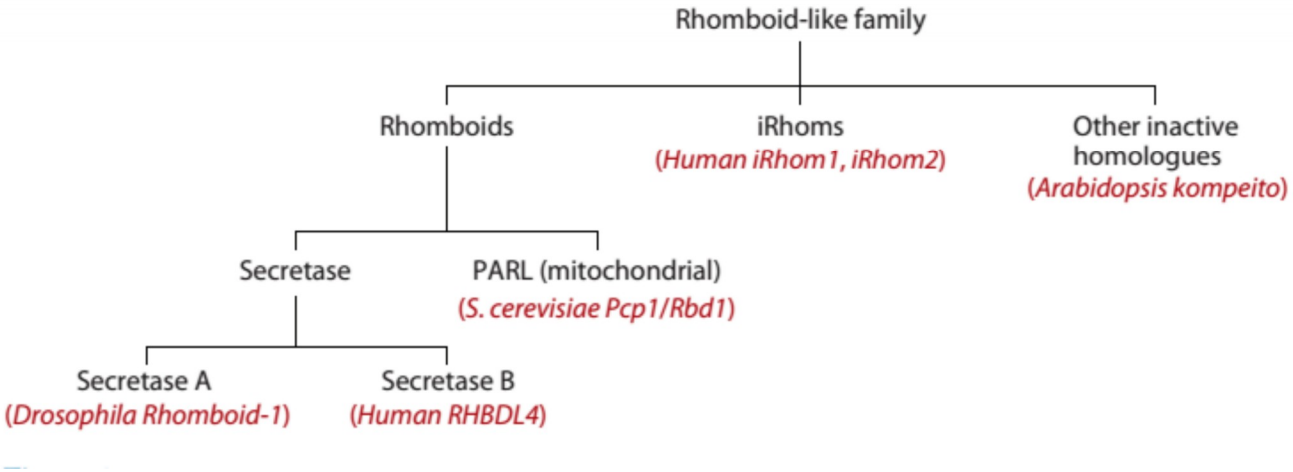
Rhomboid-like family
Rhomboids
iRhoms
(Human iRhom1, iRhom2)
Other inactive homologues
(Arabidopsis kompeito)
Secretase
PARL (mitochondrial)
(S. cerevisiae Pcp1/Rbd1)
Secretase A
(Drosophila Rhomboid-1)
Secretase B
(Human RHBDL4)

Figure 1.2: The eukaryote rhomboid-like family. Systematic classification of rhomboids separates them into three major groups of rhomboid-like proteins: the active proteases; a tightly clustered group of apparently inactive rhomboid-like proteins (termed iRhoms), which resemble rhomboids in most regards but which lack catalytic residues; and a number of other rhomboid-like proteins that are predicted to be inactive but which do not cluster with themselves or with the iRhoms. The active proteases can in turn be further subdivided into secretase and presenilin associated rhomboid-like (PARL) proteins (From Freeman, 2008).

morphology and fusion (Herlan *et al.*, 2003; McQuibban *et al.*, 2003). In mammals, mitochondria fusion is mediated by two outer mitochondrial membrane (OMM) proteins, mitofusin (MFN) -1 and MFN-2. The mammalian homolog of *S. cerevisiae* Mgm1p, Optic atrophy 1 (OPA1) is also a dynamin-related protein that promotes mitochondrial fusion by cooperating with MFN-1 (Cipolat *et al.*, 2006). Several mitochondrial rhomboids have also been implicated in regulation and control of mitochondrial morphology and function through the PINK1/PARKIN pathway, and in mammals, apoptotic regulation (Noble *et al.*, 2012).

1.3 Protease presenilin-associated rhomboid-like (PARL): Rhomboid Catalytic Mechanism

The mitochondrial rhomboid protease, presenilin-associated rhomboid-like (PARL), is the human ortholog of yeast Pcp1p/Rbd1p (Jeyaraju *et al.*, 2006). PARL was originally identified in a two-hybrid screen to interact with presenilin-2, the enzymatically active core protein of gamma-secretase (Pellegrini *et al.*, 2001). It is now known that PARL does not interact with presenilin *in vivo,* and the interaction was due to an artifact.

PARL is a 379 amino acid long protein residing exclusively in the inner mitochondrial membrane. Similarly to Pcp1p/Rpd1, PARL has its C-terminus exposed to the inner membrane space (IMS), and N-terminus facing the matrix (Jeyaraju *et al.*, 2006). Like other rhomboid family members, PARL has a conserved core of six transmembrane helices (TMH), with the serine (S277) and histidine (H335) residues required to form the catalytic dyad embedded in TMH4 and TMH6, respectively. Within the conserved core, there is also a domain within the first loop and TMH2 which has an unknown function and a highly-conserved tryptophan-arginine (136W137R) motif which has been hypothesized to be required for proteolytic activity (Freeman, 2008; Lemberg

and Freeman, 2007; Lemberg *et al.*, 2005; Wang *et al.*, 2007). As a eukaryotic rhomboid and member of the mitochondrial PARL subfamily, PARL has an additional TMH located at the N-terminus, on top of the conserved six TMH core, giving it the 1+6 TMH topology (Lemberg and Freeman, 2007). PARL contains unique differences in its structure compared to other rhomboids by missing the arginine in loop 1 and glutamate between TMH2 and TMH3 and by having the characteristic serine protease catalytic dyad shifted over from TMH4 and TMH6, to TMH5 and TMH7.

The active site of PARL is about 10 Å below the mitochondrial membrane surface, closer to the matrix side, allowing the cleaved substrate to be released into the IMS (Freeman, 2004; Noble *et al.*, 2012). More specifically, based on crystallography, the active site is located within a cavity that is open to the aqueous environment with the catalytic serine positioned on top of a short, tilted TMH4. This serine is further surrounded by longer TMHs that span the lipid bilayer of the mitochondria, shielding the serine from its hydrophobic environment. The corresponding histidine of the catalytic dyad is oriented so that it can convert the catalytic serine into a reactive nucleophile by stripping it of a proton (Freeman, 2008).

PARL is still a subject of debate in terms of its substrate specificity, cleavage site determination, and entry into the active site. Few substrates, and further, their cleavage sites, have been conclusively identified (Hill and Pellegrini, 2010). There are several theories as to how PARL and other mitochondrial rhomboids interact with their substrates. The most popular theory is that substrates enter between helices 2 and 5, with TMH5 acting as a gatekeeper. Mutational analysis on *E. coli* rhomboid GlpG revealed increased proteolytic activity upon the disruption of TMH5, allowing for increased lateral entry of it substrates. The sequence variability of TMH5 has

been suggested to reflect differences in rhomboid substrate specificity (Lemberg and Freeman, 2007).

Another theory is termed alternative topogenesis and involves the substrate (Herlan *et al.*, 2004). An ATP-driven motor translocates the substrate's primary transmembrane domain into the mitochondria matrix, pulling a secondary hydrophobic domain into the membrane itself. This secondary hydrophobic domain contains the rhomboid's cleavage site, and its shift in position into the IMM allows it to be accessible to PARL for proteolysis. In yeast, Pcp1p/Rpd1 and Mgm1 undergo this form of mechanism of substrate cleavage in which the single TMD of Mgm1 is not cleaved but instead, an alternative hydrophobic domain normally located outside the membrane is cleaved. During cleavage, their topology is rearranged to allow for the substrate cleavage site, contained in a secondary hydrophobic domain, separate from the primary transmembrane domain (TMD).

1.4 PARL Cleavage

PARL itself undergoes two constitutive cleavage events and a third cleavage event believed to be involved in negative regulation of PARL function. The N-terminal domain of PARL contains the α-site (position G52-F53) and the vertebrate specific β-site (position S77-A78). The exact location of the γ site is unknown, but likely between amino acids 121-167, within the first loop connecting TMH1 to the 6 TMH core. Cleavage at the α-site leads to the removal of the mitochondrial localizing sequence and is associated with the import of PARL into the mitochondria. Cleavage at the γ site appears to be tissue-specific, and in mammals, appears to destabilize PARL, serving as a control on PARL activity (Jeyaraju *et al.*, 2011). The β-cleavage is

mammalian specific, and developmentally controlled. The β-cleavage occurs through PARL I-Clip activity supplied *in trans* and liberates the Pβ domain which spans amino acids 40-100, containing a nuclear localizing sequence (Sík et al., 2004). A study performed by Jeyaraju *et al.* showed that the phosphorylation of residues S65, T69, and S70 within the Pβ domain by PDK2, inhibits PARL β-cleavage, ultimately leading to the inhibition of PARL-induced mitochondrial fragmentation, a process required for efficient mitophagy (Shi and McQuibban, 2017). Along with the high sequence conservation, this suggests that the development of the Pβ domain during vertebrate evolution may be associated with the emergence of a new mechanism for the regulation of PARL activity (Jeyaraju *et al.*, 2006; Jeyaraju *et al.*, 2011).

Once cleaved, the Pβ-peptide is expelled into the cytosol where it is directed to the nucleus (Hill and Pellegrini, 2011). Here, it is believed that the Pβ-peptide functions in mitochondrial retrograde signaling (MRS). Since the majority of mitochondrial proteins are encoded in the nucleus, it is important for there to be a feedback communication system between the mitochondria and the nucleus of a cell. MRS is responsible for this compensatory communication, involving factors that can sense and transmit mitochondrial signals to effect changes in nuclear gene expression, allowing for the coordination of mitochondrial protein synthesis. MRS can sense mitochondrial activity and dysfunctions, relaying this information to the nuclease for reconfiguration of metabolism to accommodate and compensate for mitochondria defects.

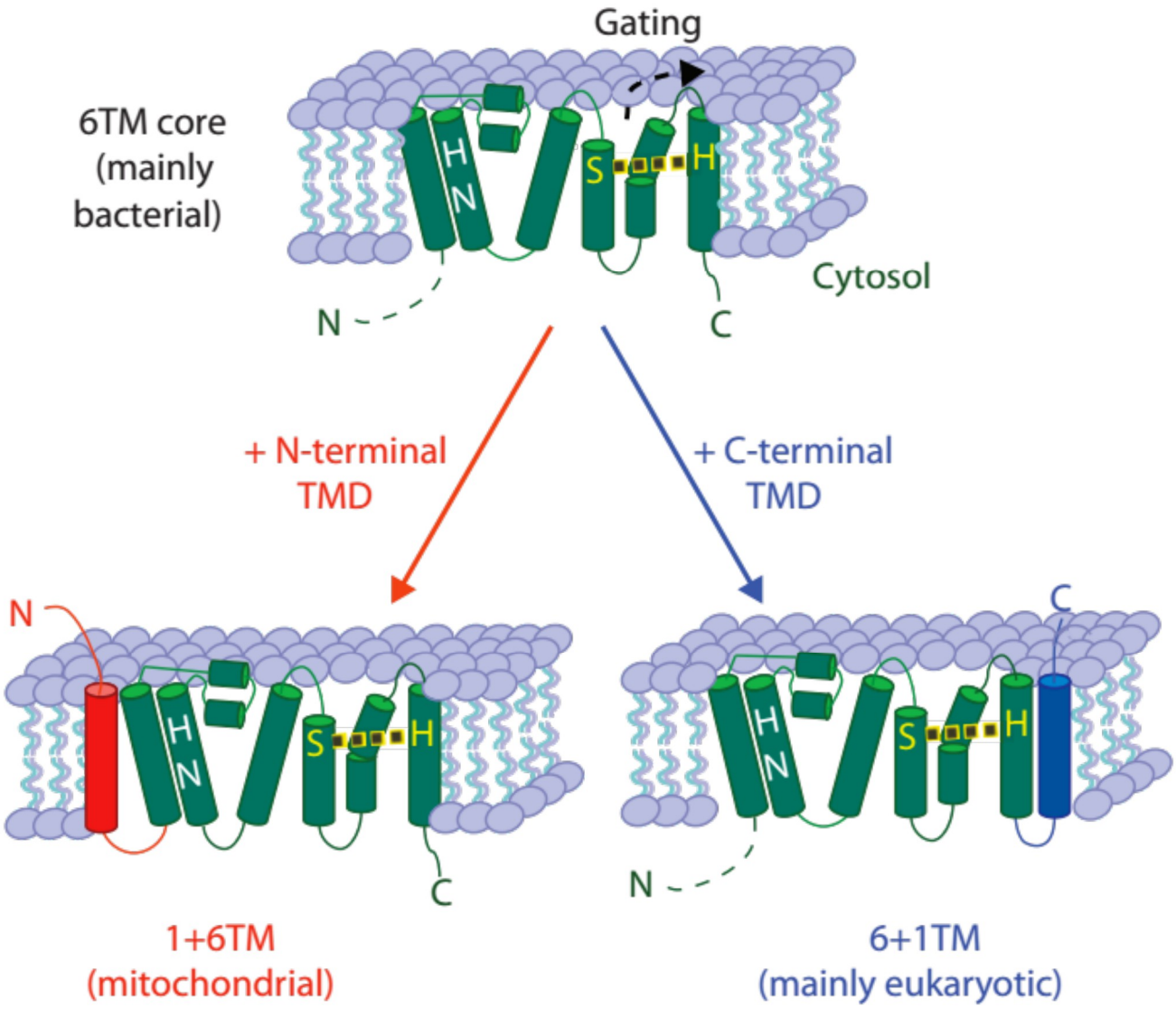
Gating
6TM core
(mainly
bacterial)
H
N
S
H
Cytosol
N
C
+ N-terminal
TMD
+ C-terminal
TMD
N
H
N
S
H
C
1+6TM
(mitochondrial)
C
H
N
S
H
N
6+1TM
(mainly eukaryotic)

Figure 1.3: Rhomboid proteins exist in three topological forms. The 'core' rhomboid domain consists of 6 transmembrane helices (TMH), with variable amino termini (dashed lines). Most eukaryotic and mitochondrial rhomboids have an additional TMH added to either the carboxy-terminus (eukaryotes, blue) or amino-terminus (mitochondria, red) to the 6TM core, as depicted. Catalytic residues are shown in yellow for nucleophilic chemistry (hydrolysis) and white for electrophilic residues (oxyanion transition state stabilization) (From Urban and Dickey, 2011).

In yeast, MRS is involved in coordinating a variety of functions, including nutrient sensing, growth control, aging, metabolism, and organelle homeostasis. In mammals, MRS has been implicated in coordinating the mitochondrial stress response. In a study performed by Cagin *et al.*, they demonstrated that neuronal function may be regulated by MRS through the knockdown of the *Drosophila* Similar (*Sima*) gene*,* ortholog of hypoxia inducible factor alpha (HIFα), and a regulator of several retrograde genes. *Sima* knockdown in *Drosophila* with induced mitochondrial dysfunction in the nervous system, showed a restoration of neuronal function without affecting the primary mitochondrial defect. This suggests that MRS may be partly responsible for neuronal dysfunction. Additionally, the knockdown restored function in the *Drosophila* models of Leigh syndrome and Parkinson's Disease (Cagin *et al.*, 2015).

The precise mechanism and components involved in mitochondrial retrograde signaling remain largely unknown. In this respect, the study of PARL's Pβ-peptide-mediated MRS could lead to novel mechanisms and models on how the nucleus monitors and responds to mitochondrial bioenergetics, a critical process in the survival and functioning of a cell. Moreover, the role of PARL's unique putative signal moiety in MRS, leads to further implications on its role in mitochondrial dynamics, neuronal development, and mitochondrial dysfunction-linked diseases.

1.5 Mitochondria in Cell Maintenance

Mitochondria, in general, are vastly important organelles for a cell and for development, especially with their role in cellular maintenance. Due to their involvement in intermediate metabolism and the production of ROS, mitochondria can rapidly fall into a death promoting cascade initiated with excessive ROS, and leading to the release of pro-death proteins, disrupted ATP synthesis, mitochondrial membrane depolarization and the activation of cell death pathways. To maintain proper functioning, a variety of mitochondrial quality control systems have evolved to regulate mitochondrial morphology and function. Among them, mitochondria constantly undergo cycles of fusion and fission to maintain a healthy population of mitochondria. Fusion events rescue bioenergetically impaired mitochondria by rejoining them with a larger, healthy mitochondria network. Fission events sequester severely damaged mitochondria and this process of the selective clearance of damaged mitochondria in cells is termed mitochondrial autophagy, or mitophagy (Kubli and Gustafsson, 2012).

If the damage is severe, mitochondria can also induce apoptosis. Apoptosis is a naturally occurring process by which a cell is directed to undergo programmed cell death and is indispensable to the normal development and function of an organism. The signals for apoptosis initiation can be extrinsic or intrinsic. The best known intrinsic pathway is through mitochondria dysfunction. The steps involved in this process start with a change in the mitochondrial membrane potential, production of ROS, opening of the permeability transition pore (PTP), and the release of the intermembrane space protein, cytochrome *c* (Cyt c). The released cytochrome *c* activates Apaf-1, which in turn activates a downstream caspase death program. Considering the

substrates it acts upon, mounting evidence suggests a role of PARL in both mitophagy and apoptosis (Gross *et al.*, 1999).

1.6 PARL in Mitophagy

One known substrate of PARL cleavage is PTEN induced kinase-1 (PINK1), a mitochondrial serine/threonine kinase involved in stress induced mitochondrial dysfunction. The PINK1/PARKIN pathway is a highly studied process in mitophagy through which PINK1 signals for the clearance of unhealthy mitochondria, acting as a cellular checkpoint for mitochondrial integrity (Meissner *et al.*, 2011). Upon synthesis, cytoplasmic PINK1 is inserted into the IMM via the TOM complex (Lazarou *et al.*, 2012). Autophosphorylation of PINK1 leads to its stabilization in the IMM. During mitochondrial depolarization, PINK1 recruits cytoplasmic PARKIN, an E3 ubiquitin ligase, activating its E3 function and leading to the initiation of mitophagy (Shi *et al.*, 2011).

Several studies have shown that PARL is a potential regulator of this canonical import pathway, suppressing mitophagy when inappropriate by proteolytically processing PINK1 in a mitochondrial membrane potential-dependent manner (Deas *et al.*, 2011; Jin *et al.*, 2010; Meissner *et al.*, 2011; Shi *et al.*, 2011). Here, PARL cleaves PINK1's signal sequence, generating a 52 kDa form of PINK1. The 52 kDa form is then rapidly removed by a proteasome-dependent pathway, most likely after its release from the mitochondrial intermembrane space (IMS) to the cytosol leading to the eventual removal of PINK1 from the mitochondria (Imai, 2012). Upon the depolarization of the mitochondrial membrane potential though, IMM insertion and the subsequent processing of PINK1 by PARL may be inhibited, leading to the accumulation of full-length PINK1 in the mitochondrial OM, initiating mitophagy.

Rhomboids in yeast and *Drosophila* also show related mitochondrial roles, indicating that PARL might be a functionally conserved subclass of rhomboid proteases (McQuibban *et al.*, 2003; McQuibban *et al.*, 2006). The *Drosophila* homologue, *Rhomboid-7*, also acts in the PINK1-PARKIN pathway with rhomboid-7 epistatic to its substrate, PINK1 (Whitworth *et al.*, 2008). Similarly, a study by Noble *et al.,* found that zebrafish *parl* genes, *parla* and *parlb* paralogs, are also epistatic to the zebrafish *pink1* gene by knockdown of *parla/b* using translation-blocking morpholinos, while simultaneously expressing *pink1* (Noble *et al.*, 2012). This evidence suggests that the *parl* genes may function upstream of *pink1*, in a conserved pathway between *Drosophila,* zebrafish and vertebrates.

PARL also mediates the cleavage of phosphoglycerate mutase 5 (PGAM5), which has been found to activate the stress-activated mitogen-activated protein kinase (MAPK) pathways. While in healthy mitochondria, PARL cleaves PINK1, during depolarization of mitochondrial membrane potential, PARL instead cleaves PGAM5. Cleavage of PGAM5 activates the protein, apoptosis signal-regulating kinase 1 (ASK1), allowing it to facilitate a stress-response through the MAP kinase pathway (Sekine *et al.*, 2012). Additionally, the Lenardo group found evidence that PGAM5 is necessary for the stabilization of full-length PINK1 on damaged mitochondria, acting as a regulator of mitophagy, and serving as a protector for dopaminergic neurons *in vivo* (Lu *et al.*, 2014). Therefore, PARL regulates differential cleavage of PINK1 and PGAM5, depending on the health status of the mitochondria in question. PGAM5 has also been implicated in mediating necrosis via mitochondrial fission, working downstream of necrosis promoting kinases, receptor-interacting protein 1 and 3 (RIP1 And RIP3).

1.7 PARL in Apoptosis

Another pathway involving PARL revolves around HtrA2/Omi, a substrate of rhomboid 7 and ortholog of OPA1. HtrA2/Omi are required for mitochondrial fusion during spermatogenesis and muscle maturation. *Drosophila rhomboid-7* mutants display severe neurological defects and have a reduced lifespan. In addition, these flies have a droopy wing phenotype, disrupted patterning of myofilaments in indirect flight muscles, and disrupted mitochondrial packing, size and inner membrane organization (McQuibban *et al.*, 2006).

OPA1, a dynamin-like mitochondrial GTPase, functions cooperatively in an intrinsic apoptotic mechanism, inhibiting cell death through stabilizing mitochondrial morphology (Cipolat *et al.*, 2006). OPA1 is anchored to the mitochondrial inner membrane, facing the intermembrane space. Haplo-insufficiency of OPA1 is responsible for the most common form of autosomal dominant optic atrophy, a neuropathy resulting from the degeneration of retinal ganglion cells and of the optic nerve.

For apoptosis initiation resulting from mitochondrial dysfunction, release of cytochrome c is key for amplifying the activation of caspases. Several apoptogenic proteins, including cytochrome c, reside in the mitochondrial inner membrane space (IMS). Based on studies using electron tomography, cytochrome c is likely sequestered in intra-cristae regions made of juxtaposed folding of the IM. Without remodeling of these intra-cristae, cytochrome c has limited access to the IMS, and thus cannot exit to the cytosol to exert its effects. OPA1 is an anti-apoptotic protein, slowing the release of cytochrome c by controlling the shape of mitochondrial cristae, keeping the junctions between the intra-cristae tight. During apoptosis, the OPA1 hetero-

oligomer is disrupted, leading to unraveling of the cristae and cytochrome c diffusion to the IMS (Figure 1.4) (Gottlieb, 2006).

Although both PARL and OPA1 are implicated in mitochondrial fusion, their role in apoptosis is independent of this process. Mitochondrial PARL cleaves the OPA1 protein, generating a pool of truncated, smaller OPA1 that is soluble in the IMS. This soluble OPA1 is critical for the anti-apoptotic effects of PARL by maintaining the bottleneck configuration of the intra-cristae and the sequestering of cytochrome c (Gottlieb, 2006). The study performed by Cipolat *et al.* revealed that $PARL^{-/-}$ mice displayed progressive multi-systemic atrophy and eventual cachectic death after the fourth postnatal week. The knockout mice showed atrophy of muscular tissue, spleen and thymus, as well as mild neurodegeneration in the thalamus and striatum (Cipolat *et al.*, 2006). All specimens died between 8 to 12 weeks likely due to moving and breathing issues and general cachexia. Interestingly, PARL is not required for mitochondrial respiration in mice, but does protect from mitochondrial dependent apoptosis. Loss of PARL led to a disruption of OPA1 in the mitochondrial cristae, which triggered the release of cytochrome c and ultimately lead to apoptosis. Through RNAi, it has been shown that PARL is genetically upstream of OPA1 in the apoptotic pathway (Cipolat *et al.*, 2006).

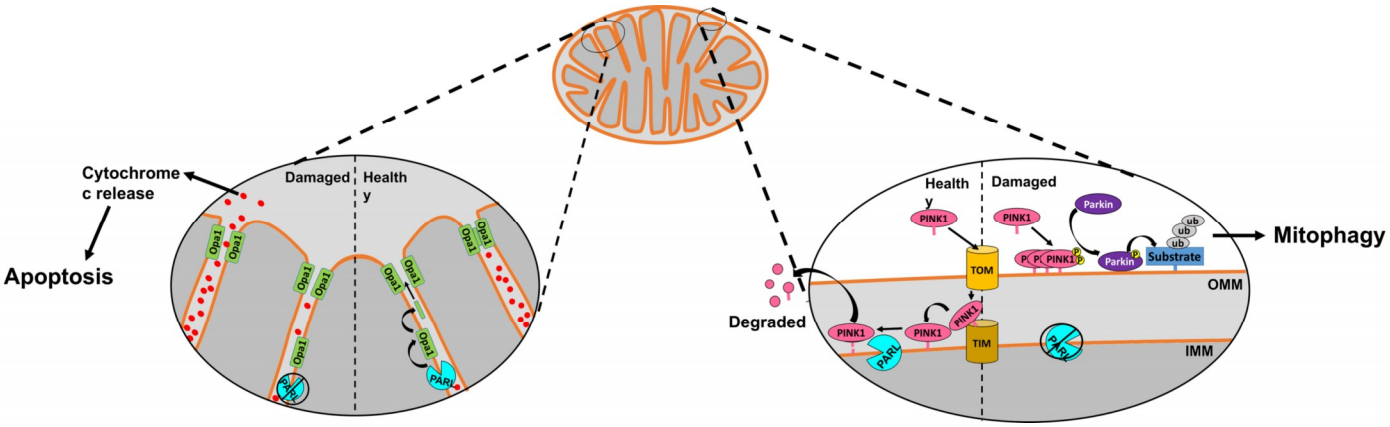
Cytochrome c release
Apoptosis
Damaged
Health y
Opa1
PARL
Degraded
Health y
Damaged
PINK1
Parkin
ub
TOM
Substrate
OMM
TIM
IMM
Mitophagy

Figure 1.4: Schematic representation of the role of PARL in mitophagy and apoptosis. Left side: Prior to the permeabilization of the mitochondrial outer membrane, matrix remodeling is required for a swift and complete release of cytochrome c. OPA1 comes in two sizes: the larger form is embedded in the mitochondrial inner membrane and the smaller soluble form is found in the intermembrane space (IMS) and plays a critical role in maintaining the bottleneck structure of the cristae. PARL, an intramembrane protease, regulates OPA1 processing. During apoptosis, the OPA1 hetero-oligomer is disrupted, leading to unraveling of the cristae and cytochrome c diffusion to the IMS. Following perforation of the mitochondrial outer membrane (usually due to Bak/Bax activity), cytochrome c is released to the cytosol where it forms the apoptosome (oligomers of Apaf-1, cytochrome c, and pro-caspase-9) and leads to further downstream events that trigger full-blown apoptosis. **Right side:** PINK1 is imported into the mitochondria and cleaved by PARL. Upon release from the mitochondrial intermembrane space to the cytosol, the shorter, cleaved PINK1 molecule is rapidly removed by a proteasome-dependent pathway. Upon mitochondrial membrane depolarization, PARL cleavage of PINK1 is inhibited and autophosphorylation activates PINK1 allowing for the recruitment and activation of Parkin, and subsequent degradation of damaged mitochondria via ubiquitylation mediated pathways.

1.8 Parkinson's Disease

Various studies have implicated mutations in PARL as contributing and causal factors in numerous disorders and degenerative diseases, including early onset type II diabetes (Walder *et al.*, 2005), obesity, glaucoma, Leber hereditary optic neuropathy (LHON) (Phasukkijwatana *et al.*, 2010), and metabolic syndromes. The most studied of these degenerative diseases, and of particular interest to this study, is Parkinson's disease (Noble *et al.*, 2012; Shi *et al.*, 2011).

Parkinson's Disease (PD) is the most common neurodegenerative movement disorder in humans, resulting in extensive and often devastating symptoms. PD is an age-related progressive disease with diagnosed individuals being predominantly older than 65 years of age, although cases of earlier onset have been observed. Clinically, affected individuals show deterioration of motor function, including bradykinesia, rigidity, postural instability and resting tremor. In addition to motor symptoms, patients can also suffer from cognitive disturbances like anxiety, depression, and dementia. Although not considered primary diagnostic criteria, other frequently seen non-motor symptoms include defects in gastrointestinal motility, impaired olfaction, autonomic failure, and responsiveness to L-DOPA therapy. The specific symptoms and progression of the disease varies and is unique to each individual, causing PD to be difficult to diagnose. Currently, there is no cure although treatment options including medication, surgery, and diet regulation have been utilized to treat the developing symptoms.

The major clinical symptoms of PD are due to the progressive loss of dopaminergic neurons in the *substantia nigra pars compacta*. The presence of intracytoplasmic inclusions known as Lewy bodies have also been linked to the pathogenesis of the disease, although not all cases of PD involve Lewy body formation, and their development is not unique to PD only.

Although not the hallmark pathological feature, neurodegeneration and Lewy bodies can also be found in the *locus coeruleus*, hypothalamus, nucleus basalis, cerebral cortex, cranial nerve motor nuclei, and central and peripheral components of the autonomic nervous system (Dawson and Dawson, 2003; Polymeropoulos *et al.*, 1997). The systemic pathology of PD in the central nervous system (CNS) and peripheral nervous system (PNS), affects not just the dopaminergic system, but the noradrenergic, cholinergic and serotonergic systems. This widespread pathology helps to explain the diverse motor and non-motor manifestations of PD.

The dopaminergic neurons of the *substantia nigra pars compacta* (SNc) are a part of the extrapyramidal system or basal ganglia, a group of subcortical nuclei in the forebrain. Other included regions are the striatum, globus pallidus (GP; internal and external), and subthalamic nucleus (STN). The basal ganglia are associated with a variety of functions including the control and refinement of voluntary motor movements, helping to suppress unwanted movements. More specifically, the basal ganglia control and regulate activities of the motor and premotor cortical areas to produce smooth, voluntary movements through selecting an appropriate motor behavior from several possibilities. In simplest terms, the basal ganglia are innervated by input from the cerebral cortex for refinement control, and output is relayed back to the motor cortex through the thalamus (Jankovic, 2008).

Cortical input to the basal ganglia comes via the striatum, which sends output signals mediated by the inhibitory gamma-amino-butyric-acid (GABA) neurotransmitter to other components of the basal ganglia. The globus pallidus receives input from the striatum and sends inhibitory output to the thalamus (internal) and subthalamic nucleus (external). The subthalamic nucleus also receives input from the striatum and cerebral cortex and projects back to the globus

pallidus (internal). The striatum itself receives excitatory and inhibitory influences from the substantia nigra pars compacta through dopaminergic input, acting as a control for the direct and indirect motor movement pathways. Through the direct pathway, the release of dopamine from the SNc leads to an excitatory effect on the cells of the striatum, via D1 dopamine receptors, leading to increased output of GABA to the GABAergic neurons of the GP (internal). This inhibition in turn lead to a decrease in suppressive signals via GABA from the GP (internal), therefore allowing for increased cortico-thalamic signals, and allowing for increased motor activity. Through the indirect pathway, dopamine released from the SNc acts through D2 dopamine receptors, leading to an inhibitory influence on striatal cells via the GP (external). Dopaminergic nigrostriatal projections innervate GABAergic neurons in the globus pallidus externa, which in turn projects to the STN, which provide excitatory input via glutamate to the internal segment of the GP. Therefore, the GP (internal) increases suppressive signals via GABA, to the thalamus, decreasing cortico-thalamic signals, and decreasing motor activity (Jankovic, 2008; Noble *et al.*, 2012).

Both the direct and indirect pathways work in parallel, functioning in the refinement of overall net signal transmission and aids in the selection of specific motor pathways from the motor cortex. The loss of nigrostriatal control of the basal ganglia due to dopaminergic neuron degeneration in the SNc causes cortico-thalamic signal over-inhibition, through a decrease in the dopaminergic drive on the direct pathway and lack of disinhibition on the indirect pathway. This suppression of signal transmission to the thalamus from the motor cortex consequently leads to the characteristic stiffness and rigidity seen in patients with Parkinson's disease (reviewed in Sulzer *et al.*, 2016).

1.10 Parkinson's Disease Etiology

Despite the number of studies performed to investigate Parkinson's Disease, its etiology is not well understood. Epidemiologic studies have indicated several factors that can increase one's risk of developing Parkinson's Disease which include exposure to pesticides, herbicides, and neurotoxins, head trauma and genetic factors (Olanow and Tatton, 1999). Several biochemical abnormalities including mitochondrial dysfunction (complex I deficiency), free radical-mediated damage, inflammatory changes and proteasomal abnormalities have been observed in the substantia nigra of patients with sporadic PD (Hauser and Hastings, 2013; Schapira and Jenner, 2011). In general, the majority of PD cases are due to a complex cascade of interactions between environmental, epigenetic and genetic factors, leading to PD being considered an idiopathic disease with the majority of cases sporadic in nature. Due to the complexity of the interactions, the etiology of PD remains elusive, and due to this, neither preventative nor effective long-term treatment strategies are available. Only <10% of cases are due to well-defined environmental or genetic factors (Dawson and Dawson, 2003). Interestingly, the motor phenotypes of the few familial cases of PD are almost identical to the sporadic, implying a commonality in their underlying mechanisms. Therefore, the analysis of the rare genetic forms of PD may lead to better understanding of the pathogenesis of both sporadic and familial forms.

Many lines of evidence suggest that mitochondrial dysfunction plays a central role in the pathogenesis of Parkinson's disease (PD) and in fact, sporadic and familial cases of PD share mitochondrial dysfunction as a common pathway in their pathology. Studies performed on the mitochondrial toxins MPTP (Langston *et al.*, 1983), rotenone (Keow, 2016), and paraquat (Day *et*

al., 1999; Richardson *et al.*, 2005) gave early evidence to the contributing role of mitochondrial dysfunction on PD. Furthermore, patients with PD show decreased mitochondrial O_2 uptake and electron transport chain (ETC) complex 1 activity and decreased brain cortex mass, as well as higher cytochrome content, higher expression of manganese-superoxide dismutase (SOD2), and greater oxidative damage in the frontal cortex. Additionally, subunits of ETC complex 1 are oxidatively damaged, functionally impaired and misassembled in PD (Ferrer, 2011; Mcteague *et al.*, 2015). Thus, evidence from these studies strongly implicates mitochondrial dysfunction in the etiology of Parkinson's disease.

Interestingly, it is hypothesized that dopamine synthesis may be oxidatively stressful due to the involvement of oxygen molecules as a substrate for its synthesis, leading to the production of ROS (Miyazaki and Asanuma, 2008). In fact, DA neurons are metabolically demanding, requiring large amounts of ATP. Mitochondria are the producers of ATP, mostly generated via the ETC. In the synthesis of dopamine from tyrosine, the generation of ATP uses oxygen and can involve the production of superoxides and ROS that can be damaging to the mitochondria and toxic to the neuron (Durcan and Fon, 2015). The combined effect of factors on the production of superoxides and ROS potentially make DA neurons more sensitive to neuronal death due to mitochondrial dysfunction, explaining why mitochondrial toxins like MPTP and rotenone, selectively ablate dopaminergic neurons faster than other cell types.

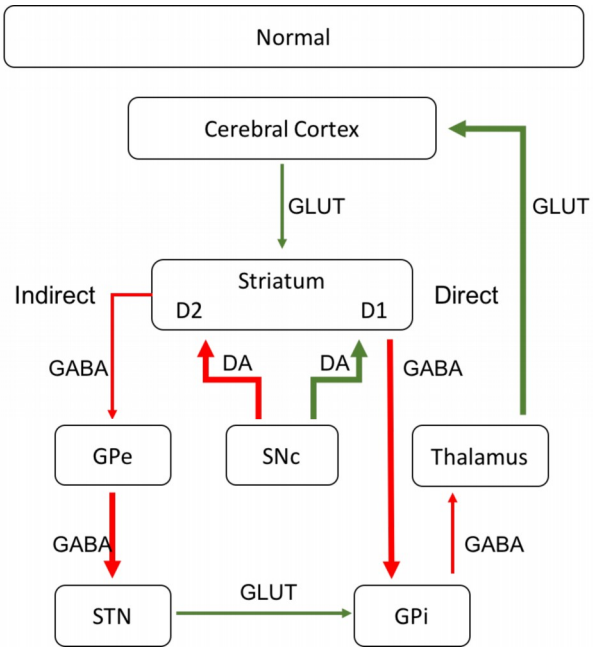
Normal
Cerebral Cortex
GLUT
GLUT
Striatum
D2
D1
Indirect
Direct
GABA
DA
DA
GABA
GPe
SNc
Thalamus
GABA
GABA
STN
GLUT
GPi

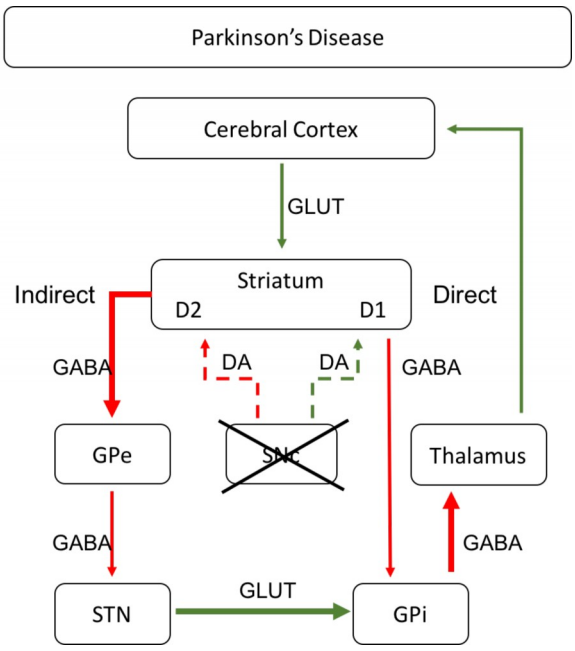
Parkinson's Disease
Cerebral Cortex
GLUT
Striatum
D2
D1
Indirect
Direct
GABA
DA
DA
GABA
GPe
SNc
Thalamus
GABA
GABA
STN
GLUT
GPi

Figure 1.5: Schematic representation of the direct and indirect pathways of the basal ganglia motor circuits in normal and Parkinson's Disease states. Red arrows indicate inhibitory projections, and green arrows indicate excitatory projections. The different thickness of the arrows in the either state indicate the proposed increase (thicker) or decrease (thinner) in activity and neurotransmitter release of specific connections. The dashed arrows in the Parkinson's Disease state indicate partial lesion or loss of function of that substantia nigra pars compacta (SNc). Globus pallidus external (GPe), globus pallidus internal (GPi), subthalamic nucleus (STN), Dopamine 1 receptors (D1), dopamine 2 receptors (D2.), dopamine (DA), gamma-amino-butyric acid (GABA), and glutamate (GLUT).

1.11 PARL in Parkinson's Disease

Several genes have been found with mutations in heritable PD including alpha-synuclein (SNCA), Parkin, DJ-1, PTEN-induced putative kinase 1 (PINK1) and leucine-rich repeat kinase 2 (LRRK2) (Cookson, 2005; Farrer, 2006; Klein and Schlossmacher, 2006; Whitworth *et al.*, 2008). Only SNCA and LRRK2 mutations cause autosomal dominant forms, whilst the other four are inherited in an autosomal recessive fashion. Recently, a mutation in the PARL gene was identified in two PD patients (Shi *et al.*, 2011).

Since PARL is involved in several pathways in response to mitochondrial dysfunction, including the PINK1/PARKIN mitophagic pathway and the intrinsic apoptotic pathway, it has been suggested that PARL may contribute to mitochondrial dysfunction in Parkinson's Disease. However, the detailed etiology of PD with respect to PARL's role in DA neuron degeneration is still not well understood. Notably, PARL deficient mice show mild neurodegeneration in the thalamus and striatum (Cipolat *et al.*, 2006). PARL deficiency only affects mice in early adulthood and since PARL is an anti-apoptotic protein that plays a role in OPA1 processing in mammals, PARL could be a drug target to control apoptosis in adults with neurodegenerative disorders, such as PD.

A study performed by Noble and colleagues investigated the role of PARL in zebrafish neurology. Interestingly, while most multicellular eukaryotes carry a single PARL gene in their genome, zebrafish have two paralogous genes recently discovered by Noble *et al.*, denoted *parla* and *parlb* (Noble *et al.*, 2012). The presence of two paralogs likely arose due to the whole genome duplication that occurred in the teleost lineage. The conservation of both paralogs in present day zebrafish suggests a functional importance and divergence in both *parla* and *parlb* genes.

Morpholino-mediated loss of *parla* and/or *parlb* function resulted in mild neurodegeneration, as evidenced by a lower density of dopaminergic neurons. Patterning of dopaminergic neurons was also perturbed in the ventral diencephalon. The morphants exhibited extensive cell death throughout the entire body as well as increased larval mortality. Rescue of the morphant phenotype was successful with the injection of human PARL mRNA, but not catalytically inactive PARL, suggesting functional conservation between the human and zebrafish proteins. More importantly, the zebrafish *pink1* mRNA as well as the human *PINK1* mRNA, but not kinase-dead nor Parkinson's disease-linked mutant *PINK1* mRNA, also rescued the morphant phenotype. This suggests that PARL genes may function upstream of *Pink1*, as part of a conserved pathway in vertebrates (Noble *et al.*, 2012).

1.12 PARL in Zebrafish

The paralog, *parla,* is located on chromosome 15, while *parlb* is located on chromosome 2. Both genes show sequence conservation at the amino acid level with other vertebrate PARL proteins, with Parla protein having a 67% a.a. identity to human PARL, and Parlb with a lower 55% identity. As mentioned previously, mammalian PARL undergoes cleavage events after localizing to the mitochondria. Zebrafish PARL proteins do not appear to conserve the S77-A78 β-site, but immunoblot analysis of FLAG-tagged Parlb gave two fragments, potentially corresponding to α- and β-cleaved forms of Parlb (Noble, 2014). The fragments were 34-35 kDa and the potential β-peptide 27-28 kDa. The theoretical size of the α-cleaved form is 39 kDa and human β-cleaved PARL is 25 kDa. FLAG-tagged Parla resulted in one fragment at 31-32 kDa, with α-cleaved Parla

theoretically 37 kDa. Therefore, the *parl* paralogs may not be processed the same way as in mammals, or produce the nucleus targeted processed β-peptide.

In terms of expression, only *parlb* mRNA was expressed maternally (at 2 hours post-fertilization (hpf)), although at very low levels. Both *parla* and *parlb* were detected throughout embryonic development starting at 4 hpf and continue to be expressed throughout adulthood. In adult zebrafish, Noble *et al.* (2012), found *parla* to be highly expressed in the brain and muscle tissues, with lower expression in the liver and heart. The *parlb* mRNA was detected in adult zebrafish brain and the liver, but transcripts were not detected in the heart nor muscles. Since PARL has been linked to mitochondrial stability and functioning, it is unsurprising to see the zebrafish paralogs more highly expressed in tissues with high metabolic needs. Noble *et al.* confirmed the expression of *parla* and *parlb* mRNA through whole-mount *in situ* hybridization from 3 dpf zebrafish larvae. It was concluded that the combined expression patterns of the two paralogs are similar to the expression pattern of PARL in adult and fetal human tissues (Noble *et al.*, 2012; Pellegrini *et al.*, 2001).

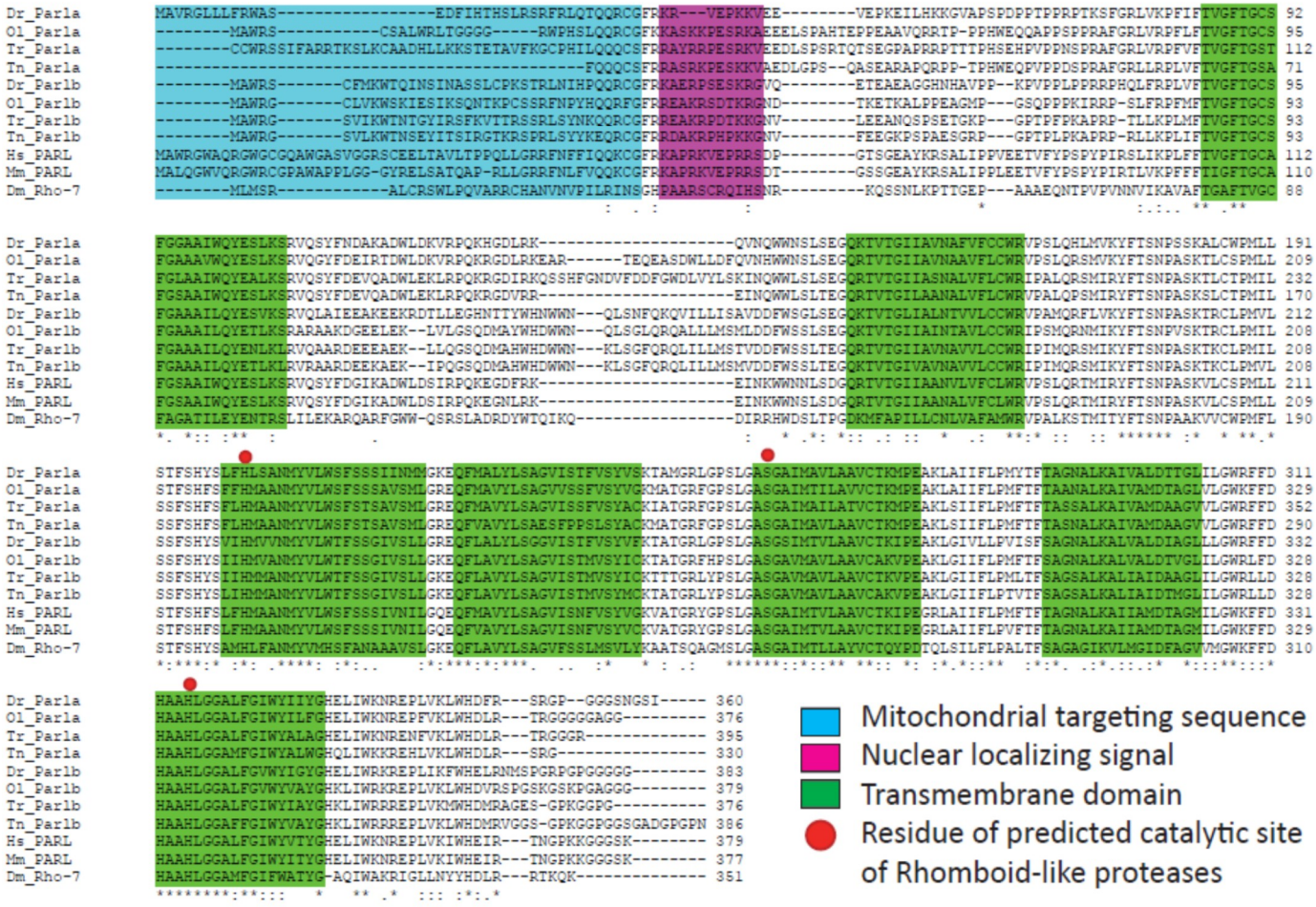
Dr_Parla
Ol_Parla
Tr_Parla
Tn_Parla
Dr_Parlb
Ol_Parlb
Tr_Parlb
Tn_Parlb
Hs_PARL
Mm_PARL
Dm_Rho-7
Mitochondrial targeting sequence
Nuclear localizing signal
Transmembrane domain
Residue of predicted catalytic site of Rhomboid-like proteases

Figure 1.6: Multiple sequence alignment of the protein domains of PARL homologues. PARL is a conserved rhomboid protease containing a mitochondrial targeting sequence (MTS) depicted in blue, a nuclear localization signal (NLS) in purple, and seven transmembrane domains in green. The amino acid residues predicted to be the catalytic diad of PARL proteases are indicated with a red circle directly above. Humans (Hs), mice (Mm) and *Drosophila* (Dm) have one PARL gene each, while the teleost fish presented, zebrafish (Dr), medaka (Ol), fugu (Tr), tetraodon (Tn), have two parl genes, denoted parla and parlb (Reprinted with permission from copyright owner: Noble, 2014).

1.13 Zebrafish as a Model for Diseases

The zebrafish, *Danio rerio*, represents an ideal alternative vertebrate model of human disease. Its popularity has arisen from the high conservation of genetic information and physiological processes between zebrafish and humans, their short generation time (~3 months) and easy and inexpensive maintenance. Additionally, they possess high fecundity, and the optical clarity of their embryos helps facilitate direct observation and imaging. Gene silencing techniques, including morpholino knockdown and transcription activator-like-effector endonucleases (TALENs), have been exploited to demonstrate how loss of function can induce human disease-like states in zebrafish. Furthermore, several behavioral assays have been developed to examine changes in motor activity and sensory responses, particularly at the larval stages. Many studies have been performed using zebrafish models leading to an accumulation of easily applicable genetic and genomic methods, and whole-genome resources and annotations (Steele *et al.*, 2014).

Many characteristics of the structure and function of the zebrafish CNS have been conserved compared with humans at the molecular, cellular, and tissue level. Zebrafish have a well-developed network of cerebral dopaminergic (DA) neurons in areas such as the telencephalon, pretectal area, and ventral diencephalon. It has been suggested that the groups of DA neurons in the posterior tuberculum of the ventral diencephalon (vDC) ascend to the basal telencephalon in zebrafish and that these are equivalent to the dopaminergic system found in the substantia nigra of the human midbrain with projections to the striatum (Rink and Wullimann, 2002). While the progression of the neural phenotype of PD symptoms cannot be tracked *in vivo* in mammalian models, it can be studied in zebrafish, with familial PD being one of the most

commonly modeled neurodegenerative MDs in zebrafish (Steele *et al.*, 2014). Therefore, zebrafish can be a crucial model for advancing our understanding of the pathogenesis of human diseases beyond the current state of knowledge, and provide a key tool in the development of novel therapeutic approaches to treat these conditions.

1.14 CRISPR-Cas9 Genome Editing

The clustered regularly interspaced palindromic repeat (CRISPR)-Cas9 nuclease system is a new approach to genetic engineering, allowing molecular biologists the ability to induce site-specific modifications of endogenous genomic loci (Li et al., 2015; Zhang et al., 2014). Distinct from the protein-guided DNA cleavage of the earlier forms of genomic editing (ZFNs and TALENs), the CRISPR/Cas9 system depends on small RNA for sequence specific cleavage of DNA, making it easily applicable. CRISPR-Cas9 has already been demonstrated to successfully knockout a variety of genes in zebrafish and other species (Cho *et al.*, 2013; Horvath and Barrangou, 2013; Jinek *et al.*, 2012; Mali *et al.*, 2013; Zhang *et al.*, 2014).

The CRISPR-Cas9 genomic editing originates from the type II CRISPR-Cas system found in bacteria and archaea as a form of adaptive immunity against viruses and plasmids. A single stranded guide RNA (sgRNA) containing a short 20 nt guide sequence, directs the CRISPR-associated protein (Cas)9 to a complementary 20 bp DNA target via Waston-Crick base pairing. The remaining sequence of the sgRNA forms secondary structures that facilitate the loading of Cas9, acting as a scaffold. Constraints on the range of targetable sequences are due to sequence requirements imposed by the T7 promoter used to make the sgRNAs (GG at the 5'end of the

transcript) and by the requirement for a protospacer adjacent motif (PAM) sequence (NGG) in the genomic DNA just 3' to the target site (Qi *et al.*, 2013).

Once bound to the sgRNA, Cas9 generates a double stranded break (DSB) in the genomic DNA at the target sequence (Fig. 1.6), using its HNH nuclease domain and a RuvC-like nuclease domain (Ran *et al.*, 2013). Typically, sequence specific cleavage occurs 3 bp upstream of the 3' end of the target sequence. Subsequent cellular DNA repair processes, induced by the targeted cleavage, are activated.

Two major processes can repair the DSB including homology directed repair (HDR or HR) or nonhomologous end-joining (NHEJ) (Fig. 1.6). HDR is the more accurate mechanism for DSB repair, requiring higher sequence homology between the lesioned and intact donor strands of DNA. If one chromosome maintains the original DNA sequence at the DSB, the repair is error-free. Exogenous donor plasmids can be applied to allow for homologous recombination to introduce very specific mutations, or add or delete entire portions of the endogenous DNA sequence (Gaj *et al.*, 2013). HDR efficiency varies widely between genomic loci, repair template, cell types and states, generally initiating in dividing cells (Ran *et al.*, 2013). NHEJ-mediated DNA repair is active throughout the cell cycle and operates in the absence of a repair template. Unlike the high fidelity HDR pathway, NHEJ is error-prone and tends to generate insertions, deletions or substitutions. These mutations can allow for the disruption or even abolish the function of target genes if the lesion occurs at an important reside for function or causes a premature termination codon (PTC). Therefore, NHEJ-mediated repair after CRISPR-Cas9 cleavage is useful for generating null or knockout alleles in a target gene of interest (Hsu *et al.*, 2014).

Several studies have successfully used the CRISPR/Cas9 system on zebrafish including a study performed by (Hwang *et al.*, 2013). Their findings suggest that frequencies of mutagenesis do not appear to depend upon which DNA strand (sense or antisense) was targeted by the sgRNA, and in comparison to ZFNs and TALENs, germline transmission of sgRNA: Cas9-induced mutations is expected to be as efficient, the frequency of deformed or dead embryos similar but with a higher risk of off-target mutations. In addition, through using Cas9 and several gRNA with different target sites, CRISPR/Cas9 can simultaneously induce genomic modifications at multiple independent sites.

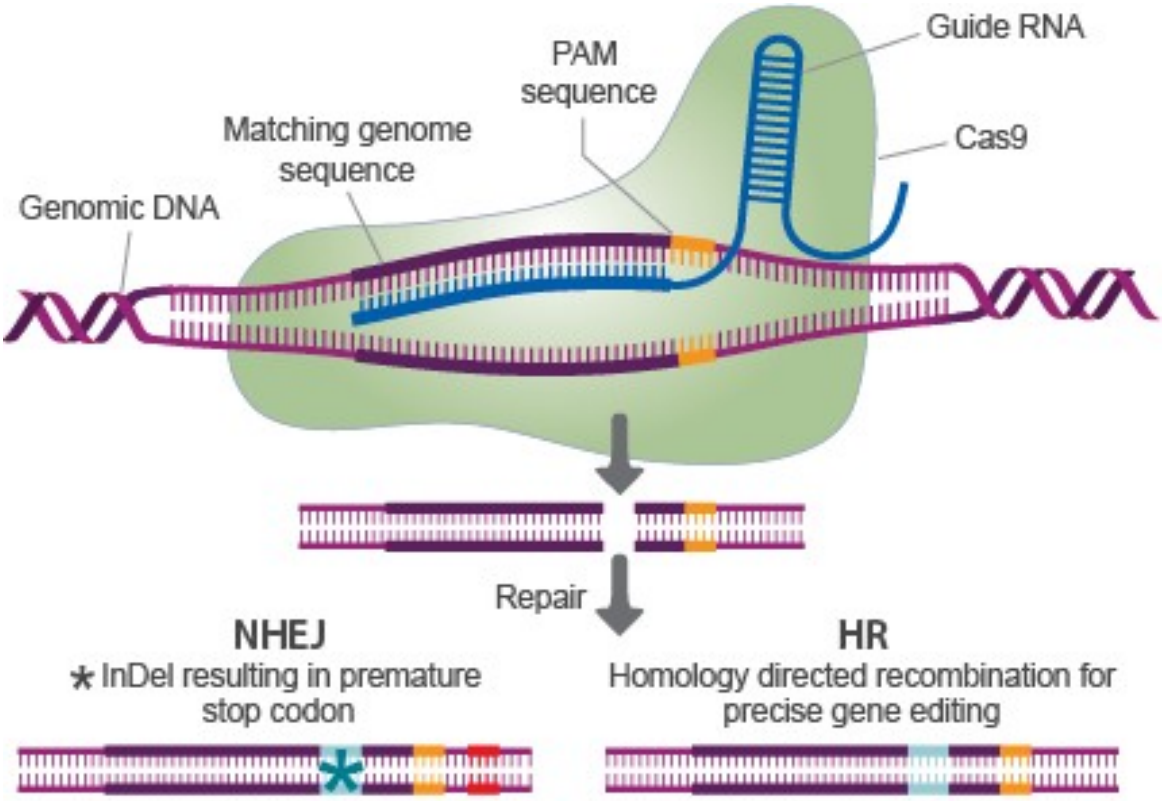
Guide RNA
PAM
sequence
Cas9
Matching genome
sequence
Genomic DNA
Repair
NHEJ
* InDel resulting in premature
stop codon
HR
Homology directed recombination for
precise gene editing

Figure 1.7: Schematic representation of CRISPR/Cas9-mediated DNA cleavage. A single-stranded guide RNA (sgRNA) binds to the complementary target genomic sequence and recruits the Cas9 protein. Cas9 binds to the sgRNA-DNA complex and cleaves the genomic DNA with the HNH nuclease domain and RuvC-like nuclease domain of Cas9, generating a DSB at the target site. The specificity of CRISPR/Cas9-mediated DNA cleavage requires a sgRNA matching the target sequence and a 3 nt NGG PAM located downstream of the sgRNA binding site. DSB is repaired by the cell in two ways, homology directed repair (HR) or non-homologous end joining (NHEJ). NHEJ can lead to InDel formation resulting in premature translation stop codons. (Reprinted by permission from Macmillan Publishers Ltd: *Hum Mol Gen*. Zhang *et al.* © 2014)

1.15 Statement of Inquiry

Previous work performed by Dr. Noble and colleagues showed that a transient loss of Parla and/or Parlb function through morpholino injections resulted in defects in the dopaminergic neurons, including mild neurodegeneration and mispatterning in the ventral diencephalon (Noble et al, 2012). Double morphants exhibited extensive cell death throughout the entire body, as well as increased larval mortality (Noble *et al.*, 2012). As effects of morpholinos are transient, and since PARL is a Parkinson's Disease-linked gene, a generally late onset disorder, we were interested in studying the effects of the heritable loss of Parl function. Therefore, the overall goal of this thesis is to create null mutant lines for *parla* and *parlb* via CRISPR-Cas9 mutagenesis to perform a functional analysis. We hypothesized that if the zebrafish paralogs, *parla* and *parlb,* function in the same processes in mitophagy and apoptosis as their mammalian homolog, PARL, then perturbing the function of these genes may lead to developmental deformities and defects. Our objectives are as follows:

1. To produce the mutant zebrafish lines with a knockout for *parla,* and *parlb* via CRISPR-Cas9 mediated mutagenesis.
2. To validate the null mutant by Western blot analysis, mass spectrometry and qRT-PCR.
3. To quantitatively assay the effect of the null mutations on RNA levels of functionally related proteins using qRT-PCR in order to assess for possible compensatory alterations in expression.
4. To determine the effect of the *parla* and *parlb* perturbations on dopaminergic neuron patterning.

2. Materials and Methods

2.1 Fish care and Husbandry

All experiments were performed according to the guidelines of the Canadian Council on Animal Care and were approved by the University of Ottawa animal care committee. Zebrafish and embryos were maintained at 28.5°C according to methods described in (Westerfield, 2007). Embryos were raised from birth up to 5 days post-fertilization (dpf) in embryo media (13mM NaCl, 0.5mM KCl, 0.02mM, Na2HPO4, 0.04mM KH2PO4, 1.3mM CaCl2, 1.0mM MgSO4, and 4.2mM NaHCO3). At 24 hours post-fertilization (hpf), embryos were bleached in a 6% sodium hypochlorite solution and raised in static tanks on a diet of rotifers and GEMMA Micro (Skretting USA). At 5 dpf, embryos are transferred to circulating system water. Wild-type adult zebrafish were kept under a controlled 14-hour light/ 10-hour dark cycle and fed a diet of Artemia and fish pellets. Embryos were killed with an overdose of tricainemesylate (ethyl 3-aminobenzoate methanesulfonate; Sigma-Aldrich,Oakville, ON, Canada). In order to prevent pigment formation in developing embryos, phenylthiourea (PTU) (Sigma-Aldrich) was added to the embryo media at 24 hpf to a final concentration of 0.2 mM.

2.2 sgRNA Design

The 20 base pair (bp) target sequences of the candidate sgRNAs were designed using the ZiFiT Targeter software (http://zifit.partners.org/ZiFiT/) (Sander *et al.*, 2010 and Sander *et al.*, 2007) and compared with the results from ChopChop (https://chopchop.rc.fas.harvard.edu) and the CRISPR online tool (http://crispr.mit.edu). Potential sgRNAs were selected based on the

following: having two guanine nucleotides at the 5' end to facilitate transcription from a T7 promoter, an NGG protospacer adjacent motif (PAM) adjacent to the 3' end, and few potential off-target sites. Potential off-target sites identified by the online tools were cross-checked against the zebrafish genome and ranked on severity.

2.3 Production of sgRNAs

Two methods for gRNA production were utilized. For *parlb* and early *parla* gRNA construction (parla target site #1 and 2), complementary oligonucleotides for each target site were designed and annealed at equal molar concentration in Annealing Buffer (10mM Tris, pH8.0, 50 mM NaCl, 1mM EDTA) and heated to 95 °C before being slowly cooled to room temperature. The annealed oligonucleotides have overhangs that are compatible with directional ligation into the *Bsa*I-digested pDR274 vector (Addgene, cat#42250), which harbors a T7 promoter positioned upstream of a partial guide RNA sequence. *E.coli* were transformed with the pDR274+insert construct and screened for the gRNA expression vector.

Generation of templates for the *parla* target sites #3-6, the protocol in the supplementary data from Gagnon *et al.* (2014) was followed. Gene-specific oligonucleotides containing the T7 (5'-TAATACGACTCACTATA-3') promoter sequence, the 20 base target site without the PAM, and a complementary region (5' GTTTTAGAGCTAGAAATAGCAAG 3') were annealed to a constant oligonucleotide (5' AAAAGCACCGACTCGGTGCCACTTTTTCAAGTTGATAACGGACTAGCCTTATTTTA ACTTGC TATTTCTAGCTCTAAAAC 3') encoding the reverse-complement of the tracrRNA tail. The annealed oligonucleotides were filled in using T4 DNA ligase to make a double stranded template. All gRNAs were transcribed using the MAXIscript T7 kit (Life Technologies, cat#AM1312). The

resulting RNA was purified using 5M ammonium acetate and ethanol precipitation. Quality of the RNA was determined by agarose gel electrophoresis and spectrophotometry.

2.4 Production of Cas9 mRNA

Capped Cas9 mRNA was transcribed using PmeI-digested Cas9 expression vector, MLM3613(Addgene, cat#42251), and the mMESSAGE mMACHINE T7 Transcription kit (Life Technologies, cat#AM1344). Following completion of transcription, the poly(A) tailing reaction was performed according to the manufacturer's instructions for the Cas9-encoding mRNA using the Poly(A) Tailing Kit (Thermo Scientific, cat#AM1350). The Cas9-encoding mRNA was purified by phenol chloroform extraction and ethanol precipitated. The MLM3613 vector containing the Cas9 mRNA was donated by the Akimenko lab (University of Ottawa). The quantity and quality of the synthesized gRNAs and Cas9 mRNA were examined by gel electrophoresis and spectrophotometry.

2.5 Microinjections

Embryos were collected at the one-cell-stage and injected with a solution containing 12.5 ηg/µl of gRNA and 300 ηg/µl of Cas9 mRNA. When more than one sgRNAs were coinjected, 12.5 ηg/µL of each sgRNA was used. A Narishige IM300 microinjector was used for microinjection. Uninjected siblings were used as controls along with embryos injected with phenol red only and Cas9 only. On the following day, injected embryos were inspected under a stereomicroscope for developmental abnormalities. Genomic DNA was collected from either single embryos or pools of embryos (as indicated) and used for PCR, indel identification and DNA sequencing as described.

Morpholino (MO) injections were performed as controls using the following splice-blocking MOs: *parla* e1i1 MO 5'- GTATGTGTGTTACCTGCTCCTCAGA-3' targeting intron 1 inclusion; *parlb* i3e4 MO 5'-GTGACCCTGCAGAAAATCAAGTGTA-3' targeting exon 4 excision (Noble *et al.*, 2012). All morpholinos were designed by Dr. Noble and obtained from Gene Tools. MOs were reconstituted in nuclease-free water and diluted for injection to a concentration of 4 mM each, in a solution containing 0.1% Phenol Red and 1X Danieau Buffer (58 mM NaCl, 0.7 mM KCl, 0.4 mM $MgSO_4$, 0.6 mM $Ca(NO_3)$, 5 mM HEPES, pH 7.6).

2.6 Genomic DNA Extraction

Tissues of either whole embryos, larvae, gametes or caudal fin clips were placed into microcentrifuge tubes and submersed in 50 mM NaOH. The volume of NaOH used for sperm was 15 µL, 20 µL for tails and single embryos/larvae, and 100–500 µL for eggs or multiple embryos/larvae. The samples were heated to 95°C for 10 min and then cooled to 4°C. To neutralize the solution, 1 M Tris-HCl, pH 8.0 was added. The sample was centrifuged to pellet the debris, and the supernatant used directly in a PCR.

2.7 Sequencing

Samples to be sent for sequencing were PCR amplified using a thermocycler with the following protocol: 95°C for 5 min, followed by 35 cycles of 95°C for 30 sec, 60°C for 20 sec and 72°C for 30 sec, followed by a final extension at 72°C for 1 min. Depending on the purity of the final product, samples were either cleaned using the QIAGEN Gel Extraction kit, or the QIAGEN

PCR Purification kit, according to manufacturer's instructions. Sequencing was performed at the StemCore Sequencing Facility (Ottawa, ON).

2.8 T7 Endonuclease I Assay

The endogenous loci were PCR amplified and denatured and reannealed in NEBuffer 2 (New England Biolabs, cat#B7002) using a thermocycler with the following protocol: 95°C, 5 min; 95–85°C at −2°C/s; 85–25°C at −0.1°C/s; hold at 4°C. The resulting hybridized PCR products were split into two halves, one half treated with the T7 endonuclease enzyme (New England Biolabs, cat#M0302) and the other without enzyme as a negative control. Samples were incubated at 37 °C for 15 min and immediately placed on ice to terminate the reaction. The products were run on a 1% agarose gel by electrophoresis and analyzed for the presence of heteroduplex bands. A list of the primers used in this study is provided in Table 2.1.

2.9 PAGE Assay

Genomic DNA was extracted for genotyping from zebrafish caudal fins, gametes or embryos and PCR amplified using primer pairs as listed in Table 2.1. After denaturing for 5 min and left for 5 min at 25°C to re-anneal, PCR products were subjected to 12% polyacrylamide gel electrophoresis (PAGE) at 150 V for 60 min. PAGE gels were stained for 30 minutes in solution containing Tris/borate/EDTA (TBE) and 0.15% RedSafe (Fischer Scientific). Gels were washed 2x15 min in TBE buffer and visualized. Purified PCR samples with positive heteroduplex bands were subjected to sequencing

Table 2.1: List of the forward and reverse PCR primer pairs against *parla* and *parlb* paralogs as used for screening and sequencing. Primer sequences were designed using Primer3 4.0 and NCBI primer BLAST. Primers were diluted in ddH2O to a 100 µM stock concentration and kept at -4ºC until selected for use.

Target Gene	Primer Name	Primer Sequence (5'-3')	Experiment
parla	Parla PAGE fw	GAGGGTCGCAGTTATGATGG	T7E1, PAGE,
	Parla PAGE rv	TGAGAGAGAAGTGTGTATGTGTGTT	Sequencing
	Parla e.d[a]. fw1	TGAATTGGATCTGCTGCGTA	Screening
	Parla e.d. fw4	GGATAAGTTGGTGGTTCATTCC	(agarose gel),
	Parla e.d. rv7	ACGCCCAGACAGACAAACAT	Sequencing
parlb	Parlb fw	AAAACACTGTCCCGAGTTGC	T7E1, PAGE,
	Parlb rv	ACCCTTGGTAGCGTTTACCC	Sequencing
	Parlb cDNA fw	AAAACACTGTCCCGAGTTGC	PAGE (cDNA)
	Parlb cDNA rv	AGGCAGGGTTCGATGTGAAG	

[a] = e.d. represents exon deletion

2.10 RNA Extraction and cDNA Synthesis

Zebrafish embryos were collected at 5 dpf and pooled into groups of 50 larvae. The pooled samples were euthanized with an overdose of tricaine and then flash frozen in liquid nitrogen. RNA was extracted using the RNeasy Plus Mini Kit (Qiagen, Mississauga, ON, Canada, cat# 74134) according to manufacturer protocol. RNA concentrations were then quantified using a NanoDrop 2000 spectrophotometer (Thermo Scientific).

A total of 200 ηg of RNA from each sample was reverse transcribed into cDNA using the Iscript Reverse Transcriptase kit (BioRad, cat#1708890), according to manufacturer's instructions. To ensure that were generating unique PCR products free of primer dimers or other contamination, a PCT-100 Peltier Thermal Cycler (Bio-Rad) was used to amplify these specific cDNAs under the following conditions: 95ºC for 10 minutes, followed by 37 cycles of 95ºC for 20 sec, 55ºC for 20 sec, then 72ºC for 20 sec. All primer pairs only produced amplicons of the expected size.

2.11 Quantitative RT-PCR

Following optimization for melting temperatures and primer efficiencies, a Bio-Rad CFX96™ Real-Time PCR Detection System was then used to assay transcripts of the genes of interest by qPCR using SsoFast EvaGreen Supermix (Bio-Rad, cat#172-5200) under the following conditions: 95ºC for 30s, followed by 40 cycles of 95ºC for 5s and 59ºC for 5s, then a melt curve progressing from 65ºC to 95ºC, at 2 sec per 0.5ºC increase. A total of 9 reference genes were tested based on their Genorm M stability value. β-actin, RPL13a and ef1α were selected and used as reference genes. The data are presented as the fold change in mRNA abundance normalized

against the geometric mean of the reference genes. The data were analyzed using CFXManager (Bio-Rad), One-way Anova and compiled using GraphPad PRISM.

Oligonucleotide primers were designed using the Primer3 Input 4.0 software (http://bioinfo.ut.ee/primer3-0.4.0/) and cross-analyzed for off targets using NCBI primer BLAST (https://www.ncbi.nlm.nih.gov/tools/primer-blast/). All primers for RT-PCR were designed to be intron spanning, so that resulting PCR products derived from the mRNA are easily distinguishable from the larger, intron-containing products derived from contaminating genomic DNA, if the latter products are even amplified due to their potential size. A list of primers used for the qRT-PCR amplification can be found in Table 2.2

Table 2.2: Forward and reverse qRT-PCR primer pairs for *parla, parlb, Opa1, PMPcβ, ClpP, afg3l2 and dat* are listed. Primer sequences for β-*actin*, *ef1α*, *RPL13a*, and *YWHAZ* were previously described in Tang *et al.* (2007). Primers were diluted in ddH2O to a 10 µM stock concentration and kept at -20ºC until selected for use.

Gene of Interest	Forward primer	Reverse Primer
parla	GTGTTTTGTTGTTGGCGGGT	ATGTAGACAGCAGCATCGG
parlb	ATCACGCAGCACATCTTGGT	TATTAGTGGCTCGCGCTTCC
Opa1	CCTGCTTGTGATGCCCTTGT	GGTGGTCTCTGTGGGTTGTT
PMPcβ	AAACGAAGCTCACGACCCTT	GAGACCTCTTTCTGGTGCCC
ClpP	GGGGCCAAGCGACAGATATT	GAGACCTCTTTCTGGTGCCC
afg3l2	ACCTGGCAAAGCCGTATTCA	GCCCATAGCTAGCCAGAAGG
β-actin	CGAGCTGTCTTCCCATCCA	TCACCAACGTAGCTGTCTTTCTG
ef1a	CTGGAGGCCAGCTCAAACAT	ATCAAGAAGAGTAGTACCGCTAGCATTAC
RPL13a	TCTGGAGGACTGTAAGAGGTATGC	AGACGCACAATCTTGAGAGCAG
YWHAZ	TCTGCAATGATGTGTTGGAGC	TCAATGGTTGCTTTCTTGTCGTC
dat	AGACATCTGGGAAGGTGGTG	ACCTGAGCATCATACAGGCG

2.12 Mitochondrial Fractionation

For whole embryo homogenate preparation, zebrafish were raised to 5 dpf, euthanized with an overdose of tricaine and flash frozen in liquid nitrogen. Samples were homogenized in lysis buffer (250 mM sucrose, 1mM EDTA, 10 mM HEPES) containing HALT protease inhibitor cocktail (Thermo Scientific, cat#78430) using a dounce homogenizer. Differential fractionation was used to separate the mitochondria from the cytosol. Homogenized lysates were centrifuged at 1500xg for 20 minutes, and supernatant harvested and the pellet of debris discarded. The supernatant was centrifuged twice at 10600xg for 10 minutes to pellet the mitochondria. The supernatant containing the cytosolic fraction was saved and stored at -20 °C. The mitochondria pellet was washed in cold lysis buffer and then resuspended in a 7M Urea solution (7M Urea, 4% CHAPS, 30 mM Tris pH 9.5). Mitochondria were lysed by vortexing for 1 minute. Protein concentrations were determined by bicinchoninic acid (BCA) assays (Bio-Rad) on a NanoDrop 2000 spectrophotometer (Thermo Scientific).

2.13 SDS-PAGE and Immunoblotting

Equivalent amounts of protein from samples were heated at 70°C for 5 minutes in Laemmli buffer (4% SDS, 20% glycerol, 10% 2-mercaptoethanol, 0.004% bromphenol blue and 125 mM Tris-HCl, pH 6.8, SigmaAldrich), placed immediately after in ice and separated on a 4-20% sodium dodecyl sulfate polyacrylamide gel electrophoresis (SDS-PAGE) running for 100 minutes at 110 V. Proteins were detected by staining gels with Coomassie Blue unless required for immunoblotting. For immunoblotting, proteins were transferred to a methanol- polyvinylene

difluoride (PVDF) membrane at a constant 100 V for 75 min and stained with Ponceau-S to confirm protein transfer.

Membranes were blocked in blocking buffer (5% skim milk in TBS-T, pH 7.5) for 1.5 hours. Primary antibodies were diluted in blocking buffer and incubated with membranes overnight at 4C [either (1:50) anti-parla (Open Biosystems, 2 rabbit 70-day protocol), (1:50) anti-parlb (Open Biosystems, 2 rabbit 70-day protocol), (1:2000) anti-VDAC1 (Abcam, AB15895), or (1:2000) anti-GAPDH (Abcam, AB8245). Membranes were then washed for 5 minutes in TBS-T four times. Secondary HRP-conjugated antibodies were diluted 1:5000 in blocking buffer and incubated with membranes overnight at 4C, then washed for 5 minutes in TBS-T four times. Membranes were then visualized with the Pierce enhanced Chemiluminescent (ECL) Western Blotting Substrate (Thermo Scientific, cat#32106) and exposed on VersaDoc Imaging Systems (Bio-Rad).

2.14 Mass Spectrometry

Mitochondrial fractions were analyzed in solution and in-gel. For in-solution samples, the filter-added sample preparation (FASP) method was utilized. For the in-gel samples, mitochondrial lysates were resolved on a SDS-PAGE gel, coomassie blue stained and bands excised. Excised bands underwent in-gel digestion with trypsin following Nature Protocoles No.1 Vol 6, 2006. All samples underwent Strong Cationic Exchange (SCX) Fractionation using 20 μL filtered tip columns for desalting. were analyzed by LC-MS/MS using a LTQ Orbitrap XL spectrometer (Thermo-Electron).

2.15 Whole Mount *In Situ* Hybridization

In situ hybridization experiments were performed according to Thisse and Thisse (Thisse and Thisse, 2008). At 24 hpf, 0.2 µM PTU was added to the embryo media to prevent pigment formation. Briefly, larvae were fixed at 3 dpf in 4% paraformaldehyde (PFA) in phosphate-buffered saline (PBS), dehydrated in methanol, and stored in 100% methanol at -20ºC. A *tyrosine hydroxylase* (*th1*) digoxigenin labelled antisense riboprobe was synthesized according to (Xi *et al.*, 2010). DA neuron patterning defects were scored according to criteria in Table 2.3 and in a blinded fashion.

2.16 Statistical Analysis:

Statistical analysis was performed using Excel and Graphpad PRISM software. qRT-PCR results were analyzed by One-way ANOVA with Tukey post-hoc test to correct for multiple comparisons. For all graphs, bars represent ± SEM. For the whole mount *in situ* experiments, the percentage of larvae in each category were analyzed using Two-way Anova, comparing row means, also using the Tukey post-hoc test. Morpholino experimental groups were compared using Chi-square analysis using excel. The number of biological replicates is indicated in corresponding sections of text or figure legends.

Table 2.3: Classification of dopaminergic neuron patterning in 3 dpf zebrafish ventral diencephalon as identified by whole mount *in situ* hybridization analysis against *tyrosine hydroxylase 1 (TH1)* mRNA.

Classification	Phenotype
Normal	Neuron density is normal and 'U'-shaped patterning is comparable to wild type patterning
Low-Density	Reduced neuron density with fewer or missing neuron clusters; neurons still aligned in the typical 'U'-shape
Mis-patterned	Normal or slightly reduced neuron density with misaligned neuron clusters with large spaces in between
Severely mis-patterned	Normal or reduced neuron density with neuron clusters severely misaligned; morphology of entire embryos potentially affected

3. Results

3.1 Design of sgRNA for *parla* and *parlb*

In order to assess the long-term effect of parla and parlb functional deficiency in a heritable model, a CRISPR-Cas9 based approach to mutagenesis was implemented to produce functional knock-outs of both proteins in zebrafish. All candidate target sequence, as initially designed by the ZiFiT targeter software, were compared to the Optimized CRISPR Design Tool and ChopChop algorithms to assess target sequence scores of specificity and efficiency. ZiFiT targeter is a simple tool that identifies possible target sites, off-targets and designs complementary oligonucleotides for subsequent cloning, based on the input FASTA sequences. The Optimized CRISPR Design Tool will only analyze a short sequence of 250 bp at a time, but gives a schematic representation of the target sites, a score for specificity, and a full list of all possible off-targets and their location in the genome (chromosome, position and whether it is a coding or non-coding region). ChopChop allows for easy visualization of candidate Cas9 target sites within your target gene, and predicts specificity using an algorithm that searches the genome for off-target sites. However, ChopChop is not ideal for searching specific regions of genomic DNA for target sites, for instance, a specific exon containing a catalytic domain or the 5' end of your target gene.

Target sequences with consistently high scores for specificity and efficiency were further assessed for potential off-targets as presented by all three software. Target sequences with the least number of off-targets only in non-coding regions were selected for use and consisted of the typical 5'GG-N18-NGG sgRNA architecture (Doudna and Charpentier, 2014). The 5' GG is required

for efficient transcription from a T7 promoter. Although a 5' GG could be artificially added to the sgRNA, this mismatch to the genomic complement cause a significant negative impact on the mutagenic activity of the sgRNA in zebrafish (Varshney *et al.*, 2015). None of the target sequences chosen had off-targets in coding regions or the same chromosome as *parla* nor *parlb,* if any off-targets were identified by the three softwares.

Out of the potential target sequences, a single sgRNA was designed and produced for *parlb,* 5'-GGAGGAGCTGCTTCATGAAA-3', while two sgRNA were required for *parla,* 5'-GGGGTTTAGTGTTGTTCAGG- 3' and 5'- GGGGTTTATTGTTGTTCAGG-3'. Initial sequencing of the population of zebrafish used in this study indicated the presence of a SNP in the middle of the highest-scoring target *parla* sequence designed by ZiFiT targeter (GGGGTTTAG^{T}TGTTGTTCAGG) and thus two sgRNA corresponding to both versions were produced and co-injected. These first set of sgRNAs were produced by cloning the complementary oligonucleotides of the target regions into a DR274 sgRNA expression vector, and transcribed. The genomic target sequences and complementary oligonucleotides can be found in Table 3.1.

Table 3.1 The zebrafish genomic target sites for *parla* (target 1 and 2) and *parlb* (target 1) for CRISPR-Cas9 mutagenesis as designed using ZiFiT Targeter Software. The 20 nucleotide target sequences and their complementary oligonucleotides for sgRNA production are depicted. Complementary oligonucleotides were annealed and cloned into a pDR274 vector for transcription.

Gene	Target site	Target Sequence (5'-3')	Complementary Oligos (5' to 3')
parla	1	GGGGTTTAGTGTTGTTCAGG	TAGGGGTTTAGTGTTGTTCAGG; AAACCCTGAACAACACTAAACC
	2	GGGGTTTATTGTTGTTCAGG	TAGGGGTTTATTGTTGTTCAGG; AAACCCTGAACAACAATAAACC
parlb	1	GGAGGAGCTGCTTCATGAAA	TAGGAGGAGCTGCTTCATGAAA; AAACTTTCATGAAGCAGCTCCT

3.2 Microinjection and Screening

Embryos were collected at the one-cell-stage and injected with a solution containing the sgRNA and Cas9 mRNA or protein. When more than one sgRNAs were co-injected, 12.5 ηg/μL of each sgRNA were used. There was no difference in the mutation efficiencies observed between injections using Cas9 mRNA or protein (data not shown). Non-injected siblings were used as controls along with embryos injected with phenol red only, and embryos injected with Cas9 mRNA or protein only.

Screening for mutants in primary injected (F_0) zebrafish was performed by T7 endonuclease 1 (T7E1) and PAGE assays (Figure 3.1). The targeted regions of *parla* and *parlb* were amplified from the extracted DNA by PCR and then denatured and reannealed to form hybridized DNA. For initial screening of primary injected embryos and to determine mutation efficiency of the *parlb* sgRNA, the hybridized PCR amplicons were digested with the T7E1 enzyme. When these digested products are run on an agarose gel, it allows for the visualization of potential mutants based on banding pattern. A mutant sample (not homozygous for the mutation), will show a band representing the normal PCR amplicon, as well as two additional bands, that approximately match the size of the original PCR product cleaved at the target site, which can be theoretically determined. The presence of these bands suggests that the target DNA underwent induced mutagenesis (Figure 3.2B).

For determining mutation efficiency, 10-15 1 dpf microinjected embryos were euthanized and tested by T7E1 assay for mutations. The percentage of embryos with a positive T7E1 result was calculated as 74% for *parlb*. Due to the presence of a SNP in the *parla* sequence and the

sensitivity of the T7E1 enzyme, a different screening method needed to be utilized, owing to the possibility of false positive results using the T7E1 method.

Screening for mutation *parlb* F1-F4 offspring (Figure 3.2B) and *parla* F_0 fish (Figure 3.3A) was performed by subjecting hybridized PCR products to 12% polyacrylamide gel electrophoresis (PAGE). Rather than utilizing an enzyme to cleave the heteroduplexes, the open angle between matched and mismatched DNA causes mutant heteroduplex DNA to migrate at a significantly slower pace than homoduplex DNA on a native PAGE gel, thus allowing for mutants to be identified (Zhu *et al.*, 2014) . To screen for homozygotes, PCR amplicons of zebrafish with unknown genotype were hybridized and run by themselves and as a "mixture" of unknown sample and wild type sample. Heterozygotes have the additional heteroduplex bands in the unknown sample only, while homozygotes only have heteroduplex formation in the "mixture". Wild types only have homoduplexes. Additionally, as different mutations have different open angles and nucleotides in the heteroduplex, each mutation has a unique banding pattern identifiable on a PAGE gel. Therefore, zebrafish with the same mutation or different mutations are easily discernable without having to sequence them, unlike with the T7E1 assay. Due to this additional specificity, PAGE was used for all further screening.

Since the CRISPR-Cas9 method initially creates mosaic mutations in the primary injected embryos, the precise location of the site and size of cleavage could not be sequenced from the F_0 treated fish. Once sexual maturity is reached (approximately 3 months old), these primary injected fish were fin clipped and those positive for somatic mutation were bred with wild type (WT) fish. Outcrossing was performed twice with the purpose of eliminating any potential off-

A

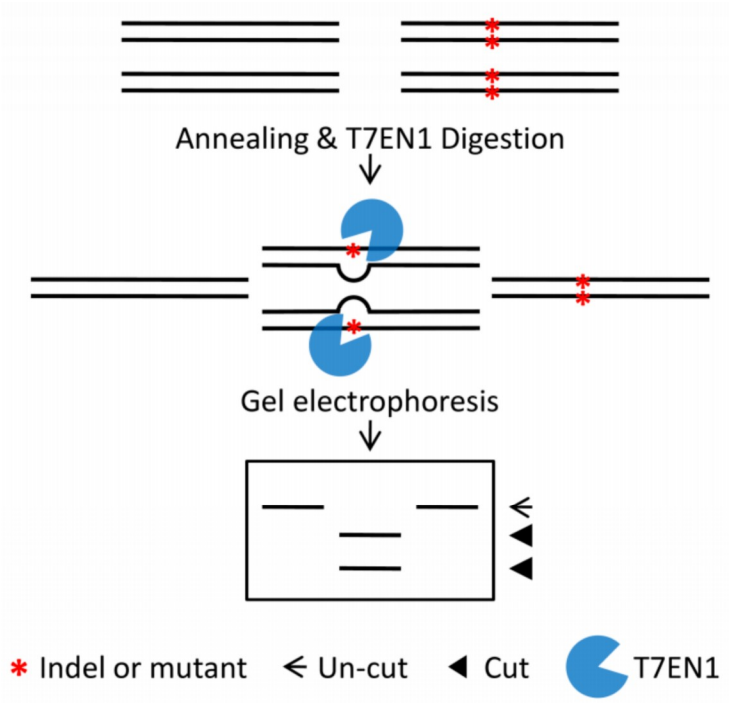
Annealing & T7EN1 Digestion
Gel electrophoresis
Indel or mutant
Un-cut
Cut
T7EN1

B

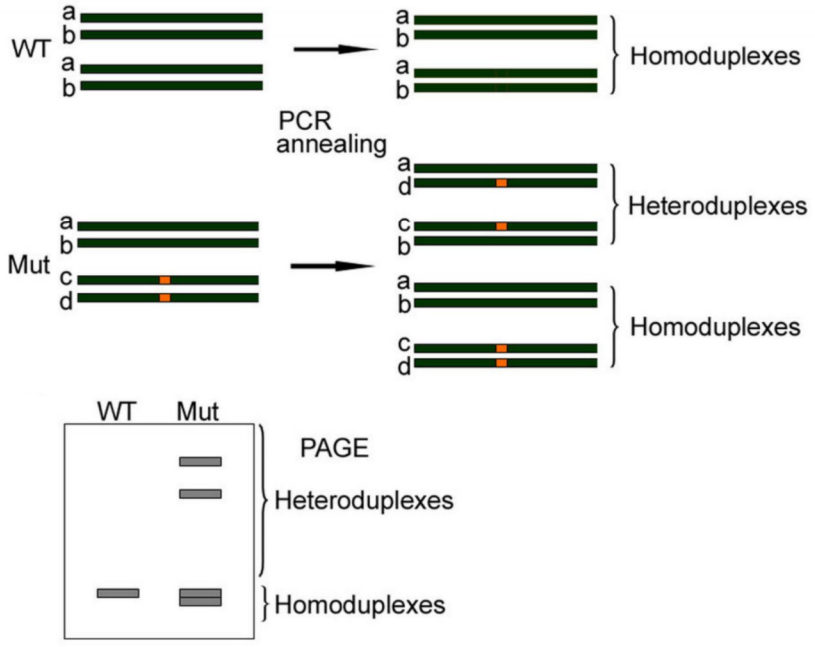
WT
Mut
PCR
annealing
Homoduplexes
Heteroduplexes
Homoduplexes
WT
Mut
PAGE
Heteroduplexes
Homoduplexes

Figure 3.1: Schematic representation of (A) T7 Endonuclease 1 (from Shen *et al.*, 2013) and (B) PAGE-based (from Zhu *et al.*, 2014) identification of insertion/deletion (indel) mutants. PCR products were amplified from CRISPR targeted region, and then subjected to slow reannealing at decreasing temperature. Slow reannealing leads to both homoduplex formation and heteroduplex formation at mismatches and extrahelical loops formed by single or multiple nucleotides. (A) Hybridized products are digested with T7E1, which can recognize and cleave heteroduplex DNA. Cleaved bands can then be detected by agarose gel electrophoresis (from Shen *et al.*, 2013). (B) Hybridized products are resolved by polyacrylamide gel electrophoresis. Heteroduplexes migrate slower than homoduplexes allowing for heterozygotes, homozygotes and wild type zebrafish to be easily distinguishable based on their banding pattern (Zhu *et al.*, 2014). (Reprinted by permission from Macmillan Publishers Ltd: *Cell Res*. Shen *et al.* © 2013).

target mutations from the mutant lines. To determine germline mutation efficiency and germline transmission rate, genomic DNA from either F_1 embryos or caudal fin clips from adult F_1 fish were analyzed by PCR amplification and PAGE analysis. Germline mutation efficiency is the percentage of F_0 fish with germline mutations while germline transmission rate is the percentage of offspring from a single F_0 founder that are heterozygote mutants. For each founder, 24 hpf F_1 embryos were collected in groups (5-10 embryos per group), and 4-10 groups were screened for germline transmission. The F_1 embryos of positive founders were raised to adulthood, and genotyped via fin clip gDNA analysis.

Germline mutation efficiencies were 0% for *parla* target 1 and 2 sgRNA (n=15) and 83% for *parlb* target 1 sgRNA (n=16). All the somatic *parla* mutant positive primary injected F0 fish that could breed naturally, produced WT offspring only. To test whether the lack of mutant offspring was due to an absence of germline mutations, gametes were collected from individual founder fish, and the genomic DNA was extracted and analyzed by PAGE. The gametes of 2 male and 4 female F_0 fish were identified to have mutations, despite no living offspring presenting these mutations, even after screening over 100 F_1 offspring each. This suggests that either *parla* target 1 and 2 sgRNA were inefficient with low penetrance, or *para* mutations affects the viability of the gametes.

Out of the *parlb* mutants, seven different mutant founder fish were identified with germline transmission rates as follows: BBf12 = 29.2%, BOf5 = 28.1%, BBf14 = 30.8%, BBf11 = 52.2%, Bof20 = 19.2%, BBm23 = 25.0% and BBm20 = 28.5%. To determine the mutant sequences, PCR amplicon from mutant F_1 genomic DNA was purified and sent for sequencing (Figure 3.2). Founder line BBf11 produced two different mutations, #1 which was a 3 bp deletion and #2, a

5bp deletion leading to a frameshift mutation. All other founder lines produced mutants with the same mutation. Only two of the *parlb* founder lines resulted in frameshift mutations: BOf5 and BBf11 mutation #2 and these became the focus for further screening and experiments.

A

```
WT          GGAGGAGCTGCTTCATGAAATGGACACAAATAAACTCGATAAATGCATC
BBf12       GGAGGAGCTGCTTCA---------CACAAATAAACTCGATAAATGCATC
BBf14       GGAGGAGCTGCTTCA---AATGGACACAAATAAACTCGATAAATGCATC
BOf5        GGAGGAGCTGCTTCATG----GGACACAAATAAACTCGATAAATGCATC
BBf11#1     GGAGGAGCTGCTTCAT---ATGGACACAAATAAACTCGATAAATGCATC
BBf11#2     GGAGGAGCTGCTTCATG-----GACACAAATAAACTCGATAAATGCATC
```

B

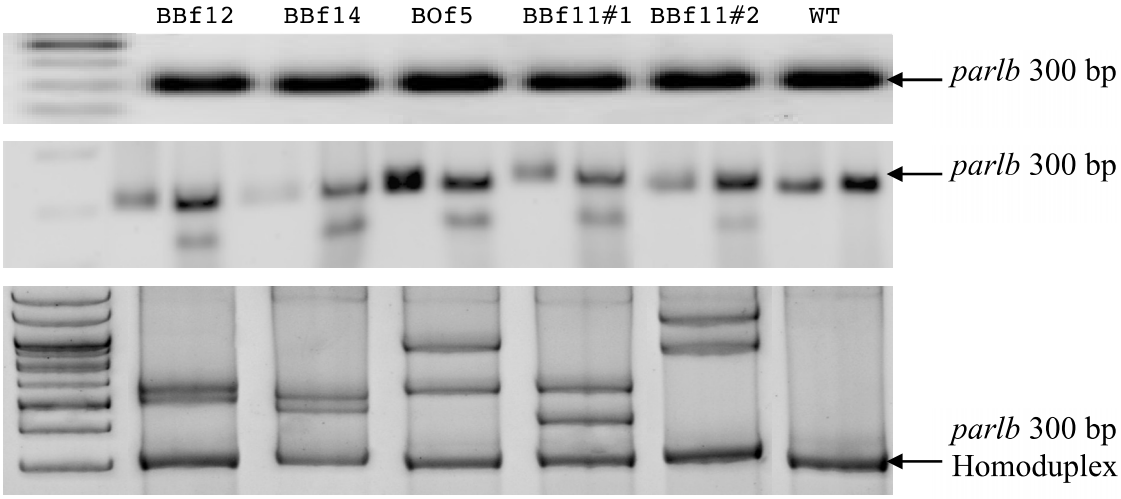

C

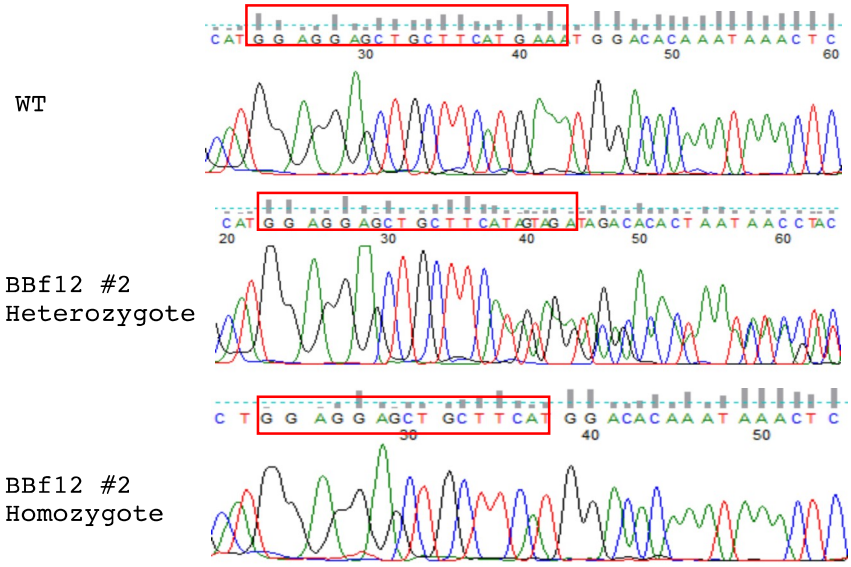

Figure 3.2: Germline transmission of CRISPR/Cas9-induced mutations in zebrafish at the parlb locus. (A) The sequencing results performed on F1 mutant zebrafish of 4 founder fish. (B)A T7E1 assay and PAGE analysis was performed on F1 mutant zebrafish of 5 founder fish. Founder fish were bred with wild type fish to produce the F1 generation. (C) Sequencing chromatogram results of BBf11 #2 mutants, later known as *parlb*^{emD9K}, comparing wild type, heterozygous mutant and homozygous mutant chromatogram readings. The target sequence is highlighted with a red rectangle.

3.3 Multi-Exon Deletion of the *parla* locus

Due to the low mutation efficiency (somatic and germline) of targets 1 and 2 for *parla*, new sgRNA were devised. The intent behind the design of targets 3-6 was for them to be injected simultaneously. The rationale behind designing and injecting four sgRNAs simultaneously is that by having 2 sgRNA designed 5' of the target region (e.g. exon 1), and 2 sgRNA designed 3' of the target region, you can increase multi-exon mutation efficiency. Target 3 and 4 are located directly adjacent to each other within the 5'UTR while targets 5 and 6 are in exon 2 and 3 respectively. Therefore, if at least one of the 5' sgRNA cuts along with at least one of the 3' sgRNA, the entire segment of DNA between the cleaved sites may be completely removed. A multi-exon deletion using targets 3-6 would remove the first exon, simultaneously deleting the translation start codon, along with the mitochondrial localizing signal. With no translation start codon, no protein should be translated and a null mutant produced. Figure 3.4 depicts a model for the targeting of all sgRNA for *parla* and *parlb*.

The sgRNAs for targets 3-6 were produced with a newly developed, faster approach published by (Gagnon *et al.*, 2014). This method also involves annealing oligonucleotides except one is gene-specific, containing a T7 promoter for *in vitro* transcription, the 20 nt target sequence and an overlap region that anneals to the constant oligonucleotide, which consists of the region of the sgRNA that forms secondary structures and acts as a scaffold for Cas9 docking. After the gene-specific and constant oligonucleotides were annealed, the rest of the sequence was filled in with T4 DNA ligase and then PCR amplified and purified. This second method for sgRNA production was found to be faster compared to the cloning method, while still producing high quality template.

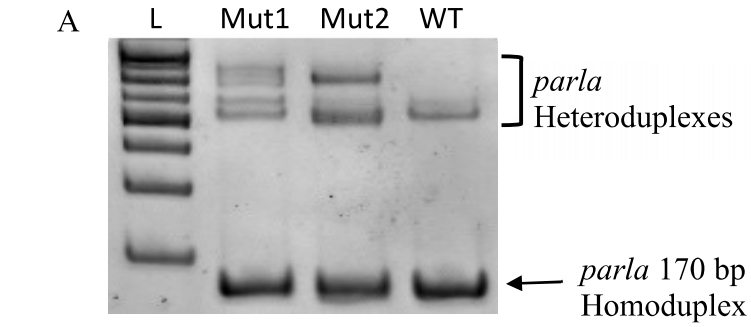
A
L
Mut1
Mut2
WT
parla
Heteroduplexes
parla 170 bp
Homoduplex

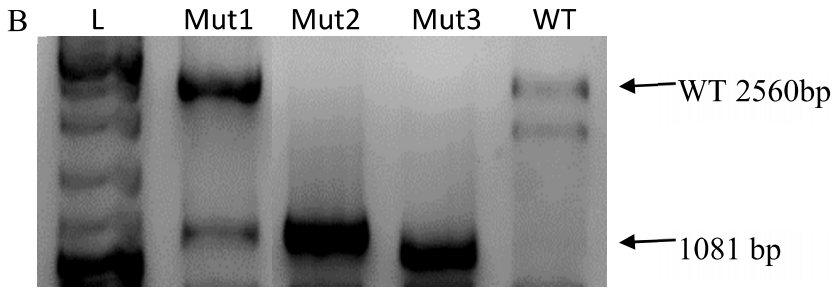
B
L
Mut1
Mut2
Mut3
WT
WT 2560bp
1081 bp

Figure 3.3: Mutation of the parla locus in zebrafish through CRISPR-Cas9 mediated mutagenesis leading to (A) indel mutations and (B) multi-exon deletions. Mut = mutant, WT = wild type. (A) Target region for mutagenesis were PCR amplified, denatured and reannealed slowly. Resulting homoduplexes and heteroduplexes were resolved on a 12% PAGE to identify potential mutants. (B) The target region was PCR amplified and resulting products resolved by agarose gel electrophoresis to identify possible mutants with multi-exon deletion.

Screening for exon deletion was performed by PCR amplification spanning all four target sites and agarose gel electrophoresis analysis. As an example, the size of the wild type amplicon was predicted at 2560 bp. A deletion caused by Cas9 cleavage of target #3 and #5 causes a loss of 1479 bp of sequence, leaving a predicted mutant product size of around 1081 bp as can be seen in Figure 3.4B. A somatic mutation efficiency was determined to be 40% based on fin clip gDNA from 2-month-old primary injected fish and confirmed by sequencing. The full list of sgRNAs used, their location, sequence and mutation efficiencies can be found in Table 3.2. At the time of writing of this thesis, germline transmission rates could not be determined as the primary injected fish were still too young to be bred.

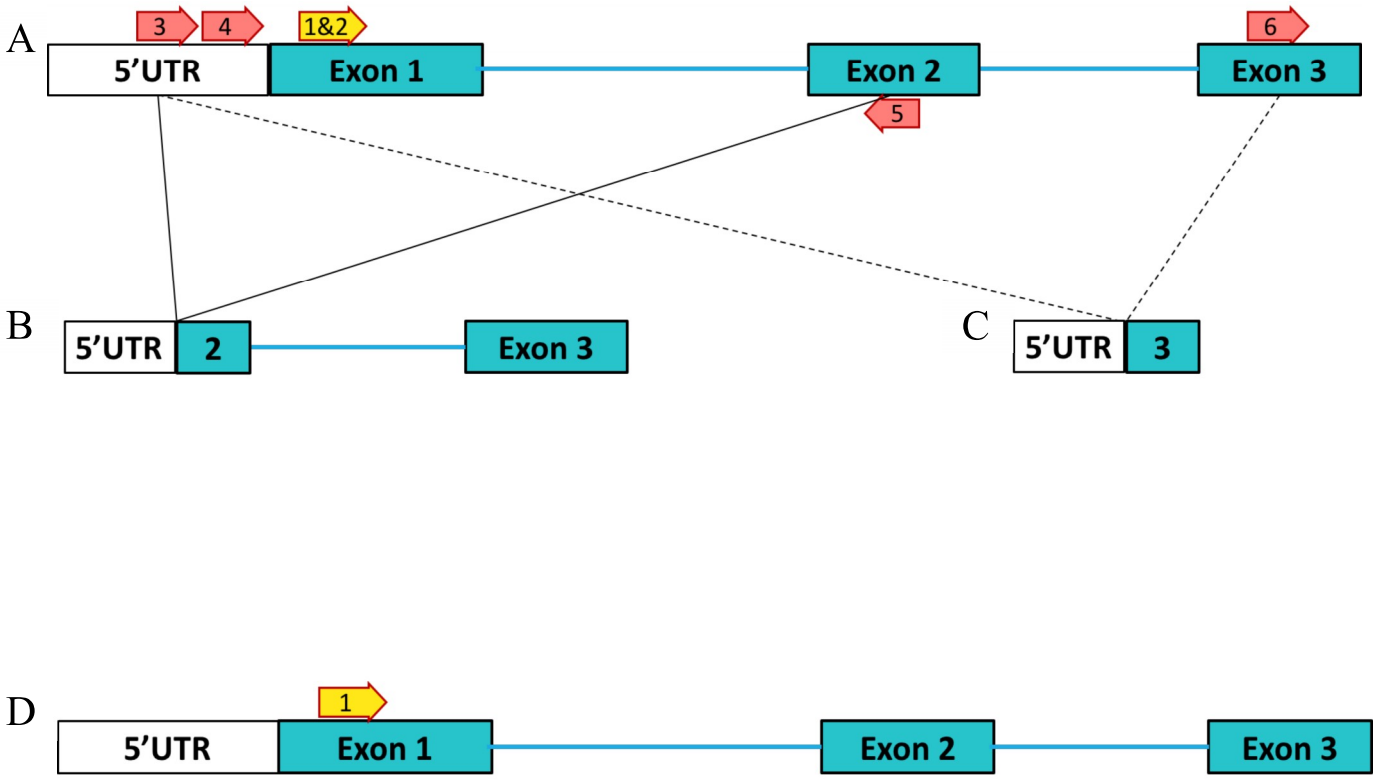
A
3
4
1&2
6
5'UTR
Exon 1
Exon 2
Exon 3
5
B
5'UTR
2
Exon 3
C
5'UTR
3
D
1
5'UTR
Exon 1
Exon 2
Exon 3

Figure 3.4: Schematic representation of the multi-exon sgRNA targeting scheme for the 5' UTR and exons 1-3 of (A - C) *parla* and (D) *parlb*. Targeting for *parla* used 6 different target sequences, with targets 1-2 designed specifically for producing indel mutations and targets 3-6 designed together for multi-exon deletion. Targets 1 and 2 for *parla* differ by one nucleotide due to a natural single nucleotide polymorphism (SNP) found in the endogenous genome. Successful targeting by (B) target 3 and 5 leads to a deletion of approximately 1479 bp of sequence while successful targeting by (C) target 3 and 6 leads to a deletion of approximately 2485 bp. Targeting for *parlb* used a single target sequence and sgRNA designed specifically for producing indel mutations. The yellow arrow represents the original sgRNA targets designed for indel mutations while red arrows represent sgRNAs designed for multi-exon deletion. Arrows above the sequence and pointing right are targets on the sense strand and arrows below the sequence and pointed left are targets on the antisense strand.

Table 3.2 The CRISPR-Cas9 target sites for zebrafish *parla* and *parlb* for CRISPR-Cas9 mutagenesis as designed using the ZiFiT Targeter Software. Location, target sequence and mutation efficiency are presented.

Gene	Target site	Location	Target Sequence (5'-3') (PAM sequence underlined)	Mutation Efficiency
parla	1	Exon 1	GGGGTTTAGTGTTGTTCAGGTGG	25% (n=74)
	2	Exon 1	GGGGTTTATTGTTGTTCAGGTGG	
	3	5' UTR	GGCGCGCTGTGAGCCGGAAGCGG	40% (n=13)
	4	5' UTR	GGAAAGCGCAGTTTTATGCAAGG	
	5	Exon 2 (antisense)	GCCAAATGACTTGGTGGGCCTGG	
	6	Exon 3	GGCTGGACAAAGTTCGCCCCAGG	
parlb	1	Exon 1	GGAGGAGCTGCTTCATGAAATGG	74% (n=40)

3.4 Two *parlb* Mutant Founder Lines Contain Premature Termination Codons

The nucleotide sequences of the mutant lines were translated to predicted amino acid sequences using ExPasy (http://web.expasy.org/translate/) to determine the effect of the mutations on the Parlb protein. The BOf5 mutant line resulted in a premature termination codon (PTC) early in the sequence, located at the 12th codon. Other than the first transmembrane helix (TMH) containing the MLS, all catalytic residues and transmembrane helices are located after the PTC. In the BOf5 founder line, the first amino acid change induced by the 4 bp deletion was a Lysine (K) to Glycine (G) at residue 9. The mutant line was termed *parlb*^{emG9K} or G9K. Similarly, the BBf11 #2 mutant lines also results in a PTC early in the amino acid sequence at codon 40. The first a.a. affected by the mutation in the BBf11 #2 founder line was also at residue 9, converting a Lysine (K) to an Aspartic acid (D) and was termed *parlb*^{emD9K} or D9K (Figure 3.6). Similar to *parlb*^{emG9K}, all TMHs are 3' to the PTC, except the N-terminal TMH, with all a.a. after position 9 differing from the original WT sequence.

Both *parlb* mutant lines were also analyzed for potential alternative start codons to further assess the value and utility of the lines. No alternative splicing variants or start codons were identified in ENSEMBL or NCBI. Additionally, the closest alternative in-frame AUG-codon is before the deletion mutations and would still produce a frameshifted protein with a premature start codon. The next in-frame AUG codon is at position 189 from the original AUG, and would result in a loss of all localizing signals and the first two transmembrane helices. As stated previously, a popular theory for PARL substrate entry is through TMH 2 and 5, so a loss of TMH2 could lead to a loss of Parl function. Therefore, neither line likely has an alternative start codon.

Currently, I have F_4 and F_5 generations for *parlb*^{emG9K} and *parlb*^{emD9K} respectively, with populations of genotyped homozygotes. Both mutants lines have been bred with Tg(*dat-eGFP*) (Xi *et al.*, 2010) and Tg(*dat:Tom20 MLS-mCHERRY*) (Noble *et al.*, 2015) transgenic lines and genotyped as homozygotes for the mutation and transgene (Figure 3.7). The Tg(*dat:eGFP*) line expresses EGFP under the control of cis-regulatory elements of the dopamine transporter (*dat*) and can be used in future experiments to visualize changes in dopaminergic neuron patterning. The Tg(*dat:Tom20 MLS-mCHERRY*) lines expresses Tom20-mCHERRY targeted to the mitochondria, and are also placed under the control of the *dat* regulatory elements. The Tg(dat:tom20 MLS-mCherry) mutants can be used in future experiments to determine if the mutations caused changes in mitochondria morphology and dynamics.

A

```
WT          ATGGCATGGAGGAGCTGCTTCATGAAATGGACACAAATAAACTCGATAAATGCATC
BBf11#2     ATGGCATGGAGGAGCTGCTTCATG-----GACACAAATAAACTCGATAAATGCATC
BOf5        ATGGCATGGAGGAGCTGCTTCATG----GGACACAAATAAACTCGATAAATGCATC
```

B

Wild type:

MetAWRSCFMKWTQINSINASSLCPKSTRLNIHPQQRCGFRKAERPSESKKGVQETEAEAGGHNRA
VPPKPVPPLPPRRPHQLFRPLVFTVGFTGCSFGAAAILQYESVKSRVQLAIEEAKEEKRDTLLEGH
DTTYWHNWWNQLSNFQKQVILLISAVDDFWSGLSEGQKTVTGIIALNTVVLCCWRVPAMQRFLVKY
FTSNPASKTRCLPMVLSSFSHYSVIHMVVNMYVLWTFSSSIVSLLGREQFLALYLSGGVISTFVSY
VFKTATGRLGPSLGASGSIMTVLAAVCTKIPEAKLGIVLLPVISFSAGNALKALVALDIAGLLLGW
RFFDHAAHLGGALFGVWYIGYGHELIWRKREPLIKFWHELRNMSPGRPGPGGGGG**Stop**

BBf11#2 line:

MetAWRSCFMDTNKLDKCIIVVSKKYQIKHPSSAKMWLPES**Stop**

BOf5 line:

MetAWRSCFMGHK**Stop**

Figure 3.5: A comparison of the wild type parlb (A) nucleotide and (B) amino acid sequence to the BBf11 #2 and BOf5 mutant sequences. Nucleotide target sequence of the CRISPR-Cas9 sgRNA is underlined (A) and sequence divergence occurs after the highlighted amino acids (B).

3.5 Primary Injected and *parlb* Mutant Homozygotes Displayed Wild Type Gross Morphology

General morphological comparisons between the non-injected wild type, and the targeted mutants for *parla*, and *parlb* were performed to test for any noticeable effects on the phenotype of the mutants. Microinjected F_0 individuals showed developmental defects including tail and eye malformations, edema and craniofacial malformation. Tail deformities ranged from light bends in the tail, to completely fused or undeveloped tails, while the eye deformities ranged from underdeveloped eye(s), partially fused eyes, cyclops, and no eyes. Edemas observed were either located at the heart or complete body edema. At 3 dpf, tail biopsies were performed on deformed and normal embryos for screening as described in (Wilkinson *et al.*, 2013). No correlation was found between deformities and the presence of mutations in the genes. Therefore, the deformities were likely due to cytotoxicity of the sgRNA and Cas9 mRNA.

The morphology of sexually mature F4 zebrafish and F5 offspring was examined, as well as embryo survival rate, breeding capability, and hatching rate. Sexually mature F_4 zebrafish were bred with a WT sibling and the embryos collected the next day and observed for survival rate and overall morphology. Zebrafish were observed for the first 7 dpf at regular intervals and at 3 months for overall morphology. There were no significant differences observed between *parlb*^{emG9K} and *parlb*^{emD9K} mutant F_4 zebrafish birth rates compared to WT siblings. The F_5 offspring displayed normal mortality and hatching rates. Phenotype analysis also showed no significant difference compared to the wild type in terms of gross morphology.

3.6 Dopaminergic Neuron Patterning in *parlb* Mutants by W.I.S.H.

Other than overall morphology, we wanted to perform a further phenotypic analysis on the *parlb* mutant lines. As stated previously, mutations in PARL have been linked to Parkinson's Disease which results in the degeneration and loss of dopaminergic neurons in substantia nigra of human patients with the disease. Therefore, we decided to examine the dopaminergic neuron patterning on 3 dpf larvae via whole mount *in situ* hybridization (W.I.S.H.). This time point was chosen due to a combination of the amenability of the small larvae to permeabilization for *in situ* analysis, and the advanced state of their CNS (Kimmel *et al.*, 1995). The riboprobe utilized was made against *th1* mRNA, a previously used marker to label various DA neuron populations including the vDc, and in the retina in zebrafish (Noble *et al.*, 2012; Yamamoto *et al.*, 2011). The focus of the analysis were DA neurons in the zebrafish posterior tuberculum of the vDc which ascend to the basal telencephalon. As mentioned earlier, these DA neurons have been suggested to be equivalent to the dopaminergic system found in the substantia nigra of the human midbrain with projections to the striatum (Rink and Wulliman, 2002). Phenotypes were classified as normal, low-density, mis-patterned or severely mis-patterned as presented in Figure 3.10A and were scored in a blinded fashion.

Our results show a slight increase in percentage of larvae showing abnormal DA neuron patterning in the homozygous *parlb*^{emD9K} mutants by 14% compared to the wild type (Chi-square test, $p>0.01$). No significant difference in phenotype distribution was seen between the other mutants and the wild types (Figure 3.6). These results corroborate with Dr. Noble's research in which the *parlb* single morphants showed no significant difference in phenotype distribution based on DA neuron patterning (Noble *et al.*, 2012).

A

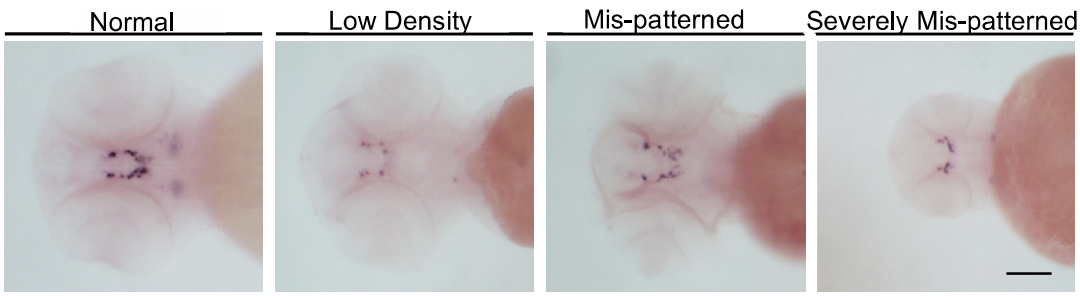
Normal
Low Density
Mis-patterned
Severely Mis-patterned

B

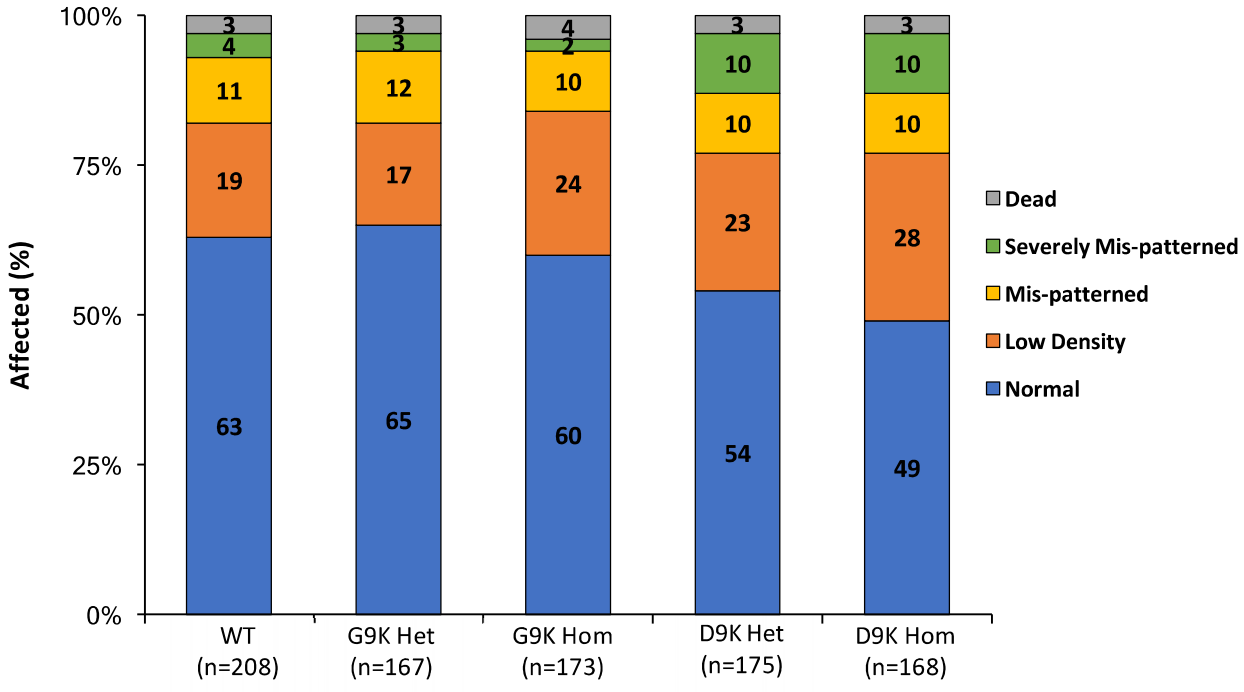
Affected (%)
100%
75%
50%
25%
0%
3
4
11
19
63
3
3
12
17
65
4
2
10
24
60
3
10
10
23
54
3
10
10
28
49
WT (n=208)
G9K Het (n=167)
G9K Hom (n=173)
D9K Het (n=175)
D9K Hom (n=168)
Dead
Severely Mis-patterned
Mis-patterned
Low Density
Normal

Figure 3.6: Dopaminergic (DA) neuron patterning in 3dpf wild type (WT), and heterozygous and homozygous *parlb*^{emG9K} and *parlb*^{emD9K} mutant. (A) Categories of dopaminergic (DA) neuron patterning using DA neuron marker, Tyrosine hydroxylase (*th1*) mRNA and (B) indicated as percentages in each bar alongside larval mortality. Scale bar represents 50 μm.

3.7 Protein Analysis by Western Blot

While direct translation of the mutant sequences in amino acid sequences resulted in the presence of PTCs that should theoretically abolish protein translation, we wanted to validate the loss of protein by immunoblot analysis. Previous work performed by Dr. Noble tested commercially available anti-human PARL antibodies. Results indicated a lack of recognition of the antibodies for Parla and Parlb in zebrafish and cell culture lysates. In addition, custom generated antibodies against Parla and Parlb (Open Biosystems, 2 rabbit 70-day protocol) also did not result in specific bands in zebrafish mitochondrial lysates and produced no signal in previous immunoprecipitation (IP) experiments in cultured cells (Noble, 2014).

Multi-pass transmembrane proteins are difficult to isolate and resuspend, therefore the antibodies were retested on zebrafish mitochondrial lysates and whole lysates for Parla and Parlb using a variety of methods, including RIPA buffer extraction, using the Mitochondrial Isolation Kit for Tissue that was used by Dr. Noble (Thermo Scientific, Rockford, IL, US), and differential fractionation (Noble, 2014). Various buffers were tested for the lysis (RIPA buffer or 250 mM sucrose, 1mM EDTA, 10 mM HEPES) and resuspension (2% CHAPS, RIPA buffer or 7M Urea) of samples. Similar to previous results (Noble, 2014), the Parla and Parlb antibodies gave a multitude of bands of all sizes in both the cytosolic and mitochondrial lysates for both the kit and differential fractionation methods. These bands were not consistently reproducible, likely due to the Parl antibodies non-specifically binding to endogenous zebrafish proteins. Results from RIPA buffer whole lysate extracts showed cleaner results with fewer non-specific bands. The custom antibodies were pre-absorbed with their respective purified peptides. Further optimizations resulted in no signals for the custom antibodies, although loading controls, anti-GAPDH and anti-

VDAC produced a signal. It was concluded that currently available antibodies are not effective against the zebrafish Parl paralogs.

3.8 Neither Parl Protein was Identified by Mass Spectrometry

With the immunoblot results being inconclusive, an alternative method we utilized to validate Parlb knockout in the mutant lines was mass spectrometry. The mitochondrial fraction of zebrafish protein lysates was sent to the laboratory of Dr. Daniel Figeys for mass spectrometry analysis (Figure 3.7). Analysis of wild type lysates did not identify either Parla nor Parlb in the lysates, potentially due to an overabundance of proteins in the sample, hiding their presence. Over 1200 proteins were identified, including: VDAC1, PGAM5, Opa1, YWHAZ, afg3l2, Tom20, and various proteins from the electron transport chain.

The predicted size of bands for full-sized Parla and Parlb are 42 kDa and 43 kDa respectively. Both Parl proteins undergo a maturation step upon integration in the inner mitochondria membrane, where the MLS is cleaved from the N-terminus of the protein. Therefore, to increase the likelihood of isolating and identifying Parla and Parlb, bands from 25-45 kDa were extracted from the electrophoresis gel after coomassie blue staining and sent for mass spectrometry analysis. Results identified 656 proteins, none of which included Parla, nor Parlb. Other transmembrane proteins were identified in both analyses performed and include VDAC1-3, YWHAZ, afg3l2, Tomm40, Tomm70a, ATP synthase, and various ETC proteins.

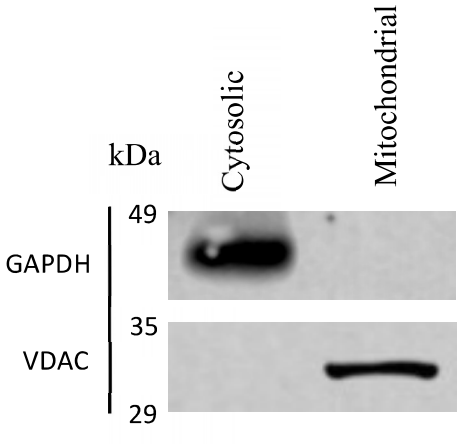
Cytosolic
Mitochondrial
kDa
49
GAPDH
35
VDAC
29

Figure 3.7: Western blots of GAPDH and VDAC on the cytosolic and mitochondrial lysates of 50 pooled 5 dpf zebrafish homogenates extracted using differential fractionation. GAPDH localizes to the cytosol and VDAC localizes to the mitochondria.

3.9 *Parlb* Mutants Maintain Normal *parla* and *parlb* RNA Expression

Due to the inconclusive results from the western blot analysis and mass spectrometry, RNA expression analysis by qRT-PCR was conducted. The *parl* paralogs were analyzed to determine if the premature translation termination codon in the *parlb* mutants would lead to nonsense mediated decay (NMD) of the aberrant mRNA, resulting in a loss of *parlb* mRNA expression. Nonsense-mediated mRNA decay (NMD) is a conserved surveillance system utilized to control for the quality of mRNA produced in a cell by detecting and degrading mRNA containing PTCs (Behm-Ansmant *et al.*, 2007). Additionally, due to the overlapping expression profile of *parla,* a decrease in *parlb* expression and protein function was predicted to lead to a compensatory upregulation of *parla.* Heterozygous and homozygous mutant samples were compared for relative fold difference in expression compared to the wild type.

Results of qPCR analysis showed no significant difference in expression levels between wild type and mutant $parlb^{emG9K}$ or $parlb^{emD9K}$ samples for either *parl* gene (Figure 3.8). To ascertain that the genomic-based mutation is transcribed into the mature mRNA, PAGE analysis of PCR amplified cDNA was performed (Figure 3.9) and sequencing confirmed the presence of the mutation in the cDNA (data not shown). This suggests that NMD is not degrading the mutant mRNA, despite the presence of a PTC in both lines. Interestingly, the $parlb^{emD9K}$ line did show a decrease in *parlb* mRNA expression by 31.6% in the homozygotes and 34.0% in the heterozygotes compared to the wild type, while the $parlb^{emG9K}$ showed no statistically significant differences in *parlb* mRNA expression compared to the wild type siblings. This suggests a possible difference in response of the NMD system to the two mutations. It has been observed that nonsense mediated decay initiation is inefficient when the triggering PTC is close to the start (AUG) codon (Popp and

Maquat, 2016). This resistance could be due to circularization of the mRNA and steric hindrance of the eukaryote translation machinery, CAP-binding complex and the NMD enzymes. Lastly, with the loss of Parlb protein, it was reasonable to expect the expression of *parla* mRNA to increase. Results from the qPCR show little compensatory changes in *parla* expression in the *parlb* mutants.

A

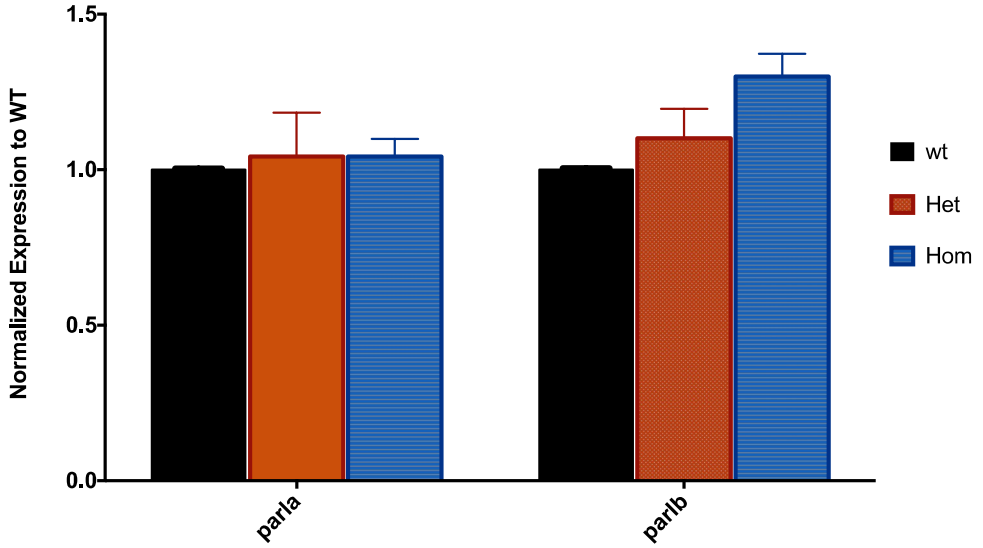
Normalized Expression to WT
1.5
1.0
0.5
0.0
parla
parlb
wt
Het
Hom

B

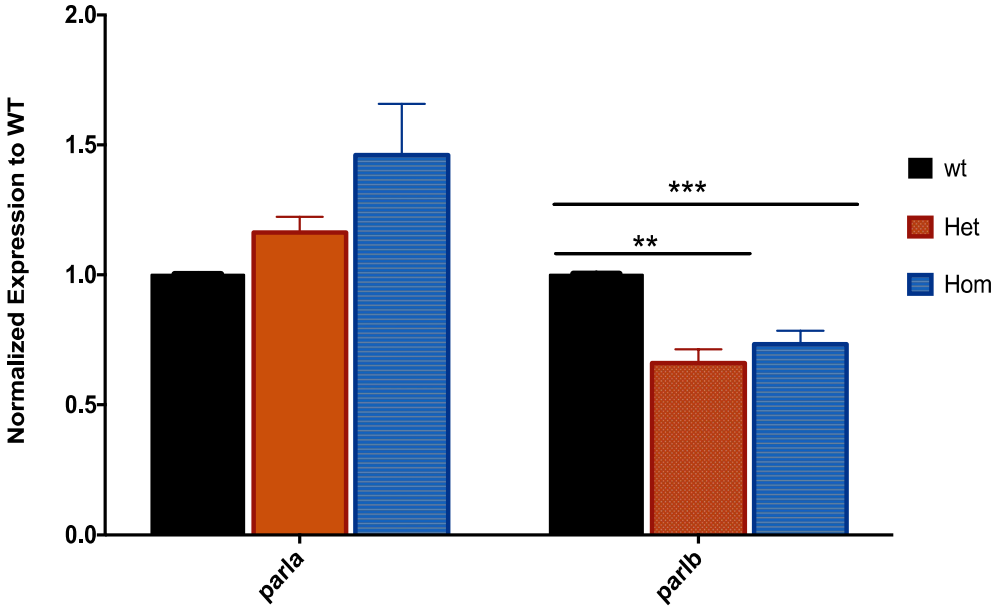
Normalized Expression to WT
2.0
1.5
1.0
0.5
0.0
***
**
parla
parlb
wt
Het
Hom

Figure 3.8: Relative expression of *parla* (n=5) and *parlb* (n=5) mRNA in wild type, and heterozygous and homozygous (A) *parlb*^{emG9K} and (B) *parlb*^{emD9K} mutants. Larvae were collected at 5 dpf and the mRNA extracted from pooled samples of 50 larvae for analysis. The relative expression levels were normalized to the geometric mean of β-actin, ef1α and RPL13α. Error bars represent ±SEM. p-values for significance are shown for mutants demonstrating **: p<0.01 and ***: p=<0.001.

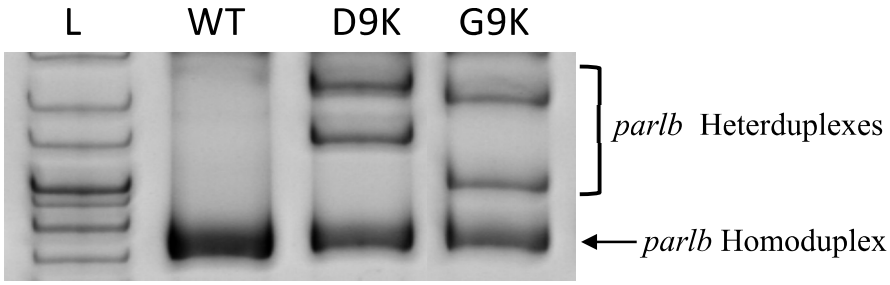
L
WT
D9K
G9K
parlb Heterduplexes
parlb Homoduplex

Figure 3.9: Detection of mutations at the *parlb* locus from *parlb*^{emG9K} and *parlb*^{emD9K} cDNA compared to wild type (WT) cDNA. Each sample was produced from mRNA extracted from pools of 50 larvae for each treatment, and converted to cDNA. Target region for mutagenesis were PCR amplified, denatured and reannealed slowly. Resulting homoduplexes and heteroduplexes were resolved on a 12% PAGE.

3.10 Potential Functionally Compensatory Proteins Showed No Changes in RNA Expression

While the Parl proteins function upstream of PINK1, cleaving and preventing PINK1 accumulation in the inner mitochondrial membrane, several other proteins also proteolytically cleave PINK1. Therefore, it has been hypothesized that these proteins could be potential compensators when there is a perturbation of Parl's inhibition of unnecessary mitophagy through the PINK1/Parkin pathway. These candidates include: 14-3-3 protein zeta/delta *(YWHAZ),* peptidase mitochondrial processing beta subunit *(PMPcβ),* caseinolytic mitochondrial matrix peptidase proteolytic subunit *(ClpP),* and ATPase family gene-like 3 *(afg3l2). YWHAZ* regulates signal transduction pathways, primarily through binding phosphoserine proteins, and regulates metabolism and apoptosis. *YWHAZ* has also been implicated in several neurodegenerative diseases, including Parkinson's Disease. *PMPcβ, ClpP,* and *afg3l2* are subunits of known proteases involved in PINK1 turnover. *PMPcβ* contains the catalytic domain of the mitochondrial processing peptidase (MPP), ClpP for caseinolytic peptidase X, and *afg3l2* is a subunit of the m-AAA protease.

Additional genes assessed for mRNA expression included optic atrophy 1 (*Opa1),* a substrate of Parl, and *dat,* a marker for dopaminergic neurons. No known alternative compensatory proteins for Parl have been identified that also cleave Opa1. qRT-PCR results once again showed no significant differences in either mutant line compared to the wild type samples for *Opa1*, *PMPc*β, *ClpP*, *afg3l2*, or *dat* (Figure 3.10). The qPCR results were once again more similar to the wild type in the *parlb*^{emG9K} line compared to the *parlb*^{emD9K} line.

A

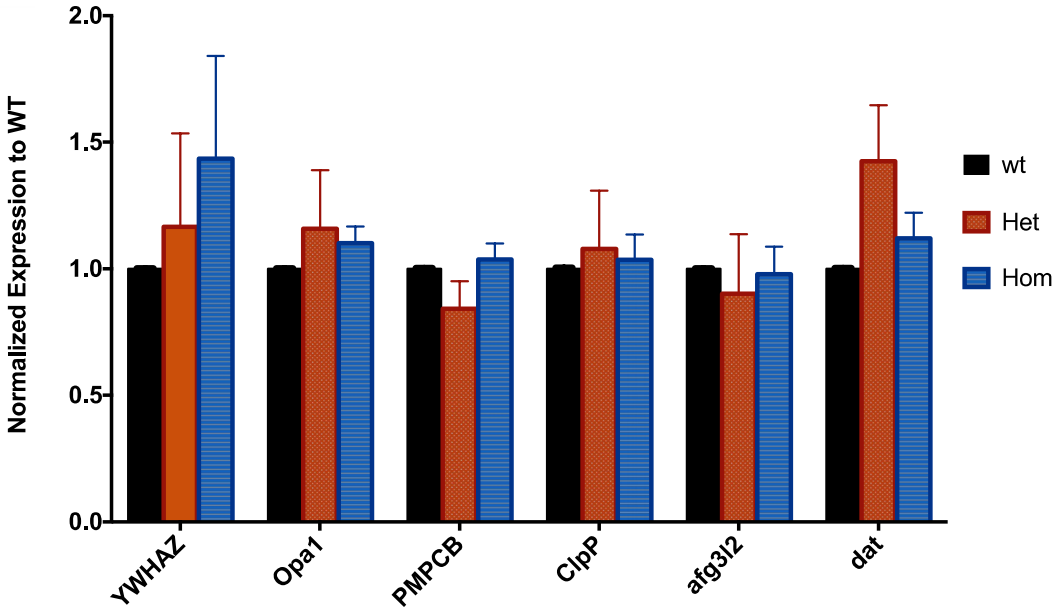
Normalized Expression to WT
2.0
1.5
1.0
0.5
0.0
YWHAZ
Opa1
PMPCB
ClpP
afg3l2
dat
wt
Het
Hom

B

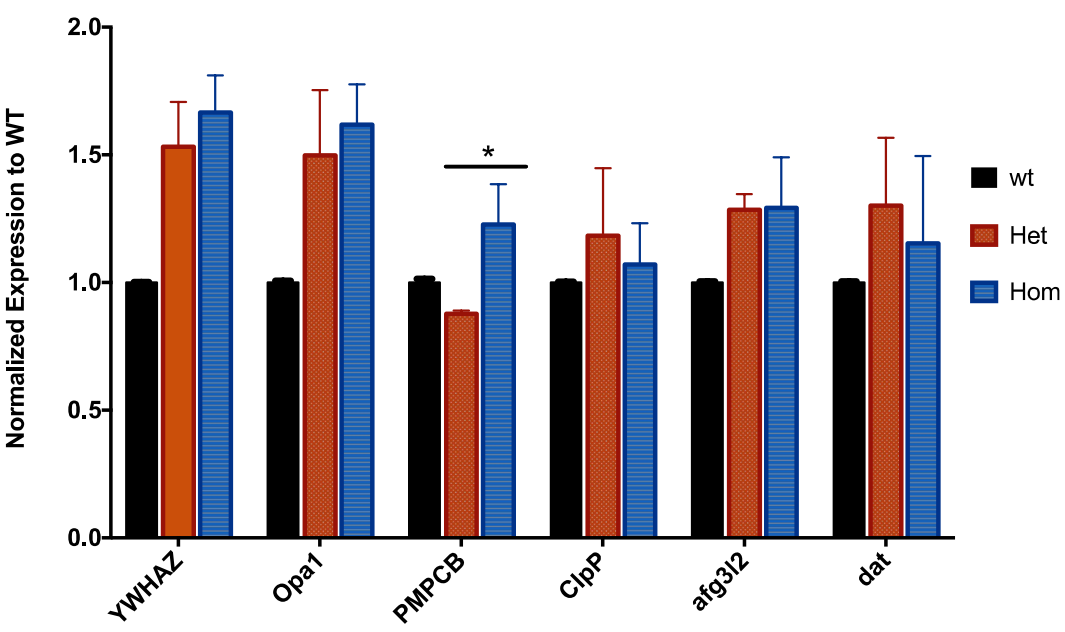
Normalized Expression to WT
2.0
1.5
1.0
0.5
0.0
*
YWHAZ
Opa1
PMPCB
ClpP
afg3l2
dat
wt
Het
Hom

Figure 3.10: Relative expression of Y*WHAZ* (n=5)*, Opa1* (n=5)*, PMPcβ* (n=5)*, ClpP* (n=5), *afg3l2* (n=4) and *dat* (n=6) for wild type, heterozygous and homozygous (A) *parlb*^{emG9K} and (B) *parlb*^{emD9K} mutants as validated by qRT-PCR analysis. Larvae were collected at 5 dpf and the mRNA extracted from pooled samples of 50 larvae for analysis. The relative expression levels were normalized to the geometric mean of β-actin, ef1α and RPL13α. The error bars represent ±SEM. P-values for significance is shown, * $p < 0.05$.

3.11 Injection of *parla* MO into *parlb* Mutants Results in Increased Larval Mortality as seen with WT Co-Injected with *parla* and *parlb* MOs

While the results from a morpholino study indicated no change in the DA neuron patterning in the *parlb* morphants (Noble *et al.*, 2012), a 37% increase in percentage of morphants with severe mis-patterning was observed in *parla* morphants compared to those that received a control MO. Additionally, double morphants, co-injected with *parla* and *parlb* MOs, showed a 17% increase in larval mortality compared to control morphants (chi-square test, $p < 0.001$) (Noble *et al.*, 2012). Therefore, to test whether Parlb function is impaired or absent in the *parlb* mutants, we injected the same splice-blocking *parla* morpholino as used in (Noble *et al.*, 2012) into wild type, $parlb^{emG9K}$ and $parlb^{emD9K}$ mutants to determine if the resulting phenotypes match the *parla* single morphants, or the *parla* and *parlb* double morphants. In parallel, co-injection of *parla* and *parlb* MOs into the *parlb* mutants and wild type zebrafish were performed as controls. The percentage of morphants that fall into each of these categories is presented alongside larval mortality in Figure 3.11.

The whole mount *in situ* hybridization results revealed a 30% increase in the proportion of morphants with severely mis-patterned DA neurons for wild type zebrafish injected with *parla* MO, compared to wild types injected with phenol red (Chi-square test, $p < 0.0001$). In addition, wild type individuals co-injected with both *parl* MOs had a 40% increase in larval mortalities (Chi-square test, $p < 0.0001$). These results corroborate with previous research (Noble *et al.*, 2012).

Interestingly, significant differences in phenotype distribution were seen between the *parlb* mutants injected with *parla* MO compared to wild type controls injected with *parla* MO. While both groups displayed an increase in the proportion of larvae with severely mis-patterned

DA neurons, this increase in the *parlb* mutants was by a much smaller percentage compared to the wild types injected with the *same* MO (Chi-square test, $p<0.001$). The *parlb* mutants injected with the *parla* MO also displayed an increase in larval mortality compared to wild type controls (21% in the $parlb^{emG9K}$ line, and 30% in the $parlb^{emD9K}$ line) (chi-square test, $p<0.0001$). This increase in larval fatalities is similar to that seen in the wild types co-injected with both *parl* MOs. In fact, no significant difference was observed in the larval mortality rates between the *parlb* mutants injected with the *parla* MO, and the wild types and *parlb* mutants co-injected with *parla* and *parlb* MO.

The similarity in the phenotypes observed in the *parlb* mutants injected with *parla* MO and the double morphants, and their dissimilarity to the phenotype of the wild types injected with *parla* MO, suggests that Parlb function is impaired in the *parlb* mutants. These results also suggest that in zebrafish, larval survival may rely on the function of both *parl* genes. Furthermore, the increase in proportion of larvae with severely mis-patterned DA neurons observed in the WT *parla* morphants, and not in any other treatment group, suggests that proper DA neuron development may depend principally on Parla function.

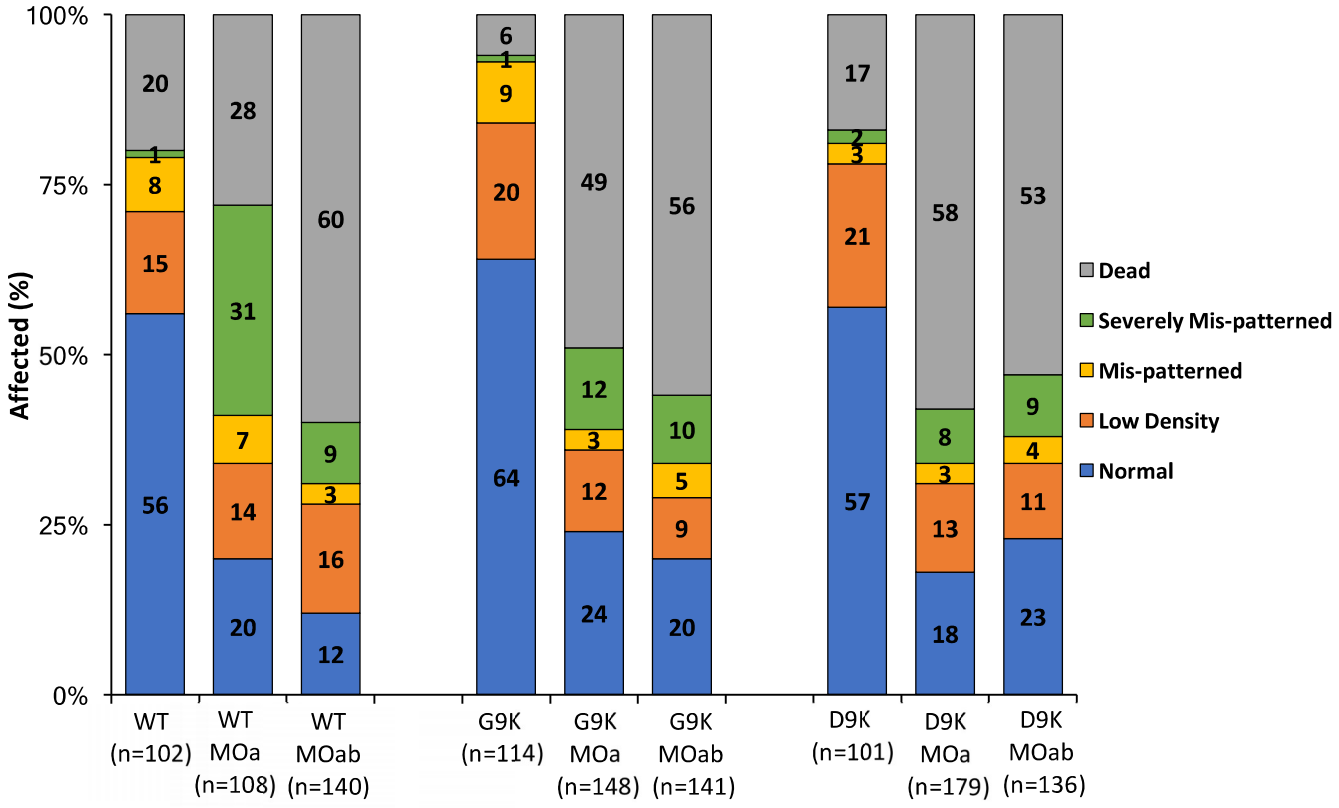
100%
75%
50%
25%
0%
Affected (%)
20
1
8
15
56
28
31
7
14
20
60
9
3
16
12
6
1
9
20
64
49
12
3
12
24
56
10
5
9
20
17
2
3
21
57
58
8
3
13
18
53
9
4
11
23
WT (n=102)
WT MOa (n=108)
WT MOab (n=140)
G9K (n=114)
G9K MOa (n=148)
G9K MOab (n=141)
D9K (n=101)
D9K MOa (n=179)
D9K MOab (n=136)
Dead
Severely Mis-patterned
Mis-patterned
Low Density
Normal

Figure 3.11: Injections of *parla* MO in homozygous *parlb*^{emG9K} and *parlb*^{emD9K} mutants, and co-injection of *parla* and *parlb* MO in wild type (WT) leads to increased larval mortality. Categories of dopaminergic (DA) neuron patterning using DA neuron marker, Tyrosine hydroxylase (*th1*) mRNA indicated as percentages. Morpholino injections were performed on four independent clutches of embryos, each with at least 100 embryos. Morphants were injected with either 2.5 ηg of *parla* MO (Moa) only, or 2.5 ηg of each *parl* MO (MOab) as indicated.

4. Discussion

We generated *parla* and *parlb* mutant zebrafish using the CRISPR-Cas9 technology to study the heritable loss of *parl* function. I have, at the time of writing this thesis, produced two *parlb* mutant lines with premature stop codons, *parlb*^{emG9K} and *parlb*^{emD9K}. Both *parlb* mutant lines show no overt phenotypes in terms of gross morphology, larval survival, hatching rate or dopaminergic (DA) neuron patterning in the ventral diencephalon. To confirm that *parlb* is knockout in the mutant lines, the presence of Parlb protein was examined through immunoblotting and mass spectrometry analysis. However, the results from immunoblotting and mass spectrometry were inconclusive. Due to a lack of protein data, qRT-PCR was performed to check for a response of *parlb* mutation on mRNA expression levels to confirm Parlb protein knockout. No change in *parlb* mRNA levels was detected in the *parlb* mutants nor was a significant change detected in the other genes of interest: *parla, Opa1, PMPcβ, ClpP, afg3l2,* and *dat*. Whole mount *in situ* hybridization experiments against *th1,* a marker for DA neurons, were performed on wild type and *parlb* mutants injected with *parla* and/or *parlb* morpholinos. The *parlb* mutants and *parlb* morphants show no differences in DA neuron patterning compared to controls, while *parla* morphants displayed an increase in proportion of larvae with severely mis-patterned DA neurons (31% in *parla* morphants, 1% in wild types). An increase in larval mortality was observed in wild type embryos injected with *parla* and *parlb* morpholinos compared to wild type controls (60% in double morphants and 20% in wild type). Lastly, *parlb* mutants injected with *parla* MO, or both *parla* and *parlb* MO also show increased larval mortality (49-58% in *parlb* mutants/*parla* morphants, 53-56% in *parlb* mutants/double morphants).

4.1 Variance in sgRNA Efficiencies

The main focus of this thesis was to generate *parla* and *parlb* knockout zebrafish lines, for the purpose of performing functional studies. We were able use CRISPR-Cas9 technology to produce several mutants through the delivery of a guide RNA (sgRNA), complementary to the target, and Cas9 mRNA or protein. Although mutations were successfully produced, not all sgRNA designed were as effective in terms of mutation ability. Out of the sgRNA utilized in this study, their efficiency ranged from 25% to 74%. The *parlb* target sgRNA produced the highest mutation efficiency at 74% compared to the numerous *parla* target sgRNAs. Target 1 and 2 for *parla* had 25% of injected zebrafish with mutations at the target site, while the multi-exon deletion sgRNAs had a combined 40% mutation efficiency. Based on these observations it could be hypothesized that *parla* and *parlb* have loci-specific variations leading to differing CRISPR-Cas9 mutational efficiencies.

It has been observed in previous studies that Cas9 binding depends on chromatin structure, DNase hypersenstiviity and the level of CpG methylation (Estep *et al.*, 2016; Kuscu *et al.*, 2014; Wang *et al.*, 2014). All sgRNA targeted to *parla* resulted in low editing efficiencies, suggesting that *parla* may be less accessible for Cas9 binding at the time of microinjection. While *parla* and *parlb* are ubiquitously expressed throughout the organism and expressed from early development to adulthood, *parlb* is expressed earlier than *parla*. First detection of *parla* in zebrafish larva was at 4 hpf, while *parlb* was observed at 2 hpf (Noble *et al.*, 2012). Microinjection of the sgRNA and Cas9 mRNA or protein is performed within the first 40 minutes post fertilization, before the first cleavage event of the embryo. It is possible that *parlb* is expressed earlier and thus the DNA at the *parlb* locus is more accessible for Cas9 binding compared to *parla,* which

becomes more highly expressed a few hours later. Therefore, *parlb* sgRNA would bind more easily to its target and recruit Cas9 compared to *parla* sgRNA.

Mutational efficiency is not only dependent on the locus subject to targeting, but also on the sgRNA themselves. Within the same gene, sgRNA have been observed to show great variability in effectiveness and activities (Doench *et al.*, 2014; Liu *et al.*, 2016; Wang *et al.*, 2014). Presumably, the variability reflects the differences in sgRNA production, sgRNA-Cas9 complex formation, and sgRNA secondary structure stability. In fact, several studies have identified sgRNA sequence determinants that underlie sgRNA activity, creating predictive models for sgRNA effectiveness (Doench *et al.*, 2014; Moreno-Mateos *et al.*, 2015; Wang *et al.*, 2014; Xu *et al.*, 2015).

Consensus from multiple studies has determined that the 8-12 nucleotides directly upstream of the protospacer adjacent motif (PAM), also known as the 'seed' sequence, is important for targeting specificity. These PAM-proximal bases interact with the arginine-rich bridge helix within the recognition lobe of the Cas9 protein. Therefore, sgRNA with more specific seed regions with few off-target mismatches can improve targeting efficiency. The PAM distal sequence is more tolerant to mismatches and is less important in terms of specificity (Liu *et al.*, 2015). Due to a single nucleotide polymorphism present in the middle of the genomic loci for target 1 and 2 in *parla,* the presence of the mismatch could be a potential reason for the low mutation efficiency of these sgRNA. Depending on the composition of the *parla* sequence in the organism (homozygous or heterozygous for either SNP variant), one of the two sgRNAs may be favored, but would need to compete with the alternative sgRNA also injected, thus leading to decreased efficiency.

While progress has been made in our understanding of CRISPR-Cas9 and sgRNA specificity and activity, current models cannot predict the efficiency of a large fraction of sgRNAs. CRISPR-Cas9 technology is becoming a power-house technology for genomic editing as a research tool and therefore we need to further optimize the design principle of sgRNAs and expand our knowledge on their workings. How sgRNAs interact with the Cas9 protein and recruit it to the DNA sequence, what components or properties limit off-target effects, and the kinetics of these processes are questions still left mostly unanswered. Our current lack of understanding on the properties of integral components of the CRISPR-Cas9 system, such as the sgRNAs, is an oversight that needs to be corrected for further evolution of this technology in genetic and medical research.

4.2 Comparison of CRISPR-Cas9 Strategies

With the current popularity of the CRISPR-Cas9 system, it is expected for new strategies and techniques to be developed. Initially, production of the sgRNA was performed through a labor-intensive process involving subcloning, screening, template extraction, purification of template and transcription. This process can take a few weeks in its entirety to complete. Although rigorous, transcription from a purified plasmid template produces a higher fidelity product compared to the more error-prone PCR method of sgRNA template production that was later utilized. The PCR method of sgRNA amplification could be completed in a single day, but required the template to be sequenced to ensure no errors were introduced into the sequence during the PCR amplification.

Between the two methods, no difference was seen on mortality rates of injected zebrafish, suggesting no change in cytotoxicity of the mRNA produced. Cytotoxicity was noted as an issue in the earliest microinjections. The cause was later identified as likely due to the use of lithium chloride (LiCl) during the RNA precipitation step. Lithium chloride is a teratogen in zebrafish (Selderslaghs *et al.*, 2009), and if it precipitated out along with the RNA at sufficient concentration, injection into embryos could lead to severe deformities and death. LiCl was replaced with an incubation with ammonium acetate and ethanol at -20°C to precipitate the RNA. Mortality rates and the proportion of deformed embryos were observed to decrease with the new method of RNA precipitation and purification.

Other than the production of sgRNA, transcribing and injecting Cas9 mRNA was the most commonly used method when this project was started. The Cas9 mRNA is injected either directly adjacent to, or in the one cell stage where translation machinery endogenous to the cell will translate the RNA into Cas9 protein. Due to the requirement for the cell to make the protein before CRISPR-Cas9 induced cleavage and mutagenesis occurs, injections needed to occur soon after fertilization. The first 15 minutes post fertilization was an ideal time as the cell would be undergoing its own replication cycle and thus Cas9 protein would be available at the single cell stage. With the Cas9 present earlier, there is increased likelihood that the injected solution would have a more penetrating mutagenic effect on the developing organism. If injected later, closer to the 45 minute mark when the single cell stage starts its first cleavage into two cells, any mutations made are likely to be different in the two cells, lending to greater mosaicism and potentially lower penetrance.

Cas9 protein eventually became available to inject rather than the RNA form. Cas9 protein is large and harder to enter the cell if injected in the adjacent yolk and thus needs to be injected into the one cell stage or risk decreased efficiency. This requires greater technical skill during microinjection to inject into the one cell stage. Since the Cas9 is already in its final protein state, injecting earlier is not as critical for efficiency, since the protein does not need to be translated first. While allowing for more time to inject embryos from the same clutch, and thus increasing the sample size, no significant difference was observed between mutation efficiencies when utilizing either the Cas9 RNA or protein. On the other hand, Cas9 protein was easier to prepare, and had a slightly lower cytotoxic effect, leading to fewer or less severe deformities in the injected embryos. In results, Cas9 protein was more effective in creating a large population of surviving primary injected zebrafish for further experiments.

Once the methods for sgRNA and Cas9 production were optimized, screening was the next major step in the process of creating CRISPR-Cas9 mutants. Initially, the T7 endonuclease 1 assay was performed to screen for zebrafish with heterogeneous DNA sequences at the target loci. Unfortunately, naturally occurring SNPs would also be detected and cleaved by the T7E1 enzyme, making analysis of the results more difficult, especially if the natural SNPs and other polymorphisms are close to the target site. If that is the case, it can become difficult to parse out which results are CRISPR-Cas9 induced mutations and which are false positives. The zebrafish used in these experiments are not from inbred lines, such as OregonAB or Tübingen, but from a mixed population of zebrafish. Zebrafish lines that possess high genetic variability breed more reliably, have higher fecundity and higher survival rates compared to inbred lines, but this maintenance of genetic variation causes SNPs to be present. Observations from dozens of T7E1

assays also noted non-specific cleavage leading to further false positive results (5%, data not shown). Therefore, to ensure a true mutant is present, sequencing was required for confirmation. Producing a homozygous line after a few generations of outcrossing requires the screening of hundreds of zebrafish, and thus having a screening method with a low false positive rate of 5% is not ideal.

Compared to the *parlb* gene, *parla,* in the zebrafish population we used, had comparatively more SNPs present in its exons and introns, making efficient targeting and screening more difficult. Due to the natural SNPs located in the *parla* gene, using the T7E1 assay as a screening method was problematic, and thus we turned to PAGE analysis. As stated earlier, PAGE analysis results in unique heteroduplex banding patterns for each mutation, allowing for easy identification of mutant zebrafish sharing the same sequence, without sequencing. No false positives were observed after screening over a thousand samples. During optimization, it was noted that a single heterozygote mutant pooled with 9 wild type zebrafish could be easily identified, allowing for faster screening for germline transmission in the F_0 mutant zebrafish. All further screening was performed using the PAGE method, due to its efficiency and reliability.

4.3 Indel Formation vs Multi-Exon Deletion

With the versatility of the CRISPR-Cas9 system, two aproaches were utilized in order to produce these mutations: 1) the use of a single target site to induce the formation of a frameshift mutations via insertions or deletions (indels), and 2) the use of multiple target sgRNAs simultaneously injected to excise an entire region of the genomic locus. Approach 1) was used to create the *parlb* mutant lines, $parlb^{emG9K}$ and $parlb^{emD9K}$. A single sgRNA was designed and used,

allowing for easy screening and sequencing. Out of 12 mutant F_0 zebrafish with germline mutations, only 2 produced mutant F_1 offspring with frameshift mutations. Therefore, although the mutation efficiency was high at 74%, very few of the mutations produced were useful for this study. Most of the mutations produced in the study had deletions near the Cas9 cleavage site three nucleotides upstream of the PAM sequence, as observed in previous studies (Cong *et al.*, 2013; Estep *et al.*, 2016).

When approach 1) was used for *parla,* the sgRNA were inefficient despite the three online sgRNA design programs we utilized assuring the opposite. Therefore, while using one target sgRNA reduces the possibilities of off-target effects, if the sgRNA turns out to be inefficient then time is wasted and the experiment must be restarted. When redesigning the *parla* sgRNA, approach 2) was used, with multiple target sites sought encompassing the first exon in the hopes of increasing the chance of at least one of the sgRNA being efficient, and to increase the chance that the mutation produced would lead to a knockout mutant for *parla.* Therefore, sgRNA were designed 5' upstream and 3' downstream of the first exon with the translation start codon, creating a potential multi-exon deletion. While having two sgRNA targeted to 5'UTR (target 3 and 4), and two sgRNA targeted to exons post exon1 (target 5 in exon 2; target 6 in exon 3) increases the chances of multi-exon deletion, it also increases the chances and number of off-target effects. Therefore, outcrossing mutant lines to eliminate these potential off-targets is important, and only sgRNA with few off-targets as predicted by the online software, were chosen. Off-targets, if predicted, were required to be on a different chromosome than *parla* to allow for easier elimination through outcrossing.

Although useful in increasing the chances of a knockout mutation, using multiple target sites that are far apart in the DNA sequences leads to its own complications, mainly in the screening process. Target 3 and 6 are separated by approximately 2.5 kb, making amplifying all four target sites difficult. The full wild type sequence was not possible to amplify consistently. Due to the smaller size of the multi-exon deleted sequences, simple agarose gel resolution allowed for easy identification of successful mutants. After gel extraction, sequencing of the resulting products allowed for identification of the mutation.

4.4 Potential Loss of Gamete Fitness in *parla* Mutants

Of the identified *parla* F_0 mutants, none have passed their mutations to their F1 offspring, at the time of writing this thesis, including those whose gametes were collected and screened positive for germline mutations. Six positive *parla* F_0 mutants with germline mutations, obtained with target 1 and 2 sgRNA, produced only wild type F_1 offspring. Of the multi-exon approach, 12 F_0 mutant zebrafish were screened and so far, none produced mutant F_1 offspring.

Of the four *parla* F_0 mutants that had their gametes screened, heteroduplex bands were observed by PAGE analysis suggesting the presence of indel mutations in the sample. Gametes were obtained 2-3 times per *parla* F_0 mutant and tested for indel mutations by PAGE analysis to confirm these results. While PAGE is more sensitive than the T7E1 analysis, and a single mutant can be observed in a pool of 10 individuals, it is not sensitive enough to recognize a single mutant in a pool of over 100 wild types. Over 100 F_1 offspring were analyzed for each of the *parla* F_0 mutants by PAGE, and none were mutants. This suggests that the *parla* mutations may affect the

viability of the gametes, lending from the function of mammalian PARL in maintaining mitochondrial stability.

PARL inhibits the PINK1/PARKIN mitophagy pathway, actively preventing the degradation of healthy mitochondria. Sperm require a vast supply of energy for motility and oocytes also require large amount of energy produced by mitochondria for oocyte and embryo development. The production of ATP as a form of energy is an oxidatively stressful process and mutations in *parl* could lead to the loss of its protective function, leading to excessive mitophagy, and therefore loss of functionality and fitness of the mutant gametes and embryos. Due to the high germline mutation efficiency in *parlb,* this may suggest a greater functional importance of *parla,* compared to *parlb,* in the case of the PINK1/PARKIN pathway and mitochondrial stability. Alternatively, Parlb may not be as necessary or vital during normal conditions, but may have a more prominent role under specific conditions, for example, in stressful and highly metabolic states.

The *parla* F_0 mutants either became sickly and their gametes could no longer be collected, or they died before further testing could be performed. Once new *parla* multi-exon deleted mutants are identified with germline mutations, the sperm could be collected and observed for decreased motility compared to sperm collected from wild type zebrafish. Sperm and oocytes could also be assessed for viability using Trypan Blue staining and thiazolyl blue tetrazolium bromide (MTT) staining, to evaluate membrane integrity and mitochondrial activity. Normal healthy cells exclude Trypan Blue dye, while nonviable cells will take up the dye(Strober, 2001). MTT assays determine cell metabolic activity by the reduction of yellow tetrazole to purple formazan by NADH-dependent oxidoreductase enzymes (Plachinta *et al.*, 2004). Therefore, cells

with high metabolic rates reduce more tetrazole and become a darker purple in colour. Another common test for oocyte viability is by cathepsin activity assays (Zhang *et al.*, 2008). Depending on the cathepsin studied, the level of apoptosis (cathepsin D) or processing of vitellogenin into yolk proteins (cathepsin B) can be assessed. All assays would compare the gametes of *parla* F_0 mutants and wild type gametes. Further tests on the gametes while under oxidativee stress could also be performed to check for increased sensitivity.

4.5 Parl Proteins are Not Identifiable by Mass Spectrometry with Current Methods

Validation of a null mutation in newly created lines is typically performed at the protein level to ensure knockout. A lack of working antibodies against *parla* and *parlb* in zebrafish led us to utilizing mass spectrometry to identify the Parl proteins in wild type zebrafish. After identification, it was intended for the mutant lines to be screened for their presence to help determine the viability of the knockout. Neither Parla nor Parlb were identified in wild type whole mitochondrial lysate fractions and from gel extracted protein samples from 25-45 kDa.

One possible cause for Parla and Parlb remaining unrecognized in the mass spectrometry analysis is due to low abundance. Their presence could become masked by the high abundance of other proteins in the samples. The whole mitochondrial lysate sample identified approximately 12000 different proteins and the gel extracted sample identified 656 proteins. There is no protein abundance information available for Parlb, but Parla abundance was estimated as 0.68-8.93 ppm (low-average protein abundance) in the whole organism. Protein abundance information was found using PaxDb[4] (http://pax-db.org). While narrowing down the range of protein sizes extracted from protein lysates resolved in an SDS-PAGE would decrease the amount of non-

target protein identified, the actual size of Parla and Parlb in the mature form present in the mitochondria is unknown.

Both Parl proteins are constitutively cleaved of their mitochondrial localizing signal at the α-site when inserted into the inner mitochondrial membrane. Therefore, the full-length protein is unlikely to be seen in the mitochondrial fractions (Sík et al., 2004). Western blot analysis of Parla-Flag and Parlb-Flag proteins indicated Parla is cleaved once, resulting in a band around 31-32 kDa, while Parlb is cleaved twice, producing bands at ~31-32 kDa and ~27-28 kDa (Noble, 2014). Dr. Noble concluded that Parla is likely α-cleaved, while Parlb undergoes α- and β-cleavage. No γ-cleavage was detected as expected since γ-cleavage is associated with destabilization and degradation of PARL in mammals. The predicted theoretical molecular weight of an α-cleaved Parla is ~37 kDa and ~39 kDa in Parlb. The Parla and Parlb bands migrated experimentally further than predicted, and this atypical migration will make extraction of these bands from a SDS-PAGE difficult to perform consistently.

Without properly working antibodies, the exact size of the Parl proteins cannot be determined. Additionally, cytoplasmic fractions are rich in proteins, so attempting to gel extract the full sized 42 kDa Parla and 43 kDa Parlb would be ineffective. Rather than subcellular fractionation, a density gradient protein fractionation using a sucrose or glycerol gradient could be utilized to reduce the size of the protein pool analyzed and bring the low abundant proteins into a dynamic range. Additionally, highly abundant proteins, such as albumin and immunoglobins could be removed using techniques including multiple affinity removal columns, to help enrich the pool with Parla and Parlb.

Another explanation is that neither protein was solubilized and, thus, the proteins were not present in the analyzed sample. Both Parl proteins are multi-pass transmembrane proteins making them particularly difficult to isolate and solubilize. An observation made after Coomassie blue staining was the presence of protein aggregates left in the wells and the interface between the stacking and resolving gels of the SDS-PAGE. It is possible that our target proteins did not solubilize from the start, or precipitated and aggregated while migrating through the SDS-PAGE, leading to abnormal migration and their absence in the gel extracted sample.

Various transmembrane proteins were identified in both types of protein extracts. For the mass spectrometry sample containing proteins extracted from a gel, most of the transmembrane proteins were indeed of the size range 25-45 kDa. However, not all the transmembrane protein identified fit within this size range. The size of proteins identified ranged from 9 kDa to 88 kDa. A few of these proteins are uncharacterized and include TMEM256 (11.7 kDa), TMEM258 (9 kDa) and TMEM50a (50 kDa). The characterized proteins identified outside the expected size range extracted were AFG3L2 (88 kDa) and TOMM70a (79 kDa), both of which undergo proteolytic cleavage events. AFG3L2 undergoes two maturation steps upon insertion into the MIM. First, its MLS is cleaved followed by an additional cleavage of an N-terminal fragment. The second maturation step is autocatalytic, allowing for AFG3L2 to hexamerize with SPG7 (Almontashiri *et al.*, 2014). TOMM70a is also proteolytically cleaved into a mature form, which is about 40 kDa (Sinzel *et al.*, 2016). Therefore, the smaller, cleaved forms of AGF3L2 and TOMM70a were potentially the ones identified by mass spectrometry and thus they migrated as expected. These results suggest that some multi-pass transmembrane proteins are being solubilized, but some may be migrating in an atypical fashion like the uncharacterized proteins. Since western blot

analysis is inconclusive and the exact size and migration of either protein is unknown, further extractions will likely be ineffective until a method for enriching protein lysates with Parla and Parlb is optimized first.

4.6 *Parlb* Mutant Lines May be Resistant to Nonsense Mediated Decay

The mRNA expression of *parlb* was analyzed to determine if the premature translation termination codon in the *parlb* mutants would lead to nonsense mediated decay (NMD) of the aberrant mRNA, resulting in a loss of *parlb* mRNA. NMD is triggered by the presence of premature translation termination codons, identified by their location relative to downstream exon-exon junctions and associated proteins. In zebrafish, this would include exon-exon junction complexes (EJCs) that are left after splicing of the premature mRNA. Upon the first read through of a ribosome along an mRNA, termed the pioneer translation, these EJCs are removed until a stop codon is reached. Normally, the termination codon is in the last exon, and thus the mRNA will contain no EJCs after this stop codon. However, if the ribosome encounters a termination codon in an mRNA which still has bound EJCs afterwards, located at least 50-55 nts downstream, then this termination codon is identified as a PTC. From there, additional proteins are recruited and NMD is initiated.

Studies performed by the Ramao Lab (Inácios *et al.*, 2004; Peixeiro *et al.*, 2012; Pereira *et al.*, 2015) and Izaurralde lab (Behm-Ansmant *et al.*, 2007) showed that PTCs located in close proximity to the start codon (AUG-proximal PTCs) trigger NMD inefficiently. When initiated, NMD normally couples its surveillance complex with eukaryotic translation termination factors and mRNA degradation enzymes. When the PTC is close to the AUG start codon, however, the

cytoplasmic poly(A)-binding protein 1 (PABPC1) binds to the poly(A) tail and with cap-binding complex subunits, eIF4G and the 40S recruitment factor eIF3, as well as the ribosome release factor, eRF3. Due to the short reading frame of an AUG-proximal PTC, the PABPC1 protein and associated cap-binding complex would be situated in close proximity to the PTC. This allows PABPC1 to bind to eRF3, sterically blocking the UPF1-eRF3 interaction required for NMD and thus effectively inhibiting NMD (Peixeiro *et al.*, 2012).

In support of this theory, another study performed by Pereira *et al.* (2015), showed that human β-globin mRNAs, containing AUG-proximal PTCs in the first exon, accumulated to similar levels as those of wild-type β-globin transcripts. Both the *parlb*^{emG9K} and *parlb*^{emD9K} mutant lines contain a CRISPR-Cas9 induced PTC in the first exon of *parlb,* 12 and 39 codons from the AUG start codon respectively. Both can be considered AUG-proximal PTCs. This observation along with the conclusions made from the studies performed in the Ramao lab could explain why neither mutant line showed the expected NMD-induced decrease in *parlb* mRNA expression compared to the wild type. The location of the PTCs prevents NMD initiation by sterically blocking the required protein interactions.

Furthermore, the apparent resistance of AUG-proximal PTCs diminishes as the distance of the PTC to the start codon increases (Inácios *et al.*, 2004; Neu-Yilik *et al.*, 2011; Pereira *et al.*, 2015). As mentioned previously, human β-globin mRNAs containing AUG-proximal PTCs showed NMD resistance. This resistance hinged upon the distance between the PTC and translation start codon. RT-PCR analysis of hβ-globin mRNA with a PTC in codon 39 (β39) resulted in an average of only 2% of the normal mRNA expression (Romão *et al.*, 2000). Analysis of expression of hβ-globin with a PTC in codon 5, 15 and 17 revealed normal levels of mRNA accumulation (70%, 90%,

and 80% respectively) (Neu-Yilik *et al.*, 2011; Romão *et al.*, 2000). Lastly, mRNA containing a PTC at codon 26 was detected at 3% of normal mRNA levels. It was concluded that NMD requires a minimal length of an open reading frame (ORF) for effective activity ((Pereira *et al.*, 2015; Romão *et al.*, 2000).

A similar effect was seen in the qPCR results with *parlb*^{emD9K} homozygotes showing a 30% decrease in *parlb* expression and a 46% increase in *parla* expression, while the *parlb*^{emG9K} line showed no change in expression of all target genes compared to wild type. As stated previously, the G9K line has a predicted PTC 11 codons from the AUG, while the D9K line has a predicted PTC 39 codons from the start codon. Since the G9K line has a more AUG-proximal PTC, and thus a shorter ORF, NMD is more greatly repressed, potentially to the point of almost complete resistance. The D9K line has a more distal PTC to the start codon, and thus can be influenced and degraded by NMD, leading to the slight decrease in *parlb* expression seen in the qPCR results.

The *parlb*^{emD9K} mutant line has a PTC at codon 40, outside the normal range of NMD-resistance, as seen in the human β-globin mRNA study (Romão *et al.*, 2000). One possibility is that another mechanism may be acting instead of NMD. Nonsense-mediated decay is not the only mechanism induced by the presence of a PTC. Previous work on the human transforming growth factor β-receptor type 2 (TGFβR2), showed that mutant cells containing a PTC located at position 273 were resistant to NMD (Hwang and Kim, 2013; Kwon *et al*., 2007). The faulty transcripts were alternatively subjected to nonsense-mediated translational repression (NMTR), which does not require Upf1 and Upf2. NMTR initiates after the formation of the 80S ribosomal complex, with the EJC core components downstream of the PTC acting as negative regulators of translation (Mockenhaupt and Makeyev, 2015). Similarly, neuronally expressed Bak1 mRNA

contain a PTC, obtained via alternative splicing, leading to NMTR rather than NMD (Jakobson *et al*., 2013). While NMTR would account for the unaltered mRNA levels observed, it may not be the specific mechanism functioning in our *parlb*^{emD9K} mutants. The lack of NMD response on RNA levels does not necessarily mean the mutation did not result in functionally-null Parlb.

4.7 Parl Proteins Retain Some Functional Overlap

Phenotype analysis showed that the *parlb* mutants displayed normal wild type characteristics in terms of gross morphology, embryo survival rate, breeding capability, hatching rate and dopaminergic neuron patterning. The absence of an overt phenotype is not unexpected as the Parla protein is still fully functioning and could compensate for any differences in Parlb deficiency. Paralogs have been known to compensate for each other, and it has been seen multiple times that deleting one of the paralogs leads to no phenotypic or fitness consequence, a phenomenon known as genetic buffering (Plata and Vitkup, 2014). Only upon removing the function of both paralogs is a phenotype observed (Diss *et al.*, 2014; Hartman *et al.*, 2001).

Due to the role PARL has in mitophagy and apoptosis, a certain level of genetic robustness is expected to maintain PARL's general function despite environmental or genetic perturbations. In fact, gene duplicates with at least partially redundant function act as a large part of genetic robustness in living organisms. The spatial and temporal expression overlap of *parla* and *parlb* mRNA (Noble *et al.*, 2012) already suggests a level of functional redundancy between the paralogs, allowing them to compensate for each other's loss.

With the decrease in Parlb protein function, it was expected for the expression of *parla* mRNA to increase. Results from the qPCR show little compensatory expression fluctuations in

parla expression in response to *parlb* mutation. Compensation for a loss of protein function does not have to occur at the level of mRNA expression, and mRNA expression levels do not always correlate to protein levels. The compensatory response of *parla* could be at the level of protein translation instead (Diss *et al.*, 2014). Alternatively, it is possible that normal expression of *parla* mRNA is sufficient for normal cellular functioning, and does not require active paralogous compensation (Diss *et al.*, 2014). In fact, DeLuna *et al.* (2010) showed cases in which duplicated genes show a responsive change in transcription due to deletion of one of the paralogs. What was noteworthy for this study, is that the responsiveness of the paralogs depended on the presence of the environmental conditions in which the paralogs are required. In other words, if the function of these genes is required or important under specific circumstances, if you remove those conditions then no compensatory change will occur in expression levels between the paralogs (DeLuna *et al.*, 2010; Diss *et al.*, 2014). The Parl paralogs function to prevent mitophagy and apoptosis when unnecessary, and this function may become more important when the cell is under metabolic stress. Therefore, under normal conditions no compensatory increase in expression of *parla* may be observed due to a lack of Parlb.

Interestingly, qPCR results for the other genes of interest also depict a similar trend: no significant differences were apparent in either mutant line compared to the wild type samples for *Opa1*, *PMPcβ*, *ClpP*, *afg3l2*, nor *dat*. Expresion of thse genes based on qPCR results was more similar to that of the wild type in the *parlb*^{emG9K} mutants compared to the *parlb*^{emD9K} mutants. The absence of a response in gene expression is not unexpected as the Parla protein is still fully functioning and could compensate for any differences in Parlb deficiency. Therefore, no change

would be expected in the mRNA expression of *Opa1* or *dat*, nor *PMPcβ*, *ClpP*, and *afg3l2,* potential proteins that could compensate for the lack of PINK1 cleavage.

Distinct phenotypes were observed when splice blocking MOs against *parla* or *parlb* were injected into wild type zebrafish embryos individually or together. The *parlb* single morphants looked similar to controls while the *parla* single morphants showed an increased proportion of zebrafish with DA neurons with severe mis-patterning in the ventral diencephalon (vDc). The double-morphant phenotype was more severe than that of the two single morphants, with a 40% increase larval mortality. This aggravated phenotype, a form of negative epistasis, indicates functional overlap and genetic redundancy (He *et al.*, 2010; Qian *et al.*, 2010). While revealing a potential buffering relationship between the two paralogous genes, these results also suggest a distinct functional difference between *parla* and *parlb*. The increase in proportion of larvae with severely mis-patterned DA neurons is observed only in the WT *parla* morphants, suggesting that proper DA neuron development may depend principally on Parla function. The increase in larval mortality in the *parla* and *parlb* double morphants suggests that larval survival may require the function of at least one of the *parl* genes.

Overall, *parla* and *parlb* seem to be genetic buffers for each other, with the phenotypic effect of the single *parlb* mutant hidden or buffered by the presence of a compensating gene, *parla.* This does not necessitate a complete functional redundancy and in fact, the presence of both paralogs in modern zebrafish suggests a possible functional divergence. Paralogs are usually transient and tend to diverge over time (Diss *et al.*, 2014). Other than gaining new functions, paralogs can both be retained due to subfunctionalization, the partitioning of the ancestral gene function between the paralogs, allowing for their retention (Plata and Vitkup, 2014). In addition,

the genetic robustness between paralogs can allow for the incorporation and retention of more deleterious mutations than would typically occur, while retaining protein fitness between the paralogs (Tokuriki and Tawfik, 2009). The high degree of stability can result in differing phenotypes between knockouts of either paralog, depending on the mutations that develop, and a greater phenotypic consequence than expected in the double knockout. This phenomenon would result in negative epistasis.

The knockdown of *parlb* leads to no overt phenotype, and thus Parla may be sufficient on its own to compensate for the loss. The knockdown of *parla,* on the other hand, results in severe mis-patterning of the DA neuron in the vDC. In this case, Parlb may not be sufficient on its own to compensate for the loss of Parla, and may have accumulated mutations that would normally be selected against if it was not for the buffering role of Parla. Therefore, loss of Parlb leads to no phenotypic consequence impacting zebrafish fitness. Compared to the human PARL sequence, Parlb is more divergent in amino acid sequence (55% identity), compared to Parla (67% identity). This coincides with the results of the morpholino experiment in which Parlb cannot sufficiently compensate for loss of Parla, while Parla can. Parlb may have accumulated more deleterious mutations over evolution, but remains due to the advantage of genetic buffering. Even so, some functional overlap is expected to be retained as a consequence of similarities in their sequence, regulation and structure.

4.8 Parlb is Impaired in *parlb* Mutants

With the potential for functional redundancy between *parla* and *parlb,* the absence of a discernable phenotype in the *parlb* mutants in terms of dopaminergic neuron patterning could be due to compensation by *parla.* In fact, the results from the morpholino study also indicated no change in the DA neuron patterning and larval mortality in the *parlb* morphants compared to the control morphants (Noble *et al.*, 2012). The loss of *parlb* function could either be due to buffering or compensation by *parla*, or the aberrant phenotype is only apparent under specific circumstances.

Another possibility, is that the *parlb* mutant lines obtained do not have a loss of Parlb function, either due to an undetected alternative start codon or other mechanism. Unfortunately, with a lack of protein data from immunoblot and mass spectrometry analysis, and inconclusive results from mRNA expression data obtained by qRT-PCR, the knockout could not be confirmed. Therefore, we examined the effects of a *parla* knockdown via morpholino injections in the *parlb* mutants compared to its effect in wild type zebrafish.

Injection of *parla* MO into wild type zebrafish embryos led to an increase in proportion of zebrafish larvae with severely mis-patterned vDc DA neurons and wild type mortality rates. Upon injection of the same *parla* MO into the *parlb* mutant lines, $parlb^{emG9K}$ and $parlb^{emD9K}$, a different phenotype was observed, with injected mutants displaying an increase in larval mortality, comparable to the increase seen in wild type zebrafish injected with both *parla* and *parlb* MOs. These results suggest that Parlb protein function is impaired in the *parlb* mutants. In further support of this conclusion, the additional injection of *parlb* MO along with the *parla* MO into the *parlb* mutants, caused no further change in phenotype compared to injection of only *parla* MO.

4.9 Future Directions

Once homozygous *parla* mutants are obtained, whole mount *in situ* hybridization experiments against *th1* can be performed to confirm the mutants mimic the *parla* morphant and the double morphant phenotypes. Morphant phenotypes do not always correlate to mutant phenotypes (Kok *et al.*, 2015), due to morpholino off-target effects or even compensation in the targeted mutants (Rossi *et al.*, 2015). Analysis of the dopaminergic neuron patterning can be observed in *parla* and *parlb* mutant *Tg*(dat:eGFP) zebrafish. Both *parlb*^{emG9K} and *parlb*^{emD9K} mutant lines have been bred into the *Tg*(dat:eGFP) line as well as the *Tg*(dat:MLS-mCHERRY) line. Once the *parla* mutants and eventually double mutants are bred into both transgenic lines, further analysis of dopaminergic neuron patterning can be observed. With the knockout mutants' lines in a *Tg*(dat:MLS-mCHERRY) background, future experiments can be performed to determine if the mutations caused changes in mitochondrial morphology and dynamics. Since Parl plays an important role in stabilizing mitochondria and protecting against unwanted mitophagy, the *parla* mutants, could potentially display increased fragmentation of mitochondria in its dopaminergic neurons (Gomes and Scorrano, 2013; Mortiboys *et al.*, 2008). In addition, loss of both Parla and Parlb protein function through morpholinos led to an increase in larval mortality. Therefore, double knockout mutants for both *parl* paralogs may be lethal, and therefore double heterozygotes for both mutations may be required, rather than homozygote double mutants.

Further qRT-PCR experiments could be performed on potential compensatory enzymes for Parl function. Similarly, changes in protein levels could also be analyzed through mass spectrometry in response to the mutations. Our qRT-PCR results indicated no change in *parla* mRNA expression in the response to *parlb* mutations. The *parla* mutants also displayed a

potential loss in gamete viability and a severe mis-patterning phenotype in the DA neurons of the vDC. One hypothesis to explain these results was that *parlb* may have a more important role in times of stress. To test this hypothesis, experiments could be performed to evaluate the sensitivity of the mutants to reagents that induce oxidative stress, and if the phenotypes in *parlb* mutants change in response to the increased stress. Due to PARL's role in mitophagy and apoptosis, the *parla* and *parlb* knockout zebrafish should be more sensitive than the wild type uninjected zebrafish when exposed to mitochondrial toxins, including rotenone, hydrogen peroxide and paraquat, but not to general deleterious agents like BME, DTT and MG132 (Meulener *et al.*, 2005). If a sensitivity is detected, further experiments characterizing the effect of mitochondrial toxin on dopaminergic neuron patterning in *parl* mutants could also be performed.

5. Conclusion

Through the experiments conducted in this body of work, the CRISPR-Cas9 system of genomic mutagenesis was successfully utilized to create indel mutation in the *parla* and *parlb* genes, as well as exon deletions of up to 1756 bp in *parla* as confirmed by PAGE analysis and sequencing. The *parla* target sgRNA 1 and 2 had a mutational efficiency of 25%, while the sgRNA for multi-exon deletion had an efficiency of 40%. The single *parlb* sgRNA had the highest mutation efficiency at 74%. The differences in mutation efficiency are likely a result of differences in accessibility at each loci for Cas9, due to the early expression of *parlb* coinciding with the time of microinjections. *Parla* mRNA is observed to be expressed 2 hours later. Parla mutants have been identified and line propagation is in progress as of writing this thesis. Two *parlb* mutant lines with premature stop codons were isolated, and termed *parlb*^{emG9K} *and parlb*^{emD9K}. No overt phenotype was observed in the *parlb* mutants in terms of gross morphology, fecundity, larval survival or in the patterning of the dopaminergic (DA) neurons of the ventral diencephalon (vDc).

Immunoblot and mass spectrometry analyses were inconclusive due to a lack of working antibodies and unsuccessful target protein identification, respectively. The *parlb* mRNA levels were examined using qRT-PCR in the *parlb* mutants and no significant differences were found between mutant and wild type. The absence of a response in mRNA levels in *parlb* mutants is potentially a result of the proximity the CRISPR-induced PTCs to the start codon. AUG-codon proximal PTCs display resistance to nonsense mediated decay (NMD) due to their short open reading frames causing steric hindrance between translation termination complexes and NMD complexes, preventing proper NMD initiation (Pereira *et al.*, 2015). In addition, *parla* mRNA levels

in the *parlb* mutants were compared to wild type controls and the results indicate no significant increase in mRNA expression in response to *parlb* mutation. The predicted compensatory response of *parla* could be at the level of protein translation or, alternatively, it is possible that normal expression of *parla* mRNA is sufficient for normal cellular functioning, and does not require active paralogous compensation (Diss *et al.*, 2014).

When splice blocking MOs against *parla* and/or *parlb* were injected into wild type zebrafish embryos and the DA neuron examined, the *parlb* morphants had no change in patterning from wild type, while the *parla* morphants showed an increased proportion of zebrafish with DA neurons displaying severe mis-patterning in the vDc (30% in *parla* morphants; 1% in controls). Double-morphants had a 40% increase in larval mortality, a phenotype more severe than expected based on the phenotypes of the two single morphants. These results suggest a negative epistatic relationship between the paralogs, indicating a genetic buffering system in which *parla* and *parlb* share some form of function overlap. The increase in larval mortality only in the double morphants suggests that larval survival may rely on the function of both *parl* genes. Despite this functional redundancy, the increase in proportion of larvae with severely mis-patterned DA neurons observed specifically in the *parla* morphants, implies that proper DA neuron development may depend on Parla function. These results suggest that a functional divergence between the paralogs may have arisen during evolution.

Whole mount *in situ* hybridization experiments against *th1* were performed on *parlb* mutants injected with *parla* and/or *parlb* MOs. The *parlb* mutants injected with *parla* MO, or *parla* and *parlb* MOs resulted in an increase in larval fatalities, a phenotype shared by wild types injected with both MOs. In fact, no significant difference was observed between all three groups

in terms of the proportions of DA neuron phenotypes observed, and larval mortality. These results confirm Parlb impairment in the *parlb*^{emG9K} and *parlb*^{emD9K} mutants.

Rhomboid proteases like PARL have been identified in all kingdoms of life and constitute an important group of quality control regulators. Studies on these two *parl* genes in zebrafish, an important vertebrate model organism, may prove to be beneficial in the understanding of not only the specific roles played by each of the genes, but on the evolution of paralogs. In turn, investigations on this conserved genetic pathway this will shed light on the function of PARL rhomboid proteases in cellular processes, Parkinson's disease and potentially in the development of therapeutic strategies.

References

Almontashiri, N. A. M., Chen, H. H., Mailloux, R. J., Tatsuta, T., Teng, A. C. T., Mahmoud, A. B., Ho, T., Stewart, N. A. S., Rippstein, P., Harper, M. E., Roberts, R., Willenborg, C., Erdmann, J., Pastore, A., McBride, H. M., Langer, T. and Stewart, A. F. R. (2014). SPG7 Variant Escapes Phosphorylation-Regulated Processing by AFG3L2, Elevates Mitochondrial ROS, and Is Associated with Multiple Clinical Phenotypes. *Cell Rep.* **7**, 834–847.

Behm-Ansmant, I., Gatfield, D., Rehwinkel, J., Hilgers, V. and Izaurralde, E. (2007). A conserved role for cytoplasmic poly(A)-binding protein 1 (PABPC1) in nonsense-mediated mRNA decay. *EMBO J.* **26**, 1591–1601.

Brown, M. S., Ye, J., Rawson, R. B. and Goldstein, J. L. (2000). Regulated intramembrane proteolysis: a control mechanism conserved from bacteria to humans. *Cell* **100**, 391–398.

Cagin, U., Duncan, O. F., Gatt, A. P., Dionne, M. S., Sweeney, S. T. and Bateman, J. M. (2015). Mitochondrial retrograde signaling regulates neuronal function. *Proc. Natl. Acad. Sci.* **112**, E6000–E6009.

Cho, S. W., Kim, S., Kim, J. M. and Kim, J.-S. (2013). Targeted genome engineering in human cells with the Cas9 RNA-guided endonuclease. *Nat. Biotechnol.* **31**, 230–2.

Cipolat, S., Rudka, T., Hartmann, D., Costa, V., Serneels, L., Craessaerts, K., Metzger, K., Frezza, C., Annaert, W., D'Adamio, L., Derks, C., Dejaegere, T., Pellegrini, L., D'Hooge, R., Scorrano, L. and De Strooper, B. (2006). Mitochondrial Rhomboid PARL Regulates Cytochrome c Release during Apoptosis via OPA1-Dependent Cristae Remodeling. *Cell* **126**, 163–175.

Cong, L., Ran, F., Cox, D., Lin, S., Barretto, R., Habib, N., Hsu, P., Wu, X., Jiang, W., Marraffini, L. and Zhang, F. (2013). Multiplex Genome Engineering Using CRISPR/Cas Systems. *Science (80-.).* **339**, 819–822.

Cookson, M. R. (2005). The biochemistry of Parkinson's disease. *Annu Rev Biochem* **74**, 29–52.

Danial, N. N., Gramm, C. F., Scorrano, L., Zhang, C.-Y., Krauss, S., Ranger, A. M., Datta, S. R., Greenberg, M. E., Licklider, L. J., Lowell, B. B., Gygi, S. P. and Korsmeyer, S. J. (2003). BAD and glucokinase reside in a mitochondrial complex that integrates glycolysis and apoptosis. *Nature* **424**, 952–6.

Dawson, T. M. and Dawson, V. L. (2003). Rare genetic mutations shed light on the pathogenesis of Parkinson disease. *J. Clin. Invest.* **111**, 145–51.

Day, B. J., Patel, M., Calavetta, L., Chang, L. Y. and Stamler, J. S. (1999). A mechanism of paraquat toxicity involving nitric oxide synthase. *Proc. Natl. Acad. Sci. U. S. A.* **96**, 12760–5.

Deas, E., Plun-Favreau, H., Gandhi, S., Desmond, H., Kjaer, S., Loh, S. H. Y., Renton, A. E. M., Harvey, R. J., Whitworth, A. J., Martins, L. M., Abramov, A. Y. and Wood, N. W. (2011). PINK1 cleavage at position A103 by the mitochondrial protease PARL. *Hum. Mol. Genet.* **20**, 867–879.

DeLuna, A., Springer, M., Kirschner, M. W. and Kishony, R. (2010). Need-based up-regulation of

protein levels in response to deletion of their duplicate genes. *PLoS Biol.* **8**,.

Diss, G., Ascencio, D., Deluna, A. and Landry, C. R. (2014). Molecular mechanisms of paralogous compensation and the robustness of cellular networks. *J. Exp. Zool. Part B Mol. Dev. Evol.* **322**, 488–499.

Doench, J. G., Hartenian, E., Graham, D. B., Tothova, Z., Hegde, M., Smith, I., Sullender, M., Ebert, B. L., Xavier, R. J. and Root, D. E. (2014). Rational design of highly active sgRNAs for CRISPR-Cas9–mediated gene inactivation. *Nat. Biotechnol.* **32**, 1262–7.

Doudna, J. A. and Charpentier, E. (2014). The new frontier of genome engineering with CRISPR-Cas9. *Science (80-.).* **346**, 1258096–1258096.

Durcan, T. M. and Fon, E. A. (2015). The three P's of mitophagy: PARKIN, PINK1, and post-translational modifications. *Genes Dev.* **29**, 989–999.

Estep, J. A., Sternburg, E. L., Sanchez, G. A. and Karginov, F. V (2016). Immunoblot screening of CRISPR/Cas9-mediated gene knockouts without selection. *BMC Mol. Biol.* **17**, 9.

Farrer, M. J. (2006). Genetics of Parkinson disease: paradigm shifts and future prospects. *Nat. Rev. Genet.* **7**, 306–318.

Ferrer, I. (2011). Neuropathology and neurochemistry of nonmotor symptoms in Parkinson's disease. *Parkinsons. Dis.* **2011**, 708404.

Freeman, M. (2004). Proteolysis within the membrane: rhomboids revealed. *Nat. Rev. Mol. Cell Biol.* **5**, 188–197.

Freeman, M. (2008). Rhomboid proteases and their biological functions. *Annu. Rev. Genet.* **42**, 191–210.

Gagnon, J. A., Valen, E., Thyme, S. B., Huang, P., Ahkmetova, L., Pauli, A., Montague, T. G., Zimmerman, S., Richter, C. and Schier, A. F. (2014). Efficient mutagenesis by Cas9 protein-mediated oligonucleotide insertion and large-scale assessment of single-guide RNAs. *PLoS One* **9**, 5–12.

Gaj, T., Gersbach, C. A. and Barbas, C. F. (2013). ZFN, TALEN, and CRISPR/Cas-based methods for genome engineering. *Trends Biotechnol.* **31**, 397–405.

Gomes, L. C. and Scorrano, L. (2013). Mitochondrial morphology in mitophagy and macroautophagy. *Biochim. Biophys. Acta - Mol. Cell Res.* **1833**, 205–212.

Gottlieb, E. (2006). OPA1 and PARL Keep a Lid on Apoptosis. *Cell* **126**, 27–29.

Green, D. R. and Kroemer, G. (2004). The pathophysiology of mitochondrial cell death. *Science* **305**, 626–9.

Gross, A., McDonnell, J. M. and Korsmeyer, S. J. (1999). BCL-2 family members and the mitochondria in apoptosis. *Genes Dev.* **13**, 1899–1911.

Hartman, J. L., Garvik, B. and Hartwell, L. (2001). Principles for the Buffering of Genetic Variation. *Science (80-.).* **291**, 1001–1004.

Hauser, D. N. and Hastings, T. G. (2013). Mitochondrial dysfunction and oxidative stress in Parkinson's disease and monogenic parkinsonism. *Neurobiol. Dis.* **51**, 35–42.

He, X., Qian, W., Wang, Z., Li, Y. and Zhang, J. (2010). Prevalent positive epistasis in Escherichia coli and Saccharomyces cerevisiae metabolic networks. *Nat. Genet.* **42**, 272–6.

Herlan, M., Vogel, F., Bornhövd, C., Neupert, W. and Reichert, A. S. (2003). Processing of Mgm1 by the rhomboid-type protease Pcp1 is required for maintenance of mitochondrial morphology and of mitochondrial DNA. *J. Biol. Chem.* **278**, 27781–27788.

Herlan, M., Bornhövd, C., Hell, K., Neupert, W. and Reichert, A. S. (2004). Alternative topogenesis of Mgm1 and mitochondrial morphology depend on ATP and a functional import motor. *J. Cell Biol.* **165**, 167–173.

Hill, R. B. and Pellegrini, L. (2010). The PARL family of mitochondrial rhomboid proteases. *Semin. Cell Dev. Biol.* **21**, 582–592.

Hill, R. B. and Pellegrini, L. (2011). NIH Public Access. **21**, 582–592.

Horvath, P. and Barrangou, R. (2013). RNA-guided genome editing à la carte. *Cell Res.* **23**, 733–4.

Hsu, P. D., Lander, E. S. and Zhang, F. (2014). Development and applications of CRISPR-Cas9 for genome engineering. *Cell* **157**, 1262–1278.

Hwang, J. and Kim, Y. K. (2013). When a ribosome encounters a premature termination codon. *BMB Rep.* **46**, 9–16.

Hwang, W. Y., Fu, Y., Reyon, D., Maeder, M. L., Tsai, S. Q., Sander, J. D., Peterson, R. T., Yeh, J. R. and Joung, J. K. (2013). Efficient genome editing in zebrafish using a CRISPR-Cas system. *Nat Biotechnol* **31**, 227–229.

Imai, Y. (2012). Mitochondrial Regulation by PINK1-Parkin Signaling. *ISRN Cell Biol.* **2012**, 1–15.

Inácios, Â., Silva, A. L., Pinto, J., Ji, X., Morgado, A., Almeida, F., Faustino, P., Lavinha, J., Liebhaber, S. A. and Romão, L. (2004). Nonsense mutations in close proximity to the initiation codon fail to trigger full nonsense-mediated mRNA decay. *J. Biol. Chem.* **279**, 32170–32180.

Jakobson, M., Jakobson, M., Llano, O., Palgi, J. and Arumäe, U. (2013). Multiple mechanisms repress N-Bak mRNA translation in the healthy and apoptotic neurons. *Cell Death Dis.* **4**, e777.

Jankovic, J. (2008). Parkinson's disease: clinical features and diagnosis. *J. Neurol. Neurosurg. Psychiatry* **79**, 368–376.

Jeyaraju, D. V, Xu, L., Letellier, M.-C., Bandaru, S., Zunino, R., Berg, E. a, McBride, H. M. and Pellegrini, L. (2006). Phosphorylation and cleavage of presenilin-associated rhomboid-like protein (PARL) promotes changes in mitochondrial morphology. *Proc. Natl. Acad. Sci. U. S. A.* **103**, 18562–7.

Jeyaraju, D. V, McBride, H. M., Hill, R. B. and Pellegrini, L. (2011). Structural and mechanistic basis of Parl activity and regulation. *Cell Death Differ.* **18**, 1531–1539.

Jin, S. M., Lazarou, M., Wang, C., Kane, L. A., Narendra, D. P. and Youle, R. J. (2010). Mitochondrial membrane potential regulates PINK1 import and proteolytic destabilization by PARL. *J. Cell Biol.* **191**, 933–942.

Jinek, M., Chylinski, K., Fonfara, I., Hauer, M., Doudna, J. A. and Charpentier, E. (2012). A Programmable Dual-RNA – Guided DNA Endonuclease in Adaptice Bacterial Immunity. *Science* **337**, 816–822.

Kimmel, C. B., Ballard, W. W., Kimmel, S. R., Ullmann, B. and Schilling, T. F. (1995). Stages of embryonic development of the zebrafish. *Dev. Dyn.* **203**, 253–310.

Klein, C. and Schlossmacher, M. G. (2006). The genetics of Parkinson disease: Implications for neurological care. *Nat. Clin. Pract. Neurol.* **2**, 136–46.

Kok, F. O., Shin, M., Ni, C. W., Gupta, A., Grosse, A. S., vanImpel, A., Kirchmaier, B. C., Peterson-Maduro, J., Kourkoulis, G., Male, I., DeSantis, D. F., Sheppard-Tindell, S., Ebarasi, L., Betsholtz, C., Schulte-Merker, S., Wolfe, S. A. and Lawson, N. D. (2015). Reverse genetic screening reveals poor correlation between morpholino-induced and mutant phenotypes in zebrafish. *Dev. Cell* **32**, 97–108.

Koonin, E. V, Makarova, K. S., Rogozin, I. B., Davidovic, L., Letellier, M.-C. and Pellegrini, L. (2003). The rhomboids: a nearly ubiquitous family of intramembrane serine proteases that probably evolved by multiple ancient horizontal gene transfers. *Genome Biol.* **4**, R19.

Kubli, D. A. and Gustafsson, Å. B. (2012). Mitochondria and mitophagy: The yin and yang of cell death control. *Circ. Res.* **111**, 1208–1221.

Kuscu, C., Arslan, S., Singh, R., Thorpe, J. and Adli, M. (2014). Genome-wide analysis reveals characteristics of off-target sites bound by the Cas9 endonuclease. *Nat Biotechnol* **32**, 677–683.

Kwon, T. Y., Long, S. L., Kim, N. G., Hyun, J. K., Kwi, H. K., Chwae, Y. J., Kyoung, M. K., Yoon, K. K., Sung, M. P., Sung, K. J. and Kim, H. (2007). Selective translational repression of truncated proteins from frameshift mutation-derived mRNAs in tumors. *PLoS Biol.* **5**, 1098–1109.

Langston, J. W., Ballard, P., Tetrud, J. W. and Irwin, I. (1983). Chronic Parkinsonism in humans due to a product of meperidine-analog synthesis. *Science* **219**, 979–80.

Lazarou, M., Jin, S. M., Kane, L. A. and Youle, R. J. (2012). Role of PINK1 Binding to the TOM Complex and Alternate Intracellular Membranes in Recruitment and Activation of the E3 Ligase Parkin. *Dev. Cell* **22**, 320–333.

Lemberg, M. K. (2013). Sampling the membrane: Function of rhomboid-family proteins. *Trends Cell Biol.* **23**, 210–217.

Lemberg, M. K. and Freeman, M. (2007). Functional and evolutionary implications of enhanced genomic analysis of rhomboid intramembrane proteases. *Genome Res.* **17**, 1634–1646.

Lemberg, M. K., Menendez, J., Misik, A., Garcia, M., Koth, C. M. and Freeman, M. (2005). Mechanism of intramembrane proteolysis investigated with purified rhomboid proteases. *EMBO J.* **24**, 464–72.

Li, J., Zhang, B., Ren, Y., Gu, S., Xiang, Y., Huang, C. and Du, J. (2015). Intron targeting-mediated and endogenous gene integrity-maintaining knockin in zebrafish using the CRISPR/Cas9 system. *Cell Res.* 634–637.

Liu, H., Wei, Z., Dominguez, A., Li, Y., Wang, X. and Qi, L. S. (2015). CRISPR-ERA: A comprehensive

design tool for CRISPR-mediated gene editing, repression and activation. *Bioinformatics* **31**, 3676–3678.

Liu, D., Hu, R., Palla, K. J., Tuskan, G. A. and Yang, X. (2016). Advances and perspectives on the use of CRISPR/Cas9 systems in plant genomics research. *Curr. Opin. Plant Biol.* **30**, 70–77.

Lu, W., Karuppagounder, S. S., Springer, D. A., Allen, M. D., Zheng, L., Chao, B., Zhang, Y., Dawson, V. L., Dawson, T. M. and Lenardo, M. (2014). Genetic deficiency of the mitochondrial protein PGAM5 causes a Parkinson's-like movement disorder. *Nat. Commun.* **5**, 4930.

Mali, P., Yang, L., Esvelt, K. M., Aach, J., Guell, M., DiCarlo, J. E., Norville, J. E., Church, G. M., Wiedenheft, B., Sternberg, S. H., Doudna, J. A., Bhaya, D., Davison, M., Barrangou, R., Terns, M. P., Terns, R. M., Jinek, M., Gasiunas, G., Barrangou, R., Horvath, P., Siksnys, V., Sapranauskas, R., Brummelkamp, T. R., Bernards, R., Agami, R., Miyagishi, M., Taira, K., Deltcheva, E., Zou, J., Mali, P., Huang, X., Dowey, S. N., Cheng, L., Sanjana, N. E., Lee, J. H., Hockemeyer, D., Kosuri, S., Pattanayak, V., Ramirez, C. L., Joung, J. K., Liu, D. R., King, N. M., Cohen-Haguenauer, O., Kim, Y. G., Cha, J., Chandrasegaran, S., Rebar, E. J., Pabo, C. O., Boch, J., Moscou, M. J., Bogdanove, A. J., Khalil, A. S., Collins, J. J., Purnick, P. E., Weiss, R., Zou, J., Holt, N., Urnov, F. D., Lombardo, A., Li, H., Makarova, K. S., Horvath, P., Barrangou, R., Deveau, H., Ploeg, J. R. van der, Rho, M., Wu, Y. W., Tang, H., Doak, T. G., Ye, Y., Pride, D. T., Garneau, J. E., Esvelt, K. M., Carlson, J. C., Liu, D. R., Barrangou, R., Horvath, P., Kent, W. J., Dreszer, T. R., Karolchik, D., Quinlan, A. R., Hall, I. M., Langmead, B., Trapnell, C., Pop, M., Salzberg, S. L., Lorenz, R., Mathews, D. H., Sabina, J., Zuker, M., Turner, D. H., Thurman, R. E., Xu, Q., Schlabach, M. R., Hannon, G. J. and Elledge, S. J. (2013). RNA-guided human genome engineering via Cas9. *Science* **339**, 823–6.

McQuibban, G., Saurya, S. and Freeman, M. (2003). Mitochondrial membrane remodelling regulated by a conserved rhomboid protease. *Nature* **423**, 537–541.

McQuibban, G. A., Lee, J. R., Zheng, L., Juusola, M. and Freeman, M. (2006). Normal Mitochondrial Dynamics Requires Rhomboid-7 and Affects Drosophila Lifespan and Neuronal Function. *Curr. Biol.* **16**, 982–989.

Mcteague, W. C., Schebywolok, T., Paterson, J., Zuloaga, J., Varin, M. P., Halliday, W., Nshogozabahizi, J. C., Choi, K., Wilson, L. D., Camargo, R. De, Groulx, A., Robillard, C., Akimenko, M. A., White, P., Gillespie, L., Brown, A., Demers, G. B., Lewis, J., Ferron, J. M. and Trudeau, V. (2015). BIO 5900/8900 Seminar Schedule – Fall 2014 - Winter 2015.

Meissner, C., Lorenz, H., Weihofen, A., Selkoe, D. J. and Lemberg, M. K. (2011). The mitochondrial intramembrane protease PARL cleaves human Pink1 to regulate Pink1 trafficking. *J. Neurochem.* **117**, 856–867.

Meulener, M., Whitworth, A. J., Armstrong-Gold, C. E., Rizzu, P., Heutink, P., Wes, P. D., Pallanck, L. J. and Bonini, N. M. (2005). Drosophila DJ-1 mutants are selectively sensitive to environmental toxins associated with Parkinson's disease. *Curr. Biol.* **15**, 1572–1577.

Miyazaki, I. and Asanuma, M. (2008). Dopaminergic neuron-specific oxidative stress caused by dopamine itself. *Acta Med. Okayama* **62**,.

Mockenhaupt, S. and Makeyev, E. V. (2015). Non-coding functions of alternative pre-mRNA splicing in development. *Semin. Cell Dev. Biol.* **47–48**, 32–39.

Moreno-Mateos, M. A., Vejnar, C. E., Beaudoin, J., Fernandez, J. P., Mis, E. K., Khokha, M. K. and Giraldez, A. J. (2015). CRISPRscan: designing highly efficient sgRNAs for CRISPR-Cas9 targeting in vivo. *Nat. Methods* **12**, 982–8.

Mortiboys, H., Thomas, K. J., Koopman, W. J. H., Klaffke, S., Abou-Sleiman, P., Olpin, S., Wood, N. W., Willems, P. H. G. M., Smeitink, J. A. M., Cookson, M. R. and Bandmann, O. (2008). Mitochondrial function and morphology are impaired in parkin-mutant fibroblasts. *Ann. Neurol.* **64**, 555–565.

Neu-Yilik, G., Amthor, B., Gehring, N. H., Bahri, S., Paidassi, H., Hentze, M. W. and Kulozik, A. E. (2011). Mechanism of escape from nonsense-mediated mRNA decay of human beta-globin transcripts with nonsense mutations in the first exon. *RNA* **17**, 843–54.

Noble, S., Ismail, A., Godoy, R., Xi, Y. and Ekker, M. (2012). Zebrafish Parla- and Parlb-deficiency affects dopaminergic neuron patterning and embryonic survival. *J. Neurochem.* **122**, 196–207.

Noble, S., Godoy, R., Affaticati, P. and Ekker, M. (2015). Transgenic zebrafish expressing mCherry in the mitochondria of dopaminergic neurons. *Zebrafish* **12**, 349–56.

Olanow, C. W. and Tatton, W. G. (1999). Etiology and pathogenesis of Parkinson's disease. *Annu. Rev. Neurosci.* **22**, 123–144.

Peixeiro, I., Inácio, Â., Barbosa, C., Silva, A. L., Liebhaber, S. A. and Romão, L. (2012). Interaction of PABPC1 with the translation initiation complex is critical to the NMD resistance of AUG-proximal nonsense mutations. *Nucleic Acids Res.* **40**, 1160–1173.

Pellegrini, L. and Scorrano, L. (2007). A cut short to death: Parl and Opa1 in the regulation of mitochondrial morphology and apoptosis. *Cell Death Differ.* **14**, 1275–1284.

Pellegrini, L., Passer, B. J., Canelles, M., Lefterov, I., Ganjei, J. K., Fowlkes, B. J., Koonin, E. V. and D'Adamio, L. (2001). PAMP and PARL, two novel putative metalloproteases interacting with the COOH-terminus of Presenilin-1 and -2. *J. Alzheimers. Dis.* **3**, 181–190.

Pereira, F. J. C., Teixeira, A., Kong, J., Barbosa, C., Silva, A. L., Marques-Ramos, A., Liebhaber, S. A. and L., R. (2015). Resistance of mRNAs with AUG-proximal nonsense mutations to nonsense-mediated decay reflects variables of mRNA structure and translational activity. *Nucleic Acids Res.* **43**, 6528–6544.

Phasukkijwatana, N., Kunhapan, B., Stankovich, J., Chuenkongkaew, W. L., Thomson, R., Thornton, T., Bahlo, M., Mushiroda, T., Nakamura, Y., Mahasirimongkol, S., Tun, A. W., Srisawat, C., Limwongse, C., Peerapittayamongkol, C., Sura, T., Suthammarak, W. and Lertrit, P. (2010). Genome-wide linkage scan and association study of PARL to the expression of LHON families in Thailand. *Hum. Genet.* **128**, 39–49.

Plachinta, M., Zhang, T. and Rawson, D. M. (2004). Studies on cryoprotectant toxicity to zebrafish (Danio rerio) oocytes. *Cryo-Letters* **25**, 415–424.

Plata, G. and Vitkup, D. (2014). Genetic robustness and functional evolution of gene duplicates.

Nucleic Acids Res. **42**, 2405–2414.

Polymeropoulos, M. H., Lavedan, C., Leroy, E., Ide, S. E., Dehejia, A., Dutra, A., Pike, B., Root, H., Rubenstein, J., Boyer, R., Stenroos, E. S., Chandrasekharappa, S., Athanassiadou, A., Papapetropoulos, T., Johnson, W. G., Lazzarini, A. M., Duvoisin, R. C., Di Iorio, G., Golbe, L. I., Nussbaum, R. L., Lazarrini, A. M., Golbe, L. I., Polymeropoulos, M. H., Uèda, K., Chen, X., Shitasaki, Y., Iwai, A., Weinreb, P. H., Jensen, P. H., Jensen, P. H., Maroteaux, L., Scheller, R. H., Doty, R. L., Pearce, R. K., Hawkes, C. H., Daniel, S. E., George, J. M., Perez-Tur, J., Sherrington, R., Sorbi, S., Wasco, W., Levy-Lahad, E., Rogaev, E. I. and Hsiao, K. (1997). Mutation in the alpha-synuclein gene identified in families with Parkinson's disease. *Science* **276**, 2045–7.

Popp, M. W. and Maquat, L. E. (2016). Leveraging rules of nonsense-mediated mRNA decay for genome engineering and personalized medicine. *Cell* **165**, 1319–1332.

Qi, L. S., Larson, M. H., Gilbert, L. A., Doudna, J. A., Weissman, J. S., Arkin, A. P. and Lim, W. A. (2013). Repurposing CRISPR as an RNA-γuided platform for sequence-specific control of gene expression. *Cell* **152**, 1173–1183.

Qian, W., Liao, B. Y., Chang, A. Y. F. and Zhang, J. (2010). Maintenance of duplicate genes and their functional redundancy by reduced expression. *Trends Genet.* **26**, 425–430.

Ran, F. A., Hsu, P. D., Wright, J., Agarwala, V., Scott, D. A. and Zhang, F. (2013). Genome engineering using the CRISPR-Cas9 system. *Nat Protoc* **8**, 2281–2308.

Richardson, J. R., Quan, Y., Sherer, T. B., Greenamyre, J. T. and Miller, G. W. (2005). Paraquat neurotoxicity is distinct from that of MPTP and rotenone. *Toxicol. Sci.* **88**, 193–201.

Rink, E. and Wullimann, M. F. (2002). Development of the catecholaminergic system in the early zebrafish brain: An immunohistochemical study. *Dev. Brain Res.* **137**, 89–100.

Rizzuto, R., Bernardi, P. and Pozzan, T. (2000). Mitochondria as all-round players of the calcium game. *J. Physiol.* **529 Pt 1**, 37–47.

Romão, L., Inácio, A., Santos, S., Avila, M., Faustino, P., Pacheco, P., Lavinha, J., Frischmeyer, P., Dietz, H., Nilsson, G., Belasco, J., Cohen, S., Gabain, A. von, Losson, R., Lacroute, F., Zhang, S., Ruiz-Echevarria, M., Quan, Y., Peltz, S., Vancanneyt, G., Rosahl, S., Willmitzer, L., Hoof, A. van, Green, P., Kessler, O., Chasin, L., Urlaub, G., Mitchell, P., Ciudad, C., Chasin, L., Cheng, J., Fogel-Petrovic, M., Maquat, L., Carter, M., Doskow, J., Morris, P., Baserga, S., Benz, E., Maquat, L., Thermann, R., Neu-Yilik, G., Deters, A., Zhang, J., Sun, X., Qian, Y., Maquat, L., Nagy, E., Maquat, L., Hentze, M., Kulozik, A., Buzina, A., Shulman, M., Takeshita, K., Forget, B., Scarpa, A., Benz, E., Baserga, S., Benz, E., Lim, S., Sigmund, C., Gross, K., Maquat, L., Lim, S., Maquat, L., Enssle, J., Kugler, W., Hentze, M., Kulozik, A., Kugler, W., Enssle, J., Hentze, M., Kulozik, A., Hall, G., Thein, S., Ho, P., Wickramasinghe, S., Rees, D., Lee, M., Eden, A., Thein, S., Russell, E., Liebhaber, A., Orkin, S., Kazazian, H., Antonarakis, S., Ribeiro, L., Baysal, E., Kutlar, F., Kozak, M., Zhang, J. and Maquat, L. (2000). Nonsense mutations in the human beta-globin gene lead to unexpected levels of cytoplasmic mRNA accumulation. *Blood* **96**, 2895–901.

Rossi, A., Kontarakis, Z., Gerri, C., Nolte, H., Hölper, S., Krüger, M. and Stainier, D. Y. R. (2015).

Genetic compensation induced by deleterious mutations but not gene knockdowns. *Nature* **Aug 13**, 230–3.

Schapira, A. H. and Jenner, P. (2011). Etiology and Pathogenesis of Parkinson ' s Disease. *Mov. Disord.* **26**, 1049–1055.

Sekine, S., Kanamaru, Y., Koike, M., Nishihara, A., Okada, M., Kinoshita, H., Kamiyama, M., Maruyama, J., Uchiyama, Y., Ishihara, N., Takeda, K. and Ichijo, H. (2012). Rhomboid protease PARL mediates the mitochondrial membrane potential loss-induced cleavage of PGAM5. *J. Biol. Chem.* **287**, 34635–34645.

Selderslaghs, I. W. T., Van Rompay, A. R., De Coen, W. and Witters, H. E. (2009). Development of a screening assay to identify teratogenic and embryotoxic chemicals using the zebrafish embryo. *Reprod. Toxicol.* **28**, 308–320.

Shen, B., Zhang, J., Wu, H., Wang, J., Ma, K., Li, Z., Zhang, X., Zhang, P. and Huang, X. (2013). Generation of gene-modified mice via Cas9/RNA-mediated gene targeting. *Cell Res.* **23**, 720–3.

Shi, G. and McQuibban, G. A. (2017). The Mitochondrial Rhomboid Protease PARL Is Regulated by PDK2 to Integrate Mitochondrial Quality Control and Metabolism. *Cell Rep.* **18**, 1458–1472.

Shi, G., Lee, J. R., Grimes, D. A., Racacho, L., Ye, D., Yang, H., Ross, O. A., Farrer, M., McQuibban, G. A. and Bulman, D. E. (2011). Functional alteration of PARL contributes to mitochondrial dysregulation in Parkinson's disease. *Hum. Mol. Genet.* **20**, 1966–1974.

Sík, A., Passer, B. J., Koonin, E. V. and Pellegrini, L. (2004). Self-regulated cleavage of the mitochondrial intramembrane-cleaving protease PARL yields P-beta, a nuclear-targeted peptide. *J. Biol. Chem.* **279**, 15323–15329.

Sinzel, M., Tan, T., Wendling, P., Kalbacher, H., Özbalci, C., Chelius, X., Westermann, B., Brügger, B., Rapaport, D. and Dimmer, K. S. (2016). Mcp 3 is a novel mitochondrial outer membrane protein that follows a unique IMP-dependent biogenesis pathway. *EMBO Rep.* **17**, 965–981.

Steele, S. L., Prykhozhij, S. V. and Berman, J. N. (2014). Zebrafish as a model system for mitochondrial biology and diseases. *Transl. Res.* **163**, 79–98.

Strober, W. (2001). Trypan blue exclusion test of cell viability. *Curr. Protoc. Immunol.* **Appendix 3**, Appendix 3B.

Sulzer, D., Cragg, S. J. and Rice, M. E. (2016). Striatal dopamine neurotransmission: Regulation of release and uptake. *Basal Ganglia* **6**, 123–148.

Thisse, C. and Thisse, B. (2008). High-resolution in situ hybridization to whole-mount zebrafish embryos. *Nat. Protoc.* **3**, 59–69.

Tokuriki, N. and Tawfik, D. S. (2009). Stability effects of mutations and protein evolvability. *Curr. Opin. Struct. Biol.* **19**, 596–604.

Urban, S. and Dickey, S. W. (2011). The rhomboid protease family: a decade of progress on function and mechanism. *Genome Biol.* **12**, 231.

Urban, S. and Freeman, M. (2002). Intramembrane proteolysis controls diverse signalling

pathways throughout evolution. *Curr. Opin. Genet. Dev.* **12**, 512–518.

Varshney, G. K., Pei, W., Lafave, M. C., Idol, J., Xu, L., Gallardo, V., Carrington, B., Bishop, K., Jones, M., Li, M., Harper, U., Huang, S. C., Prakash, A., Chen, W., Sood, R., Ledin, J. and Burgess, S. M. (2015). High-throughput gene targeting and phenotyping in zebrafish using CRISPR/Cas9. *Genome Res.* **25**, 1030–1042.

Walder, K., Kerr-Bayles, L., Civitarese, A., Jowett, J., Curran, J., Elliott, K., Trevaskis, J., Bishara, N., Zimmet, P., Mandarino, L., Ravussin, E., Blangero, J., Kissebah, A. and Collier, G. R. (2005). The mitochondrial rhomboid protease PSARL is a new candidate gene for type 2 diabetes. *Diabetologia* **48**, 459–468.

Wang, Y., Maegawa, S., Akiyama, Y. and Ha, Y. (2007). The Role of L1 Loop in the Mechanism of Rhomboid Intramembrane Protease GlpG. *J. Mol. Biol.* **374**, 1104–1113.

Wang, T., Wei, J. J., Sabatini, D. M. and Lander, E. S. (2014). Genetic screens in human cells using the CRISPR-Cas9 system. *Science* **343**, 80–4.

Weihofen, A. and Martoglio, B. (2003). Intramembrane-cleaving proteases: Controlled liberation of proteins and bioactive peptides. *Trends Cell Biol.* **13**, 71–78.

Westerfield, M. (2007). The Zebrafish Book. A Guide for the Laboratory Use of Zebrafish (Danio rerio), 5th Edition. *Univ. Oregon Press. Eugene*.

Whitworth, A. J., Lee, J. R., Ho, V. M.-W., Flick, R., Chowdhury, R. and McQuibban, G. A. (2008). Rhomboid-7 and HtrA2/Omi act in a common pathway with the Parkinson's disease factors Pink1 and Parkin. *Dis. Model. Mech.* **1**, 168–174.

Wilkinson, R. N., Elworthy, S., Ingham, P. W. and van Eeden, F. J. M. (2013). A method for high-throughput PCR-based genotyping of larval zebrafish tail biopsies. *Biotechniques* **55**, 314–316.

Xi, Y., Ryan, J., Noble, S., Yu, M., Yilbas, A. E. and Ekker, M. (2010). Impaired dopaminergic neuron development and locomotor function in zebrafish with loss of pink1 function. *Eur. J. Neurosci.* **31**, 623–633.

Xu, H., Xiao, T., Chen, C. H., Li, W., Meyer, C. A., Wu, Q., Wu, D., Cong, L., Zhang, F., Liu, J. S., Brown, M. and Liu, X. S. (2015). Sequence determinants of improved CRISPR sgRNA design. *Genome Res.* **25**, 1147–1157.

Yamamoto, K., Ruuskanen, J. O., Wullimann, M. F. and Vernier, P. (2011). Differential expression of dopaminergic cell markers in the adult zebrafish forebrain. *J. Comp. Neurol.* **519**, 576–598.

Zhang, T., Rawson, D. M., Tosti, L. and Carnevali, O. (2008). Cathepsin activities and membrane integrity of zebrafish (Danio rerio) oocytes after freezing to -196 °C using controlled slow cooling. *Cryobiology* **56**, 138–143.

Zhang, F., Wen, Y. and Guo, X. (2014). CRISPR/Cas9 for genome editing: Progress, implications and challenges. *Hum. Mol. Genet.* **23**, 40–46.

Zhu, X., Xu, Y., Yu, S., Lu, L., Ding, M., Cheng, J., Song, G., Gao, X., Yao, L., Fan, D., Meng, S., Zhang, X., Hu, S. and Tian, Y. (2014). An efficient genotyping method for genome-modified animals and human cells generated with CRISPR/Cas9 system. *Sci Rep* **4**, 6420.

Appendix A

Figure A.1: Partial DNA sequence of sgRNA expression vector pDR274 in the opening reading from of the M13 promoter. The sequence of an M13 primer binding site is highlighted in purple, the T7 promoter is shown as bold, italicized and underlined text, and the transcriptional start site (+1) is highlighted in green. The pair of BsaI restriction sites used for cloning are indicated in bold text and the DraI restriction site used to linearize the plasmid for run-off transcription is highlighted in grey. All cut sites are indicated with "▾NNNNN▴". The “stuffer” sequence that is replaced with the annealed oligonucleotides to create customized sgRNAs is highlighted in yellow and the remainder of the full length sgRNA is shown as underlined text.

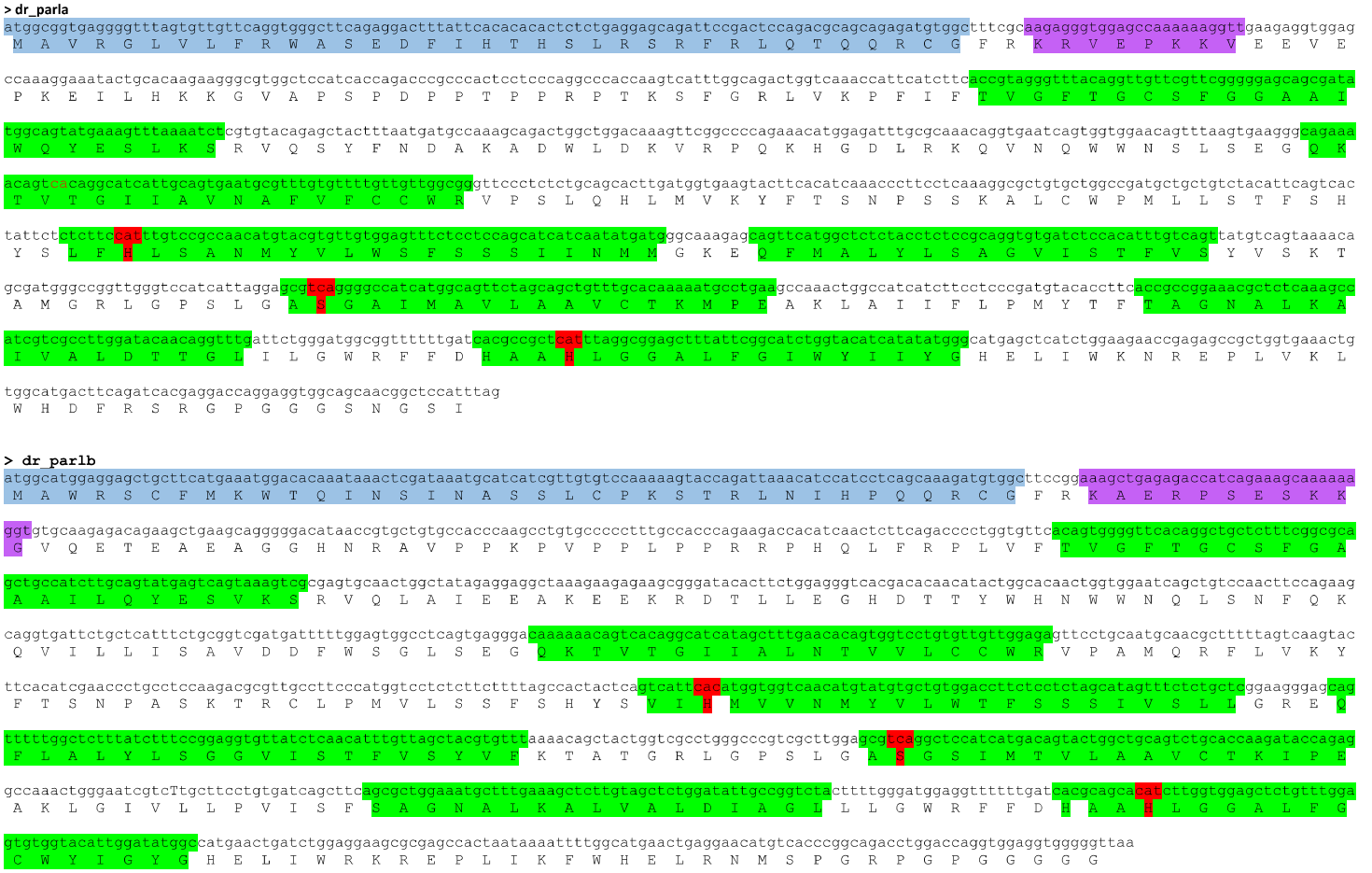

Figure A.2: DNA and amino acid sequences aligned for *parla* and *parlb* paralogs. Functional domains and catalytic sites are indicated by colour: The mitochondrial localizing signal is shaded in blue, the nucleur localizing signal is shaded in purple, transmembrane domains are shaded in green, and catalytic sites are red.

Appendix B

Permission to use Figures:

Figure 1.1 &1.3: Urban, S. and Dickey, S. W. (2011). The rhomboid protease family: a decade of progress on function and mechanism. *Genome Biol.* **12**, 231.

Free articles

All articles in BioMed Central journals are available online without charge or other barriers to access. The following journals have published a small number of articles that, while freely accessible, are not open access as outlined in the section above:

Alzheimer's Research & Therapy
Arthritis Research & Therapy
Breast Cancer Research
Critical Care
Genome Biology
Genome Medicine
Stem Cell Research & Therapy

These articles may be flagged as 'Free' content and their bibliographic information may indicate that copyright rests with the publisher or another organization. With the exception of a few co-published articles (see below), these free articles may be reproduced for non-commercial purposes without formal permission from BioMed Central or payment of fees, provided full attribution is given. If you wish to reproduce such an article, or parts thereof, for commercial purposes (other than original figures and/or tables), please contact us to check whether formal permission is needed.

Co-publications: Different rules may apply to articles which are co-published (i.e. published in a BioMed Central journal and simultaneously in another publication); in such cases a statement of co-publication is included in the bibliographic information. Please contact us for permission to reproduce content from these articles.

Figures and tables

Reproduction of figures or tables from any article is permitted free of charge and without formal written permission from the publisher or the copyright holder, provided that the figure/table is original, BioMed Central is duly identified as the original publisher, and that proper attribution of authorship and the correct citation details are given as acknowledgment. If you have any questions about reproduction of figures or tables please contact us.

Figure 1.2: Freeman, M. (2008). Rhomboid proteases and their biological functions. *Annu. Rev. Genet.* **42**, 191–210.

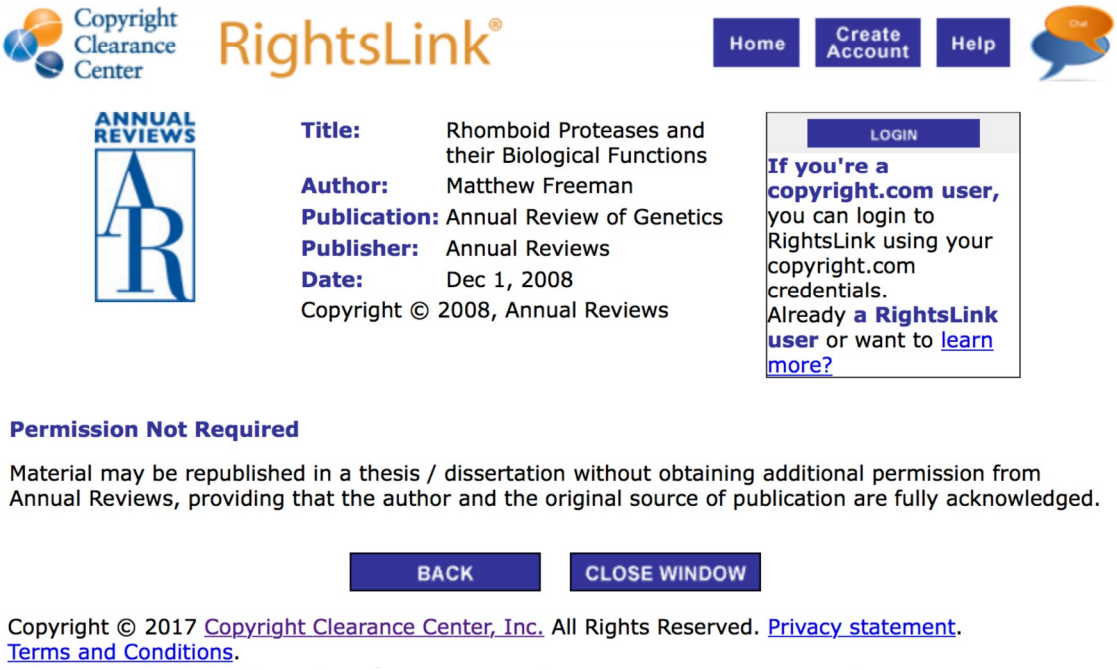

Copyright Clearance Center RightsLink®

Home | Create Account | Help

ANNUAL REVIEWS

Title: Rhomboid Proteases and their Biological Functions
Author: Matthew Freeman
Publication: Annual Review of Genetics
Publisher: Annual Reviews
Date: Dec 1, 2008
Copyright © 2008, Annual Reviews

LOGIN
If you're a copyright.com user, you can login to RightsLink using your copyright.com credentials.
Already **a RightsLink user** or want to learn more?

Permission Not Required

Material may be republished in a thesis / dissertation without obtaining additional permission from Annual Reviews, providing that the author and the original source of publication are fully acknowledged.

BACK | CLOSE WINDOW

Copyright © 2017 Copyright Clearance Center, Inc. All Rights Reserved. Privacy statement. Terms and Conditions.

Figure 1.7: Zhang, F., Wen, Y. and Guo, X. (2014). CRISPR/Cas9 for genome editing: Progress, implications and challenges. *Hum. Mol. Genet.* **23**, 40–46.

OXFORD UNIVERSITY PRESS LICENSE TERMS AND CONDITIONS

May 12, 2017

This Agreement between Megan Jung ("You") and Oxford University Press ("Oxford University Press") consists of your license details and the terms and conditions provided by Oxford University Press and Copyright Clearance Center.

License Number	4106600190802
License date	May 12, 2017
Licensed content publisher	Oxford University Press
Licensed content publication	Human Molecular Genetics
Licensed content title	CRISPR/Cas9 for genome editing: progress, implications and challenges
Licensed content author	Zhang, Feng; Wen, Yan
Licensed content date	2014-03-20
Type of Use	Thesis/Dissertation
Institution name	
Title of your work	Functional Analysis of Zebrafish Paralogs, parla and parlb, by CRISPR-Cas9 Mediated Mutagenesis

Figure 3.1 (A): Shen, B., Zhang, J., Wu, H., Wang, J., Ma, K., Li, Z., Zhang, X., Zhang, P. and Huang, X. (2013). Generation of gene-modified mice via Cas9/RNA-mediated gene targeting. *Cell Res.* **23**, 720–3.

NATURE PUBLISHING GROUP LICENSE TERMS AND CONDITIONS

May 12, 2017

This Agreement between Megan Jung ("You") and Nature Publishing Group ("Nature Publishing Group") consists of your license details and the terms and conditions provided by Nature Publishing Group and Copyright Clearance Center.

License Number	4106590448135
License date	May 12, 2017
Licensed Content Publisher	Nature Publishing Group
Licensed Content Publication	Cell Research
Licensed Content Title	Generation of gene-modified mice via Cas9/RNA-mediated gene targeting
Licensed Content Author	Bin Shen, Jun Zhang, Hongya Wu, Jianying Wang, Ke Ma et al.
Licensed Content Date	Apr 2, 2013
Licensed Content Volume	23
Licensed Content Issue	5
Type of Use	reuse in a dissertation / thesis
Requestor type	academic/educational
Format	print and electronic
Portion	figures/tables/illustrations
Number of figures/tables/illustrations	1
High-res required	no
Figures	Supplementary Information, Figure S4
Author of this NPG article	no
Your reference number	
Title of your thesis / dissertation	Functional Analysis of Zebrafish Paralogs, parla and parlb, by CRISPR-Cas9 Mediated Mutagenesis

Figure 3.1 (B): Zhu, X., Xu, Y., Yu, S., Lu, L., Ding, M., Cheng, J., Song, G., Gao, X., Yao, L., Fan, D., Meng, S., Zhang, X., Hu, S. and Tian, Y. (2014). An efficient genotyping method for genome-modified animals and human cells generated with CRISPR/Cas9 system. *Sci Rep* **4**, 6420.

Copyright Clearance Center RightsLink®

Home | Create Account | Help

nature publishing group

Title: An Efficient Genotyping Method for Genome-modified Animals and Human Cells Generated with CRISPR/Cas9 System

Author: Xiaoxiao Zhu, Yajie Xu, Shanshan Yu, Lu Lu, Mingqin Ding et al.

Publication: Scientific Reports

Publisher: Nature Publishing Group

Date: Sep 19, 2014

Copyright © 2014, Rights Managed by Nature Publishing Group

LOGIN

If you're a copyright.com user, you can login to RightsLink using your copyright.com credentials. Already **a RightsLink user** or want to learn more?

Creative Commons

The article for which you have requested permission has been distributed under a Creative Commons CC-BY license (please see the article itself for the license version number). You may reuse this material without obtaining permission from Nature Publishing Group, providing that the author and the original source of publication are fully acknowledged, as per the terms of the license.
For license terms, please see http://creativecommons.org/

CLOSE WINDOW

Are you the author of this NPG article?

To order reprints of this content, please contact Springer Healthcare by e-mail: reprintswarehouse@springer.com, and you will be contacted very shortly with a quote.